SNOW CELLS AND SHOWERS

by

Richard H. Douglas

Being a thesis submitted to the Faculty of Graduate Studies and Research, McGill University, in partial fulfillment of the requirements for the degree of Doctor of Philosophy.

Montreal. April, 1957

TABLE OF CONTENTS

PREFACE.

The occurrence of precipitation trails, formed in the wind field as snow falls from isolated sources aloft, has been noted by Marshall (1953), Browne (1952) and L'hermitte (1952). Later, Gunn, Langleben, Dennis and Power (1954) studied ten cases of snow generation in isolated and compact cells; they found that cells occur in stable air at a level which is related closely to a frontal surface. Langleben (1954) applied the concepts of trail geometry to the form of snow trails, as observed by radar, and derived the terminal speeds of the constituent particles; these were found to be appropriate to aggregate snow rather than to crystals, suggesting that the cell itself is a centre of aggregation.

Part I of this thesis represents an extension of the work of Gunn et al and of Langleben, using a zenith-pointing radar with a height-time display rather than the range-height display of the radar used earlier; this work consists of a study of 14 cases of cellular snow generation, the results of which confirm the earlier findings noted above.

Radar reveals that the cells resemble small convective elements, even though the environment is stable; furthermore, the presence of aggregated snow throughout the trail suggests that the cell is a centre of aggregation and hence presumably of turbulence. In part II, the possibility is examined of significant vertical motion

and of turbulence in stable air, the latent heat of sublimation providing the energy. The significance of the latent heats of sublimation, condensation and fusion to atmospheric processes has long been recognized, and is discussed, with particular reference to the thermodynamics of moist air, in most meteorological textbooks. Various recent notions concerning the significance of heat exchange between precipitation elements and the environment have been reviewed by Möller (1951). The idea, developed in Part II, of vertical motion in stable air, driven by heat of sublimation, resembles that used by Hewson (1948) in considering the effects, upon cloud, of subsidence due to cooling.

Langmuir (1948) has studied the collection characteristics of droplets in cloud, and his results have been applied by many researchers in studying the growth, by coalescence, of precipitation elements; the most recent study of this kind is that of East (1957). Others (e.g. Ludlam, 1950; Wexler, 1953; Magono, 1953) have examined growth of solid particles (graupel) due to the collection of liquid droplets which freeze upon the primary particle to form an accretion element. Such studies of accretion have usually been concerned with large particles for which accretion is the major growth process; the lower limit to the particle size has been taken as that size for which accretional growth rates exceed sublimational ones, the two processes being deemed independent. Houghton (1950) compared sublimational growth of ice crystals with coalescent growth

of droplets, two processes which are clearly separate and independent. In Part III, growth of spherical particles by sublimation and accretion, occurring simultaneously, is studied and the effects, upon sublimation, of the concurrent accretion are examined.

ACKNOWLEDGMENTS

This work has been done under the supervision of Prof. J. S. Marshall, whose guidance and encouragement it is a pleasure to acknowledge; the work has benefitted immeasurably from numerous discussions with the members of the Stormy Weather Research Group. The writer is indebted to Mr. A. Thomson, Director, Meteorological Division, with whose permission and encouragement this work was undertaken.

Radar data were obtained with equipment maintained by the Defence Research Board of Canada, under contract D.48-95-11-08; the research has been sponsored, in part, by the Geophysics Research Directorate, Air Force Cambridge Research Centre, under contract AF-19(122)-217.

The writer gratefully acknowledges the assistance, in preparing this thesis, of Miss Frances Oshowski, who typed the manuscript, and of Dr. M. P. Langleben and Miss Sylvia Deleu, who prepared the prints of the figures. The help of Mrs. Czalay, and of the author's wife, in the various stages of assembly, is much appreciated.

More specific references to assistance are made in the introductory sections of the three parts of this thesis.

PART ONE

SNOW PATTERN IN THE VERTICAL

PART I: SNOW PATTERN IN THE VERTICAL

1. INTRODUCTION AND ACKNOWLEDGMENTS.

One of the notable contributions of radar to the study of precipitation has been the revelation of the fact that much of the precipitation which reaches the ground as continuous rain or snow has its origin aloft in compact and discrete cells, whose horizontal dimensions may be of the order of a mile or so and which extend vertically for several thousands of feet. Marshall (1953) published RHI* photographs of such cells and the snow trails which derive therefrom, and formulated the geometry of the trail shaped in the wind field; similar analyses were performed independently by L'hermitte (1952) and Browne (1952). Trail geometry has since been further developed and used in studies of showers (Gunn and Marshall, 1955). A study of snow generating cells (Gunn, Langleben, Dennis and Power, 1954) revealed that the cells tend to occur just above a frontal surface, a stable environment being more favourable for distinctive cell occurrence than an unstable one. Langleben (1954), applying the principles of trail geometry to RHI radar observations, deduced that the fall speeds of the snow particles constituting the trail were comparable to those of aggregate snowflakes, and were (in the cases studied)

---

* RHI: range-height indication, the presentation of a vertical cross section along a specific azimuth.
CAPI: constant altitude plan indication, a plan map at any selected height.
PPI: plan-position indication, a plan map at zero angle of elevation.

invariant with height, suggesting that the cell itself is a region of aggregation, even at relatively low temperatures.

The following sections report on further studies of snow generating cells, observed by means of a zenith-pointing radar. Much of the work reported was done by members of the Stormy Weather Group other than the author, and is included here in as much detail as is necessary to insure completeness and continuity of account. Design and operation of the high-resolution system for recording the radar display (sec. 2) was directed by Dr. T.W.R. East. Trajectory analysis, pattern fitting and determination of terminal speeds (secs. 6 and 8) was performed almost entirely by Prof. K.L.S. Gunn, assisted in the early stages by Dr. Roger L'hermitte; the author contributed to the study of possible errors in the terminal speeds (sec. 8). The analysis of standard meteorological data (secs. 4 and 5) is entirely the work of the author, who made full use of the routine maps and charts prepared at the Central Analysis Office, made available through the courtesy of Mr. J.M. Leaver. The author is happy to acknowledge the assistance of Profs. J.S. Marshall and Gunn in the study and preparation of the material in secs. 7 and 9-12.

2. RADAR EQUIPMENT.

The radar in use during this phase of the work was a Marconi type LN27*, the beam of which was stationary and directed vertically upward. The display was modified to give a height/time

---

* Wavelength 3 cm; peak power 40-50 kw; pulse length 0.2μsec; pulse repetition frequency 1000 sec^{-1}; beamwidth 1 deg.

presentation. The intensity-modulated trace on the CRT was moved automatically in small steps, parallel to itself, crossing the screen in 26 minutes, during which time the camera shutter remained open. At the end of this time the trace was returned to the opposite side in preparation for the next cycle, while the camera shutter was closed and the film advanced one frame. The resulting photographic record (fig. 1) is a height/time record of the precipitation which moved through the stationary beam. Continuous records of this sort were obtained throughout the winter 1953-54.

3. PATTERNS OBSERVED.

Several different patterns of echo were revealed in the height/time records; not all of the echo showed such distinctive cell-and-trail pattern as is strikingly evident in fig. 1a. There were frequent prolonged periods during which the echo was relatively homogeneous and patternless, such as in fig. 1b. Snowfall at the ground was usually preceded for a few hours by echo aloft (fig. 1c), the base of which lowered gradually with time. Sometimes as in fig. 1c the base of this echo was scalloped in a manner suggestive of mammatus; these pendulous extensions, or "stalactites", are apparently a consequence of evaporational chilling as the snow falls from aloft into a dry stratum below.

The 14 cases examined were of the patterned type of fig. 1a or c. They were selected to coincide as nearly as possible with the times of the twice-daily upper-air ascents (0300 and 1500 GMT); the times of these 14 cases are indicated in fig. 2 by the

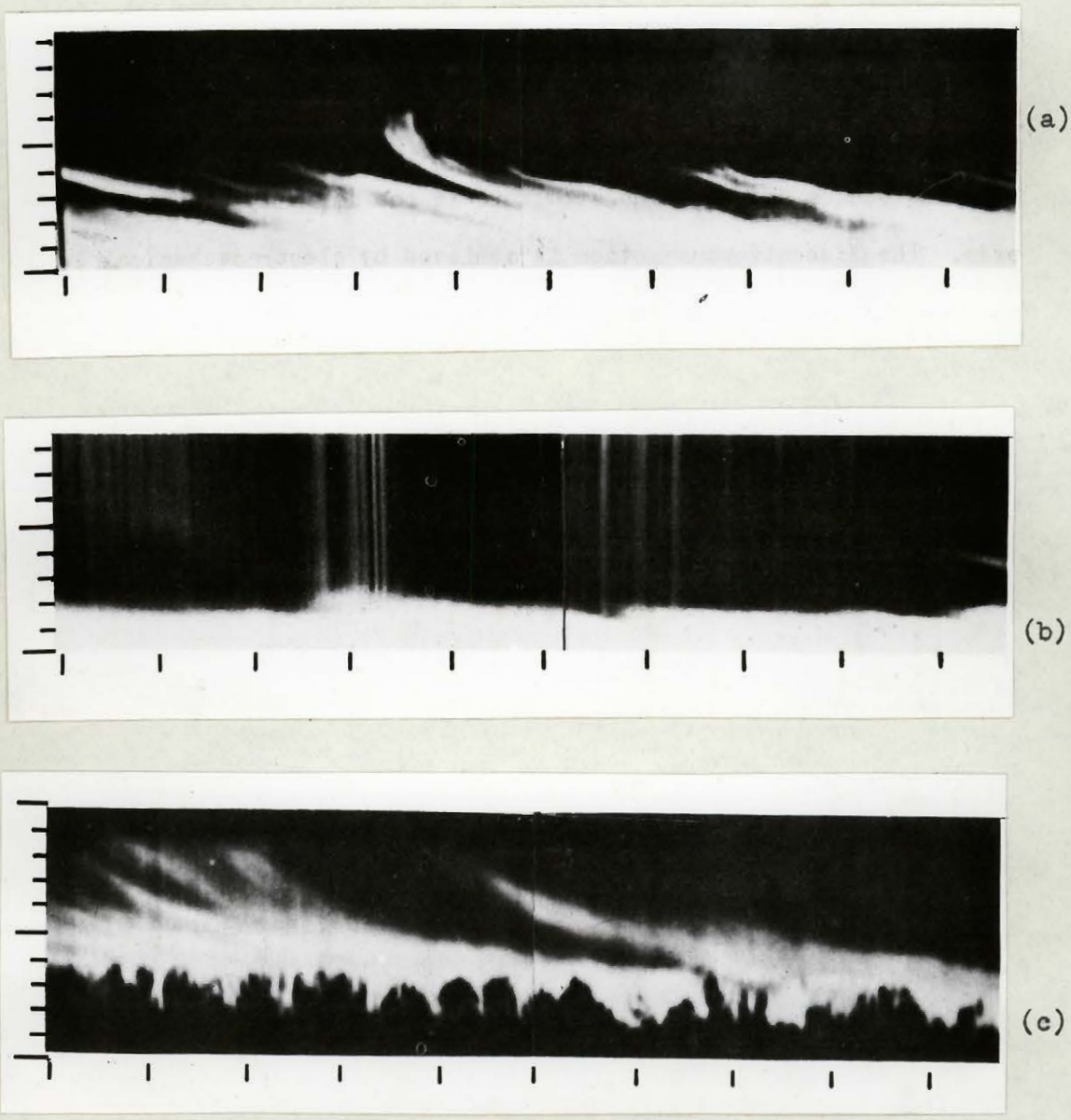

FIG. 1. Height/time radar records of (a) well-defined trail pattern, (b) relatively homogeneous unpatterned echo, (c) snow trails and stalactites. The abscissa is time, indicated at 5-minute intervals; the ordinate is height, indicated at 2000-ft intervals.

letters "A".

4. SYNOPTIC DATA.

Snowfall data were obtained from the observatory, McGill University, and were reduced to hourly precipitation rates, as shown in fig. 2. During the period investigated (1 January to 17 February 1954), a total of 6.61 in (melted) was recorded during 426 hours of snowfall.

Frontal positions aloft over Montreal were determined from the radiosonde data from Maniwaki (station 722, about 130 miles northwest of Montreal) and from the routine frontal contour analyses prepared by the staff of the Central Analysis Office (Meteorological Service of Canada) at Montreal Airport. Additional radiosonde data from other stations (such as Rome, RME, about 180 miles to the southwest) were examined when necessary. On the basis of these data, time cross-sections of the frontal structure over Montreal were prepared, on which were superimposed the radar echo levels.

Pilot balloon ascents at Montreal Airport were found inadequate because of their short duration during the snowstorms and so the upper winds, necessary for the trail geometry, were obtained from the Maniwaki rawin. Whenever a substantial shear existed through a frontal zone, and that zone lay at a different height over Montreal than over Maniwaki, a suitable adjustment to the wind-shear hodograph had to be made. These adjustments were made by using certain frontal properties discussed by Godson (1951).

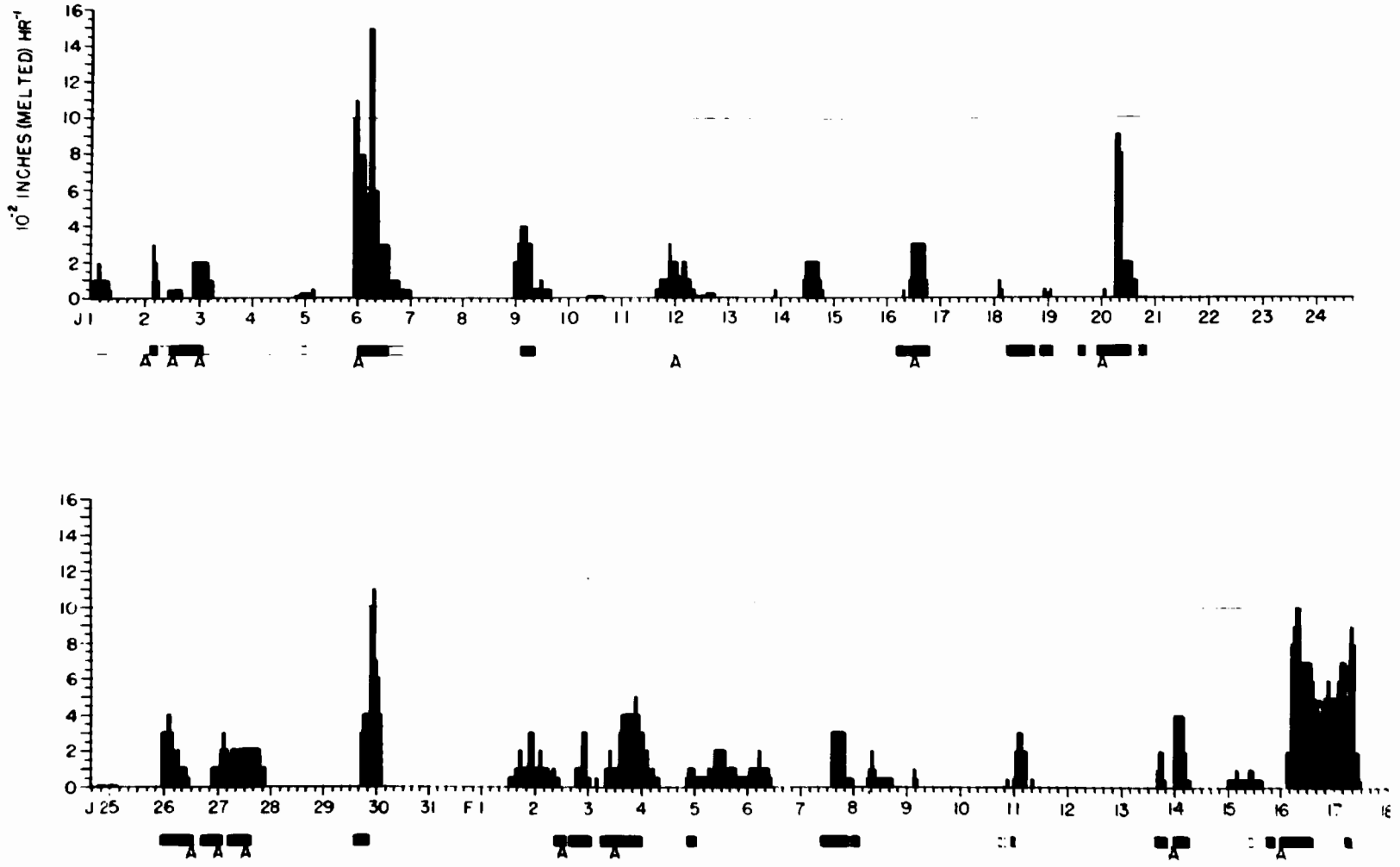

FIG. 2. Hourly precipitation, January-February 1954. Date appears at 1500 GMT. Double line indicates hours of radar operation; solid and stippled portions indicate hours of patterned and unpatterned echo, respectively. Times of analyses indicated by "A".

as described in the following section and in Appendix A. An example of a complete case history is presented in Appendix B.

5. MODIFICATION OF THE SHEAR HODOGRAPH.

Godson (1951) has derived the following expression for the slope m_p of a frontal surface in terms of the thermal gradients on either side of the boundary:

$$m_p = (\beta'_H - \beta'_w) / (\gamma'_w - \gamma'_H) \qquad (5.1)$$

where, using Godson's terminology, $\beta' = -(\partial T / \partial x)_p$ and $\gamma' = (\partial T / \partial p)$. Subscripts w and H refer here to the warm air and the hyperbaroclinic (H-) region, respectively; a similar expression may be derived for the slope of the boundary between the cold air and the H- layer. The coordinate system is the usual right-handed one, the x-axis being horizontal and normal to the frontal boundary, directed positively into the cold air. Substitution of the β'- terms in (5.1) from the thermal wind relation results in:

$$m_p = \frac{\lambda T}{g} \left\{ (\partial v / \partial z)_w - (\partial v / \partial z)_H \right\} \Big/ (\gamma'_w - \gamma'_H), \qquad (5.2)$$

where λ = Coriolis parameter; g = gravitational acceleration; v = horizontal wind component in the y-direction; thus, $\partial v / \partial z$ is the vertical shear of the wind component parallel to the front.

If, over a restricted horizontal and vertical range, the slope of the front and the vertical lapse rate difference $(\gamma'_w - \gamma'_H)$ remain unchanged, then

$$(\partial v/\partial z)_W - (\partial v/\partial z)_H = \text{constant}, \qquad (5.3)$$

since λ and T will vary but little; and if winds are reported at specific height intervals, such as every thousand feet, then

$$\Delta v_W - \Delta v_H = \text{constant}. \qquad (5.4)$$

A similar condition can be derived for the other frontal boundary, viz:

$$\Delta v_C - \Delta v_H = \text{constant}. \qquad (5.4a)$$

The constants in (5.4) and (5.4a) are not necessarily the same.

If moreover the orientation of the frontal surface remains unchanged over the horizontal and vertical distances considered, a further condition applies at the two boundaries, viz:

$$\Delta u_W = \Delta u_H \qquad \text{and} \qquad \Delta u_C = \Delta u_H \qquad (5.5)$$

where u is the horizontal wind component normal to the front; as Godson (1951) points out, the conditions expressed by (5.5) can be used to determine the orientation of the frontal boundaries from the wind shear hodograph.

The application of the above to the modification of the hodograph is best shown by means of a simple example illustrated in detail in Appendix A. Wind modifications were only made when considered absolutely necessary (i.e. when the frontal shear was highly developed), and in some cases served more as a qualitative guide to the required changes than a rigorous quantitative one.

Certainly, in several cases, very distinctive inflections in the vertical pattern of precipitation echo could only be matched, at the proper level, when pronounced wind shears over Maniwaki were adjusted to allow for the difference in frontal height over Montreal.

6. PATTERN FITTING.

A three-dimensional trail in space is formed by snow as it falls continuously from a source at the generating level (G/L) through the varying wind field below. In time Δt snow falls through a distance $\Delta z = v \Delta t$, where v is the fall velocity; at the same time it suffers a horizontal displacement $\vec{\Delta s}$ which is given by

$$\vec{\Delta s} = (\vec{W} - \vec{W_c})\Delta t = \frac{\vec{W} - \vec{W_c}}{v} \Delta z$$

where $\vec{W} - \vec{W_c}$ = average wind vector, relative to the source, through the layer of thickness Δz;

$\vec{W}$ = wind vector in the layer, relative to the ground;

and $\vec{W_c}$ = velocity of the source relative to the ground, which tends to be equal to the wind velocity (relative to the ground) at the G/L.

Fig. 3 shows the trajectory* in plan for a case when snowflakes with a terminal speed of 4 ft sec^{-1} are falling from

---

* Trajectories are consistently taken with reference to axes moving with the generating cell, and constitute the pattern created in space by snow emitted from a continuously generating point source.

a point source at 12 thousand feet. The trajectory consists of a series of vectors $\overrightarrow{\Delta s}$, each representing the horizontal displacement experienced as the particles fall through a layer of thickness 1000 ft. Trajectories such as this are readily obtained from the wind-shear hodograph, with the aid of a drafting machine. The orthogonal projection of this plan-trajectory, on the vertical plane containing the cell velocity, is shown in the lower part of fig.3. When the horizontal (abscissa) scale is divided by the cell speed, it becomes a time scale, and the pattern is that which is observed on the height/time display of the zenith-pointing radar.

It is clear that a single cell, or a short line-array of cells, may pass to one side of the vertical radar beam and thus escape detection, but that the wind field may be such as to carry a portion of the trail through the beam. Therefore one cannot assume that the maximum level of observed echo is the level of generation. However, one can consider several possible G/L's, compute the corresponding trajectories and their orthogonal projections (which will in general vary in form as the G/L is changed, due to the usual variation of wind with height) and compare these derived patterns with that observed by radar.

The constant of proportionality between the wind vectors $(\vec{W} - \vec{W_c})$ and the true horizontal displacement $\overrightarrow{\Delta s}$ is $1/v$. Thus the derived pattern (in the lower half of fig. 3) is expanded or

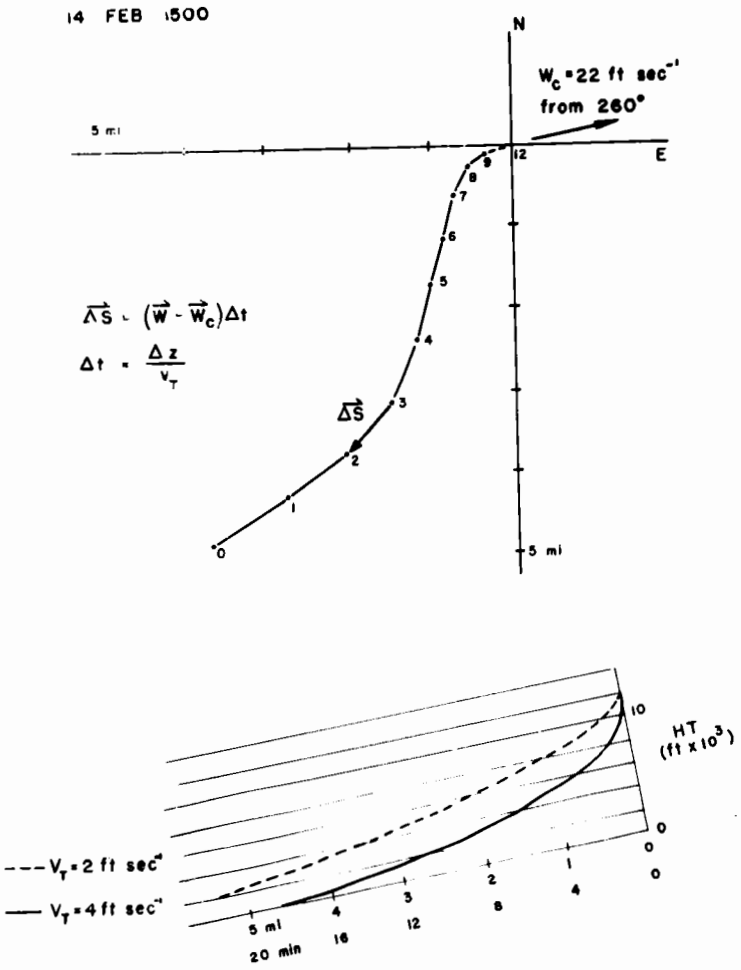

FIG. 3. (Above) Plan trajectory of snowflakes emitted from a point source, with terminal speed of 4 ft sec^{-1}; heights indicated at thousand-foot intervals along trail. (Below) Projection of the plan trajectory on a vertical plane containing the cell velocity W_c.

contracted along the abscissa until fit with the observed radar pattern is achieved; the scale factor required to accomplish this fit is convertible into the terminal speed v. Thus, fitting enables one to estimate the G/L and the terminal speed, even though the cell itself may remain undetected by the radar. A serious complication is introduced due to the unknown orientation of line-arrays of cells; present calculations have been made on the assumption that line-arrays are aligned normally to the direction of motion, and the implications of this drastic assumption will be discussed in sec. 9.

Terminal speeds of the constituent particles can also be determined from the slope of the trail, as described by Marshall (1953) and by Langleben (1954). The 14 cases analysed yielded 20 speeds by the fit method and 46 by the slope method; these are tabulated in Appendix C and discussed in sec. 8.

7. THE GENERATING LEVEL.

In fig. 4 the 14 G/L's are plotted against temperature and height; areas of the circles are proportional to the total snow from the storm in which the trails were observed, and the fraction of the circle shaded indicates the fraction of the total snowfall derived from patterned echo. Total snowfall at the ground (in hundredths of an inch, melted) is indicated below each circle; the letter "E" indicates that evaporation was occurring in the lower air mass. Large snowfalls at the ground appear equally likely with any G/L height. The majority of G/L's lay between 11

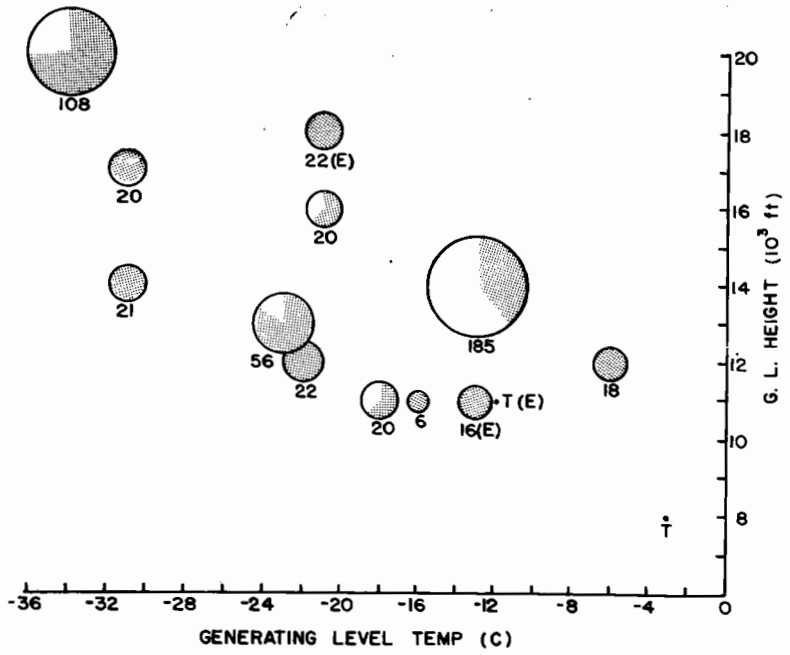

FIG. 4. Heights above ground, and temperatures, of the generating levels. Areas of circles are proportional to total precipitation in the storms (given below circles in 10^{-2} in, melted; T=trace). Letter E indicates evaporation. Shading indicates precipitation associated with patterned echo.

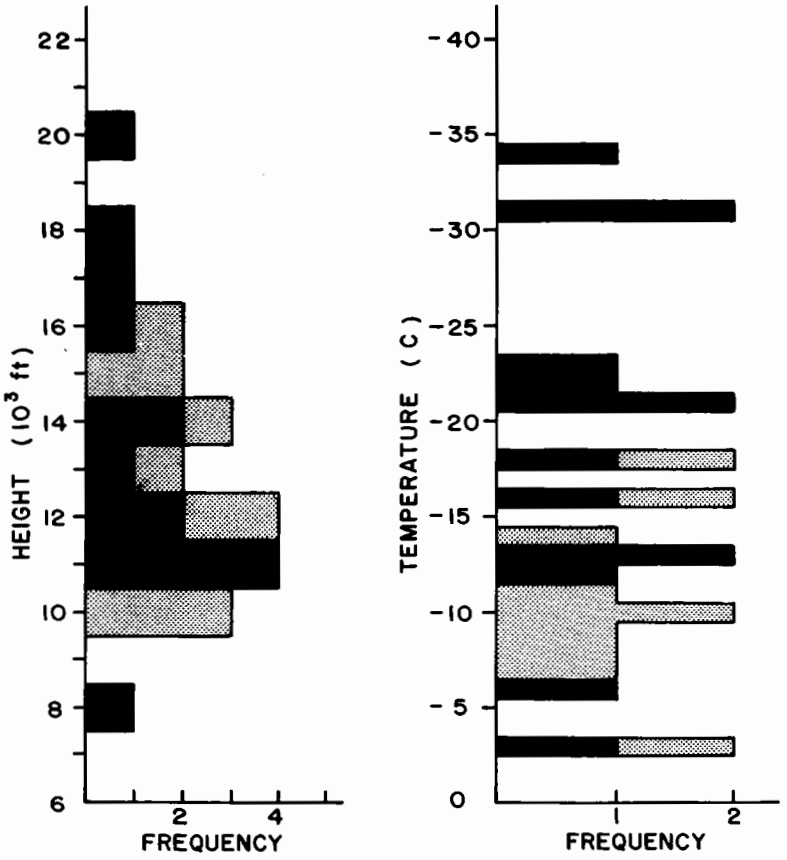

FIG. 5. Frequency distributions, with height and temperature, for combined generating level data. Ten cases for 1952 are shaded, 14 for 1954 are black.

and 20,000 ft and at temperatures between -12 and -34C. In an earlier study of cells during 1952, Gunn et al (1954) determined 10 G/L's; distributions of the combined data, with height and temperature, are shown in fig. 5. From figs. 4 and 5 it is apparent that there is a large and rather uniform spread of G/L's, both with height and temperature, providing some evidence against the notion of a preferred temperature for cellular snow-generation.

The stability of the air mass at the G/L (expressed as a stability index $\frac{\gamma_w - \gamma}{\gamma_w}$) is shown in fig. 6. Of the 14 cases examined, only 3 were unstable; the median stability index corresponds to a lapse rate which is roughly 85% of the saturated (water) adiabatic value. These data confirm the earlier findings of Gunn et al (1954) that well-defined cell structure tends to be associated with stable rather than unstable lapse rates.

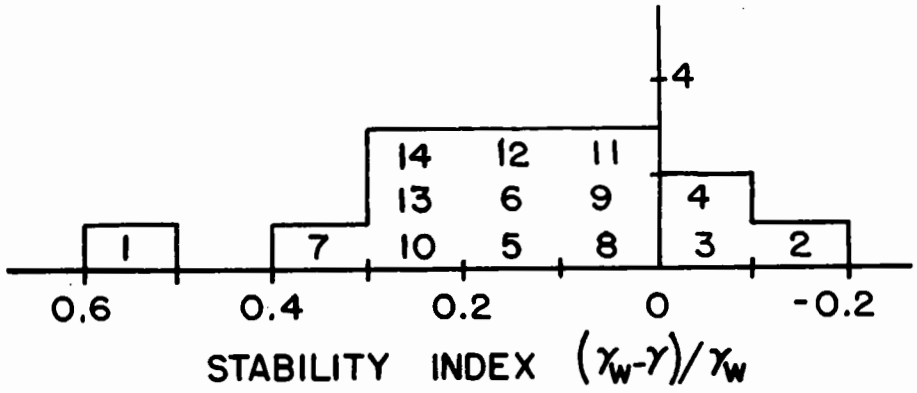

FIG. 6. Histogram of stability index at the generating level. Median value of 0.13 corresponds to a lapse rate, at 700 mb, -15C, of 6.6 deg km^{-1}. Case numbers shown are those used in Fig. 8.

Fig. 7 shows a plot of the distance from the G/L to the nearest front, as a function of the height of that front. The earlier (1952) data of Gunn et al (1954) have been added for comparison. Most of the G/L's lie above the nearest front, the majority within 3000 ft. The mean distance, for both the earlier and the new data, is +1200 ft; so there is confirmation of the earlier observation that the cells tend to occur above and within a few thousand feet of a frontal surface. There appears to be little trend of proximity to the front with the frontal height itself, although the pronounced negative values are associated with high-level fronts; this may be due to difficulties and uncertainties in locating fronts at these high levels.

Fig. 8 shows the position of the G/L with respect to the specific frontal surfaces. The air mass containing the G/L is shaded. The fronts themselves are identified as Arctic, Maritime, and Polar, separating the four air masses cA/mA/mP/mT in accordance with the 3-front synoptic model in current use in Canada (Anderson, Boville and McClellan, 1955; Penner, 1955); fronts and air masses are indicated schematically in fig. 10.

From fig. 8 it is seen that at least 2 fronts are present on each of the 14 occasions investigated; the Maritime front is present on all 14 occasions, the Polar and Arctic 9 times each. In only 2 cases did the G/L lie below the Maritime front; of the remaining cases, over one half lie within 2000 ft of the Maritime

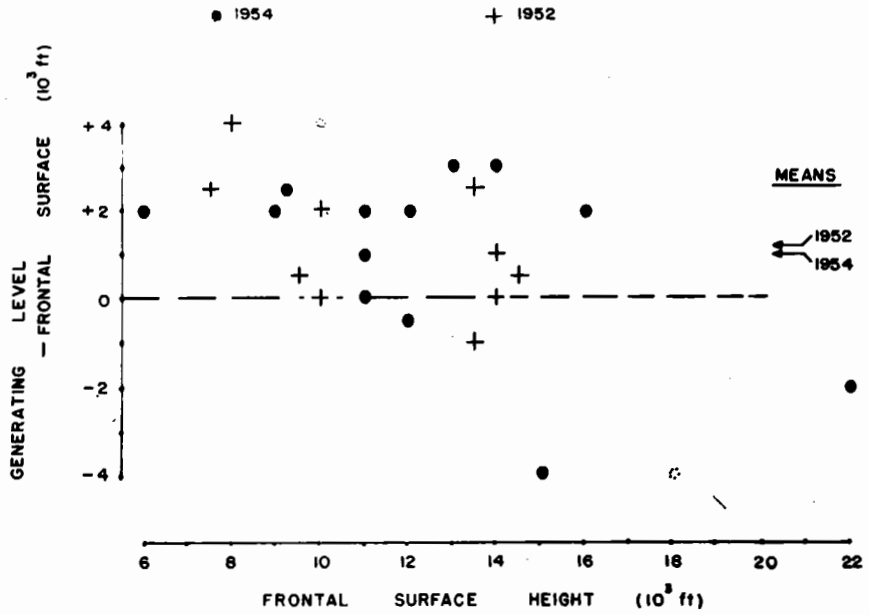

FIG. 7. Distance of generating level from nearest front versus height of front, showing both 1952 and 1954 data.

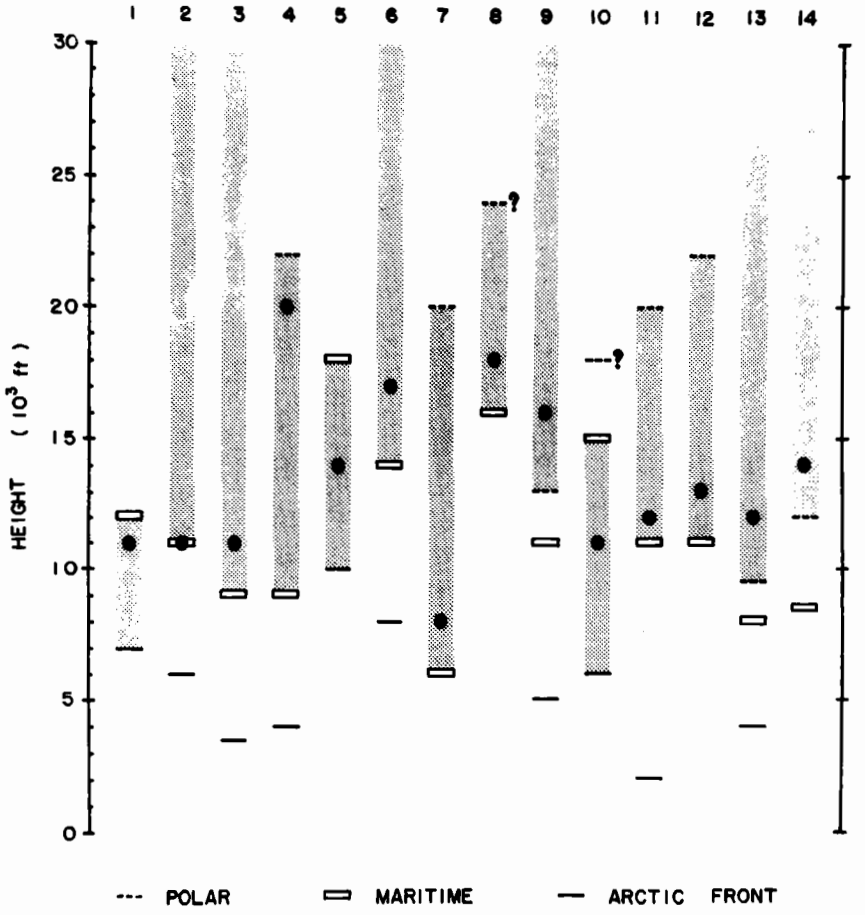

FIG. 8. Heights of fronts and of generating levels for 14 cases studied. Shading indicates air mass in which the cell resides.

front (although on 3 occasions the Polar front intervenes). The G/L is nearest to the Maritime front twice as often as to the other two fronts combined. Examining the G/L's with specific reference to this particular front, we find that in all but one case the G/L was within 5500 ft of the Maritime front, and in only 2 cases was it below. Of the occurrences above the Maritime front (neglecting case#5), the 3 most remotely removed (#s 9, 13, 14) were associated with the intervening presence of the Polar front.

Viewing the matter from the standpoint of the air masses involved, we refer to fig. 9 in which are shown the frequencies of fractional heights of the G/L within the air mass. (In some cases the top of the air mass was taken as the tropopause, arbitrarily set at 30,000 ft). Both the present (1954) data and those (1952) of Gunn et al (1954) show the predominance of cell-occurrence within the mP air mass; for both sets of data combined, cells are contained within this air mass on 15 occasions out of 24, and on 11 of these 15 occasions the cells were located within the lowest 1/5 of the air mass. These results are summarized in schematic form in fig. 10.

8. TERMINAL SPEEDS.

Terminal speeds were computed by fitting the derived trail pattern to the observed radar pattern, as described in sec. 6; in addition, terminal speeds were derived from measurements of trail slope (after Marshall,1953). In most cases, the more clear-cut leading edge of the trail was used, but on a few occasions the trailing

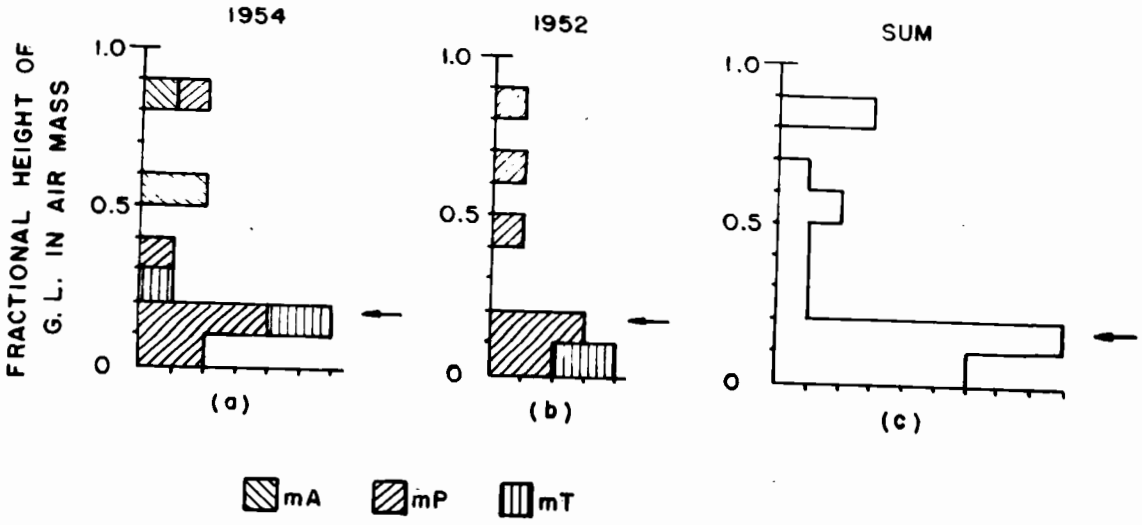

FIG. 9. Distributions of the relative heights of the generating levels within the air mass. (a) 1954 data; (b) 1952 data; (c) combined data. Arrows indicate median values.

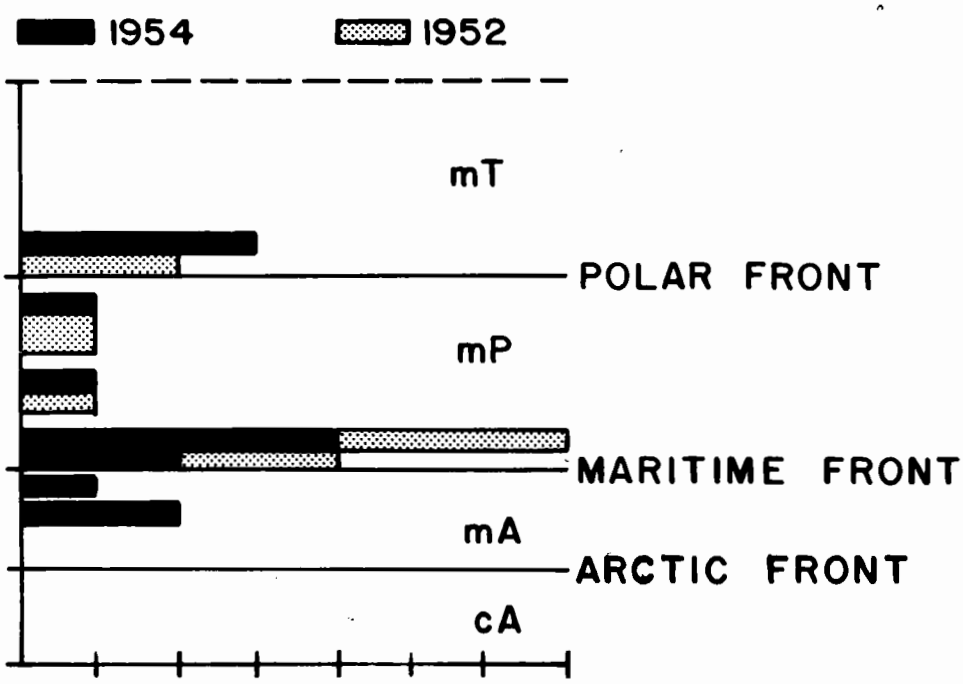

FIG. 10. Schematic diagram of air masses and fronts in the three-front model. Histogram gives relative position of each generating level within its air mass (from Fig. 8).

edge was used. Speeds thus derived are shown in fig. 11, and are tabulated in Appendix C. Clearly, about half the speeds measured are greater than the highest speeds directly observed for aggregates (Langleben 1954). Unfortunately very little data were collected regarding the type of snow particles reaching the ground, but such as were available did not suggest the presence of snow pellets or graupel with such high terminal speeds. Various possible causes of these rather high measured speeds were examined.

(a) The effect upon terminal speed of air density and of viscosity was considered, and the observed speeds were normalized to a standard environment at 1010 mb and 0C. This correction served to reduce the speeds in every case, the corrections varying from about 3 to 20%, the median correction being about 9%.

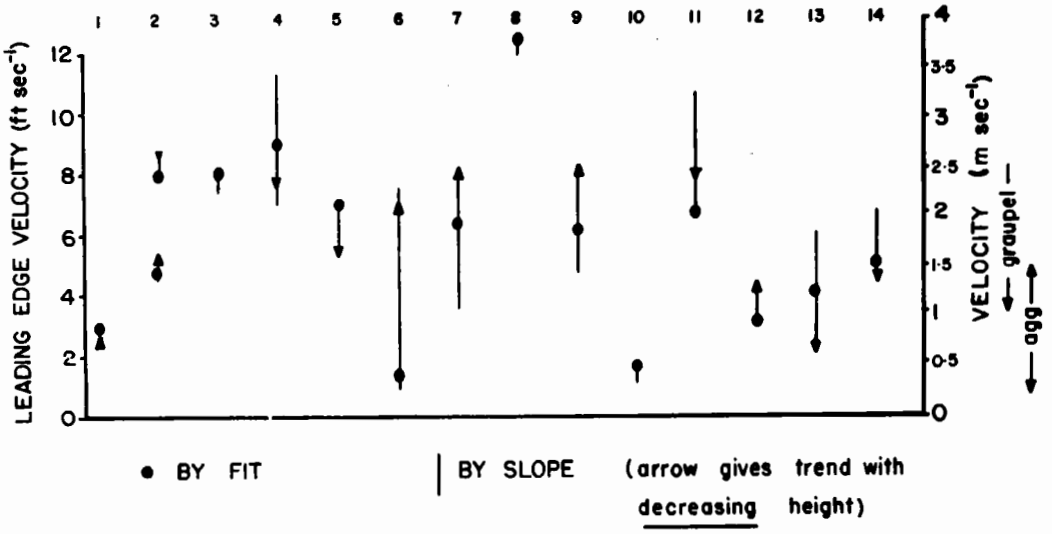

Fig. 11. Terminal speeds of precipitation particles computed by fit of pattern and by trail-slope. Line indicates range of terminal speeds obtained by slope at several points along the trail.

(b) The sensitivity of the radar was considered. The technique of measuring v has been based upon the assumption that the leading edge of the radar pattern consists, throughout its length, of particles having one and the same terminal speed, whereas in fact the edge is a contour of Z/r^2, where Z is the sum of the sixth powers of the melted particle diameter and r is the range. The Z-contours below an extended source have been computed, for the case of a rain shower, by Gunn and Marshall (1955), and their technique was applied to snow (fig. 12). A radar set equipped with STC (sensitivity-time-control) corrects for the inverse range-squared effect, and detects these Z-contours. It will be clear from fig. 12a that the Z-contours may differ appreciably from a constant fall velocity trajectory, particularly where the Z-contours converge and peak upon the central axis (which is itself a constant fall velocity curve). If the radar is not equipped with STC (as was the case with the set used) the range effect must be considered; the contours are then those of fig. 12b, and again these differ materially from those of constant fall velocity.

Consideration of these effects, based upon a model generating source and wind field, enabled a further correction to be estimated to the calculated fall speeds; this correction served to further reduce the deduced speeds.

(c) Since the trail geometry was derived on the basis of purely horizontal motion of the generating source, the effect,

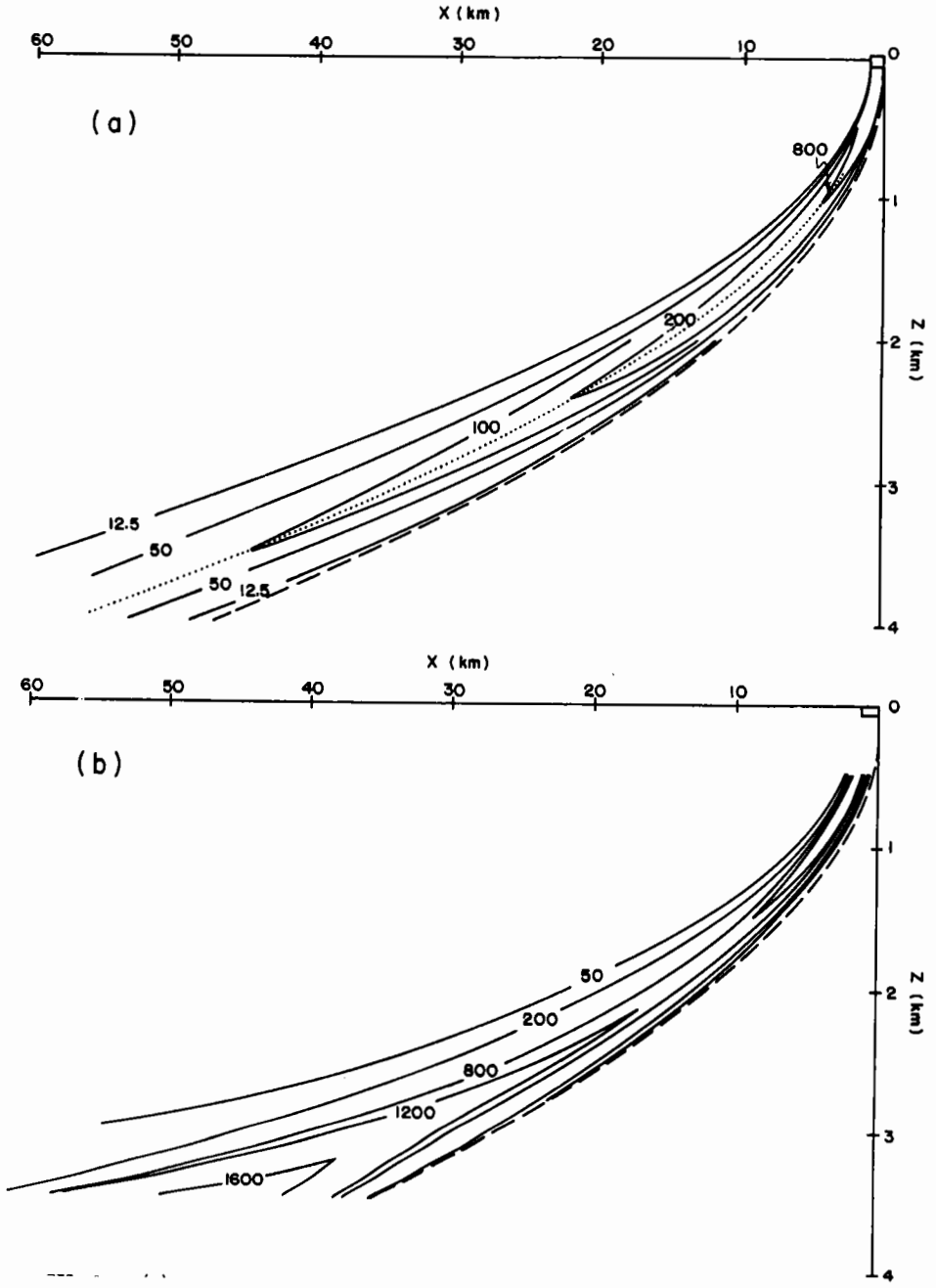

FIG. 12. (a) Contours of Z below a cell of 1 km extent in which the precipitation rate at cell is 10 mm hr^{-1}. Wind is assumed entirely in plane of diagram, with shear of 10^3 cm sec^{-1} km^{-1}. Dashed and dotted curves are particle trajectories for comparison. (b) Contours of constant signal at radar 4 km below generating level, labelled by Z-values at the generating level that would yield same signal. Precipitation rate and wind field same as in (a).

upon the computations, of vertical cell motion was investigated. With vertical motion (as over a frontal surface) the trail in space is steepened, the terminal speed derived therefrom being the sum of the true speed and the vertical component of cell velocity. This modified pattern is translated with the same vertical component, which tends to reduce the slope as viewed on the height/time display. The terminal speed v' measured from the slope of the height/time record is related to the true speed v by the equation $v' - v = \frac{W}{W_c} \cdot w$ where W_c is the horizontal wind (relative to the ground) at the generating level, W is the horizontal wind component (in the direction of W_c) at the level in question, and w is the vertical component of the cell velocity. This correction was calculated for all the terminal speeds derived from slope measurements, assuming the air at the generating level to be gliding up the relevant frontal surface. The largest correction, 13%, reduced the absolute fall speed by only 0.6 ft sec^{-1}, all other corrections being of considerably less significance; neglect of this effect was therefore considered justifiable.

A histogram of calculated terminal speeds, corrected for density, viscosity, and radar sensitivity is shown in fig. 13. (obtained by taking a running mean over 3 successive intervals, weighted in the ratio 1:2:1). While this histogram shows a peak in the region of aggregate fall speeds, it extends to values as high as 10 ft sec^{-1}. This extreme range to very high terminal speeds

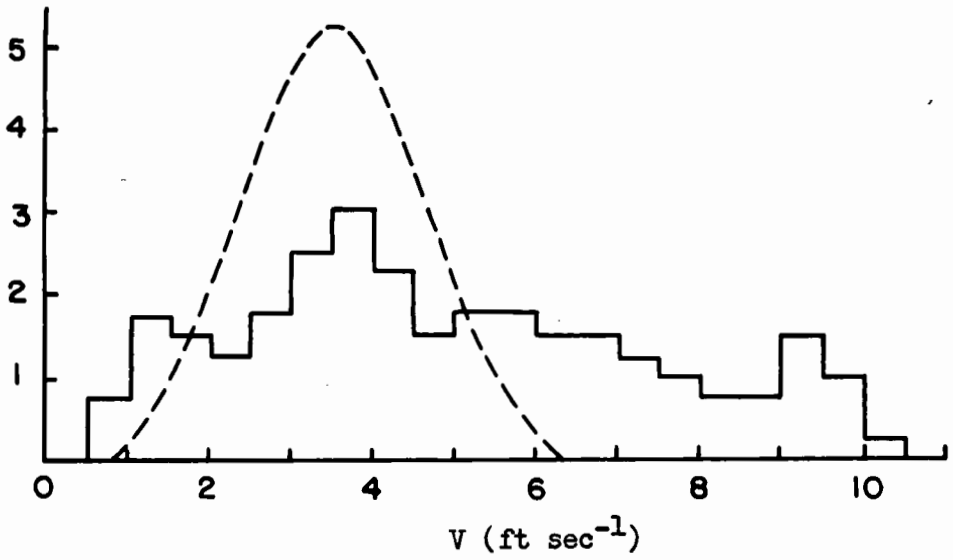

FIG. 13. Histogram of terminal speeds derived from slope measurements, corrected for radar sensitivity and adjusted to 1010 mb and 0C. Dashed curve is likely distribution, recognizing discrepancies between assumed and true orientation of cell arrays at the generating level (sec. 9).

can be explained, to some extent at least, when the effects of the orientation of linear cell arrays is considered, as in the following section.

9. ORIENTATION OF LINE ARRAYS OF GENERATING CELLS.

Langleben (1956) has examined the plan patterns of generating elements at the generating level, and finds that individual cells are often arranged in line arrays. Of 7 cases examined, he found only 2 in which the cells occurred in random fashion. When line arrays are observed, it appears that they may be oriented in almost any fashion; this same conclusion, with regard to line arrays of tropical showers, has been reached by Soane and Miles (1955). The assumption made in the analysis of radar height/time records, that the snow generation occurs in lines perpendicular to the

direction of motion, is therefore likely to be invalid in most cases.

Fig. 14 shows the plan trajectory (0-2-3 etc.) of particles (with some specific terminal speed) emitted from a point source at 0, which is moving to the left with speed W_c. If the emitting source is a line aa normal to the direction of motion ($\phi = 90^\circ$) then each point on the line acts as a source and the single trail becomes a sheet, the height contours of which lie parallel to aa and thus perpendicular to the velocity of translation. The fixed radar beam may be considered as moving along the line 0x with a speed W_c, and the height/time pattern detected is defined by the orthogonal projections of the various levels 0, 2, 3, etc. upon the 0x axis, which results in the height/time profile shown in the lower figure for $\phi = 90^\circ$. Now let the generating line be rotated through 45° to the position bb ($\phi = 135^\circ$). The contours of the snow sheet are likewise rotated, and intersect the 0x axis at different positions, resulting in the height/time profile indicated for $\phi = 135^\circ$. Similarly, rotation of the line source by 45° in the opposite sense results in the profile for $\phi = 45^\circ$. Although based upon the same particle terminal speed and wind field, these three profiles are decidedly different; terminal speeds based upon slope measurements, with the assumption that $\phi = 90^\circ$, may differ substantially from their true values.

If a terminal speed v' has been computed on the assumption that $\phi = 90^\circ$, then it can be shown that the true speed

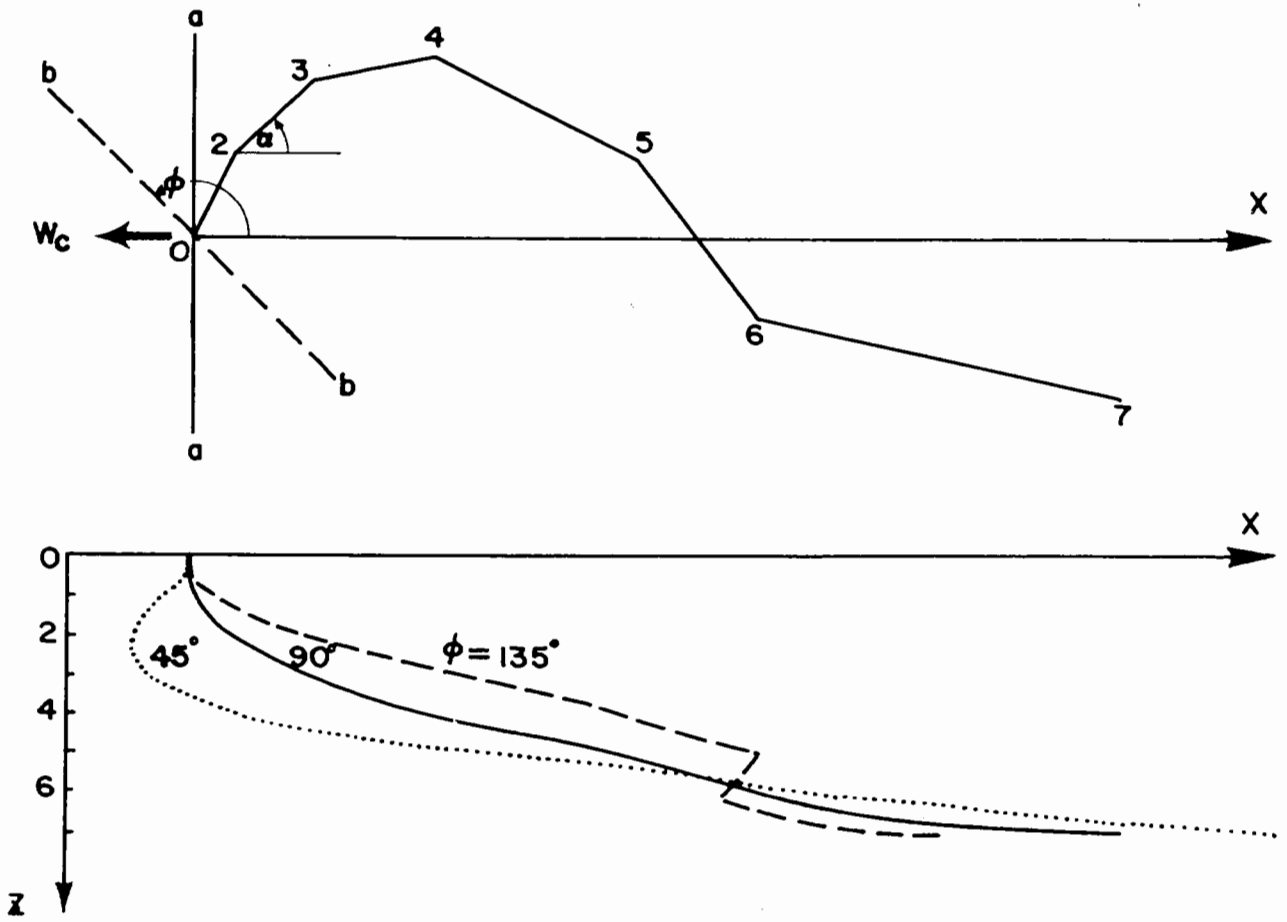

FIG. 14. The effect on the height/time pattern of different orientations of a line of generating elements. Top: A schematic plan trajectory of snow emitted from a point source O. The angle α is determined by the wind shear. Bottom: The projection onto the vertical plane containing W_c of the pattern when $\phi = 45°$, 90° and 135°.

v is given by

$$v = v'(1-\cot\phi\tan\alpha)^{-1}$$

or alternatively, that the relative error E in the speed is

$$E = (v-v')/v = \cot\phi\tan\alpha$$

where ϕ is the true orientation and α is the angle between the plan trajectory and the direction of motion, as indicated in fig. 14. Note that $\tan\alpha$ is the ratio of the crosswind to the along-wind components of shear (relative to the wind at the generating level). The relative error includes two terms, one dependent upon the orientation of the line array and the other upon the orientation of the trail, i.e. upon the wind shear. If the terminal speed is estimated from a slope measurement, assuming a generating line perpendicular to the direction of motion, then terminal speed can be plotted as a function of ϕ; if an estimate is made at several levels, the several equations relating v and v' can be solved simultaneously for v and ϕ.

Plots of terminal speed versus orientation angle are shown in fig. 15, for 6 occasions on each of which slope measurements were made at 3 or more levels. In a few cases a rather wide variation in ϕ makes relatively little difference to the computed terminal speed; in case #11, for example, speeds computed on the basis of $\phi = 90^\circ$ are valid, within a factor 2, over a broad range of ϕ from about 30° to 130°. On the other hand, in case #13, there is a very wide variation of v with ϕ

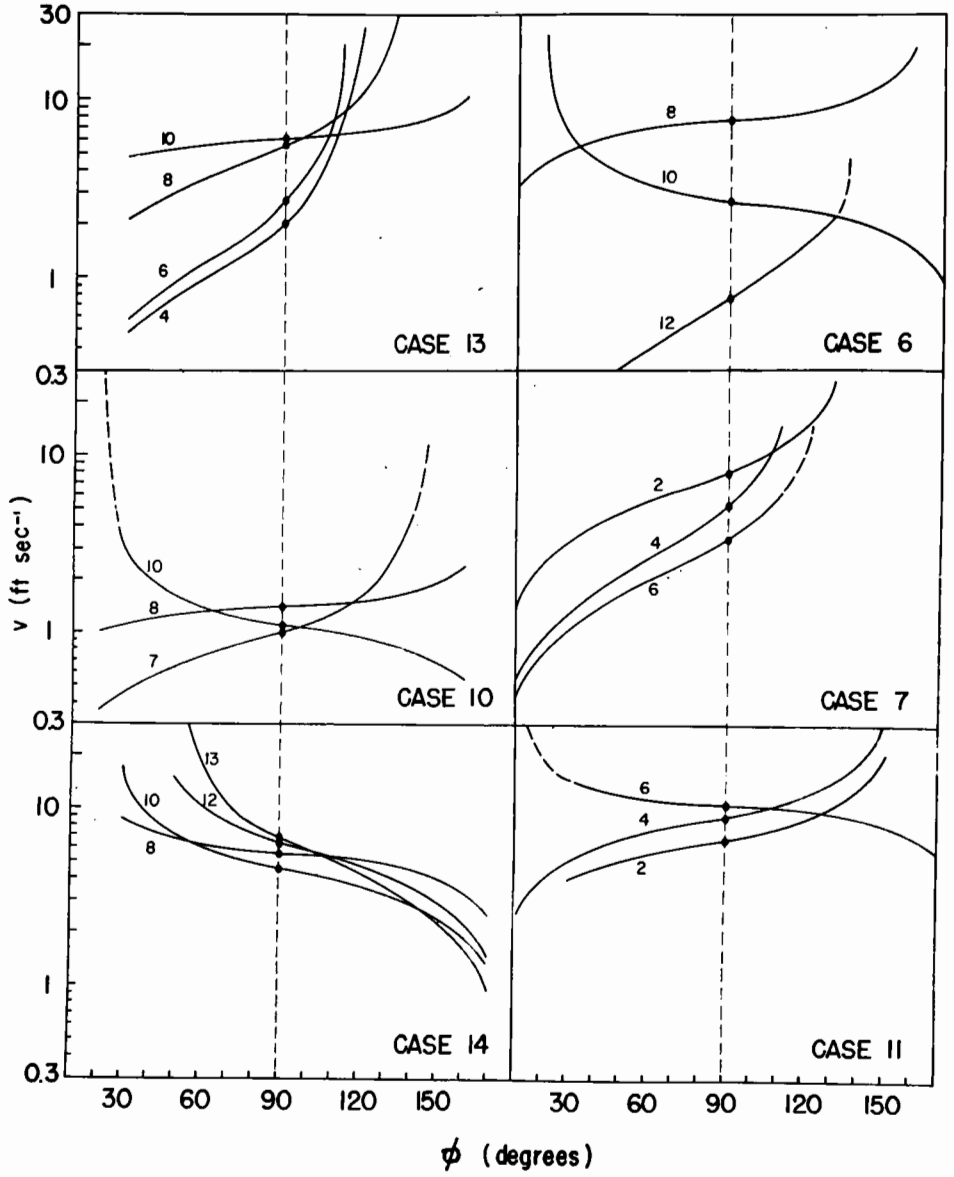

FIG. 15. The effect of orientation of a line of generating elements upon the apparent terminal speed as measured by trail slope. A terminal speed v', measured with the assumption that ϕ 90 (full circles) may be due to a true speed v coupled with an orientation ϕ. Curves show v as a function of ϕ for 6 cases. Numbers on curves indicate heights (thousands of feet) at which trail slope measured.

at the 4 and 6000 ft levels; in this particular case, a constant (with height) terminal speed of about 7-8 ft sec^{-1}, coupled with a line orientation of about 110°, might reasonably be inferred. In case #10 a fall speed invariant with height is most likely in the range of ϕ from about 80° to 100°, but other values of ϕ may be found for which v increases or decreases with height.

The calculated terminal speeds, listed in Appendix C show in some cases a very marked variation with height, but the curves of fig. 15 suggest that discrepancies between the assumed and the true orientations of line arrays may be responsible for these apparent variations. Of course the terminal speed may indeed vary with distance fallen, but in the absence of information regarding the line orientation, it is not possible to determine the true variation from the height/time records.

Fig. 15 shows the wide variation possible in terminal speed due to orientation. An attempt was made to study the effect of orientation upon the frequency distribution of fall speed shown in the histogram, fig. 13. An approximately Gaussian distribution of terminal speeds was used as the starting point (fig. 16a), and orientations ϕ, in 10° intervals from 30° to 150° (roughly the range observed by Langleben, 1956) were assumed equally likely. Using a set of randomly-chosen values of ϕ within this range as true orientations, values of the error ratio v/v' were determined from the curves of fig. 15; applying 3 such sets

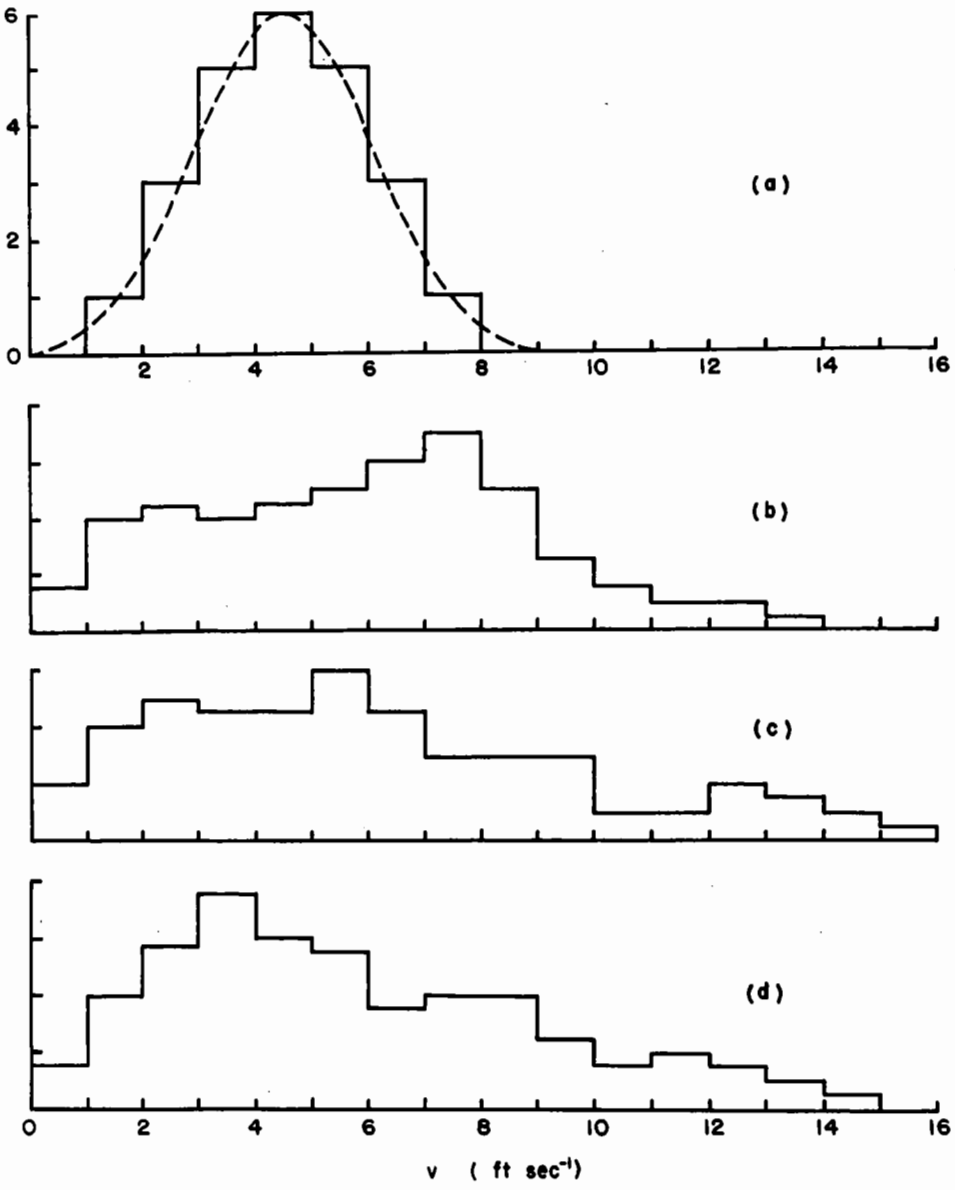

FIG. 16. Effect of discrepancies between true and assumed orientation upon the spread of a distribution of terminal speeds. (a) Assumed original distribution. As the result of random selections of ϕ, the original distribution became broadened in the manner of (b), (c) and (d). Note the resemblance of (c) and (d) to Fig. 13.

of random errors to the assumed (Gaussian) distribution yielded the 3 histograms of fig. 16b,c,d. Note the resemblance of (c) and (d) to the observed distribution of fig. 13. Clearly, the introduction of a random distribution of orientation serves to increase, about two-fold, the range of terminal speeds. Thus, the observed range up to about 12 ft sec^{-1} should probably extend only to about 6 ft sec^{-1}, which is within the range of directly measured speeds of aggregate snowflakes.

Determinations of the G/L must also be affected by the orientation factor, but an estimate of the error involved is all but impossible. However, the range of possible G/L's is usually restricted, since the level cannot be lower than the highest observed echo; other clues are occasionally furnished by careful inspection of the radar record. Furthermore, the relation between G/L and frontal surface, deduced by the present technique, agrees very well with the relation found earlier (Gunn et al, 1954) by analysis of range/height records, which are unaffected by any assumptions regarding orientation.

10. STALACTITES.

Prior to the onset of snow on the ground, radar usually detects echo aloft which lowers gradually with time. On occasions the lower edge of this echo shows a serrated structure, with numerous pendulous extensions protruding downward (fig. 1c); these resemble the mammatus-type pouches sometimes observed on the lower surfaces of overhanging cumulonimbus. These protuberances have been given

the name "stalactites".

Through January, February and March, 1954, there were 18 occasions on which echoes aloft were observed at or very near the time of a radiosonde ascent. Of these, there were 6 occurrences of sharply defined stalactites, 9 non-occurrences, and 3 doubtful cases (i.e. with only slight indecisive protrusions). The mean relative humidity with respect to ice, within the layer from ground to echo base, was determined for each case, using the Maniwaki radiosonde data. For the appearances of stalactites, these humidities ranged from 35 to 71%, with a mean of 58%; for the non-occurrences they varied from 52 to 102%, with a mean of 89%. The occurrences of stalactites are therefore associated with the presence of dry air in the lower levels, into which snow is falling from aloft and in which evaporation occurs.

Consider a moist air mass overlying a dry one, with a transition zone through which the moisture content decreases downward (fig. 17), and let snow fall from the upper into the lower air mass. Evaporational cooling will be zero at the top of the transition layer (A) and again at some lower level (B) to which the snow has just penetrated, and a maximum at some intermediate level (C). If evaporation occurs rapidly enough, a steep lapse of temperature will be established in the layer BC, in which there will develop a tendency for overturning.

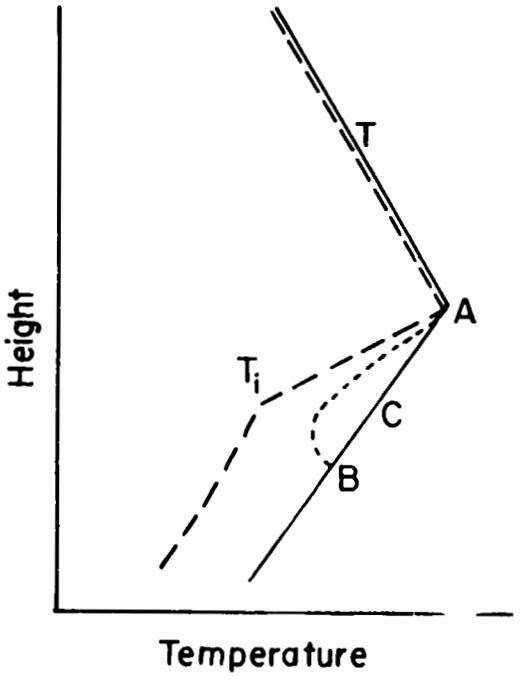

FIG. 17.

Schematic temperature (T) and ice-bulb (T_i) distributions, with height, corresponding to a saturated air mass overlying a dry one. The dotted curve indicates the temperature structure, modified by evaporational chilling, when snow has reached B.

The concept of overturning is more familiarly associated with the development of convection in a layer due to strong heating from below, leading to the formation of thermal updrafts. The instability in a thin stratum of surface air breaks down into a series of vertical jet-like thermals (which may become visible as cumulus if the condensation level is reached); each thermal is fed by the convergent flow, into its base, of the superheated surface air from some distance around. Thus, thin "disks" of warm air are converted into vertical columns or chimneys, topped at the level where the warmest surface air reaches hydrostatic equilibrium with the environment. In the case of the chilled air with which stalactites are associated, the breakdown of the unstable layer BC

(fig. 17) might be expected to result in vertical pendants as chilled air surges downward, each pendant being fed by the horizontal inflow, into its top, of cold snow-filled air. An essential difference between an ordinary snow trail and a stalactite is that, while the former consists only of small particles, possessing little inertia, the latter consists of a substantial mass of air, filled with snow, which not only possesses considerable inertia but must in addition displace the environment through which it descends; in this respect the stalactite resembles a growing cumulus. Deformation of a stalactite (or of a cumulus) in the wind field will not be as pronounced as that of the simple snow trail. Furthermore, the "generating level" from which the stalactite evolves may reasonably be expected to be the level of the chilled air from which descent occurs. Thus, it does not seem necessary to postulate a new snow generating level in order to explain the near-verticality of the pendants, as has been suggested by Atlas (1956).

So long as snow remains within, or continues to fall into, a parcel of air, chilling and descent will proceed until the parcel has become saturated; the descent of the air is dependent upon its initial moisture content and the ambient lapse rate. Such evaporational chilling and descent, which depletes the snow content, is analogous to the cooling, subsidence and dissipation of cloud through radiation, as discussed by Hewson (1948). By reasoning along these lines, one

can deduce the maximum depth to which a chilled snow-filled parcel will descend. This depth, computed for 3 well-defined occurrences of stalactites, was compared with the maximum depth observed. The results (Table 1) suggest that simple computation (made by tephigram in these cases) tends to overestimate the depth, but that the magnitude is of the right order. Since overturning likely begins before the complete maximum chilling is achieved, and probably continues in "surges" as further evaporation occurs, the overestimate by tephigram of the stalactite depth is not inconsistent with the above mechanism. Compensatory upward motion in the dry but unchilled air will occur, and may be sufficient to produce cloud in which snow growth or regeneration would occur; however, in view of the dryness of this air and the probably small upward compensation, saturation of this air would seem difficult to achieve, and may perhaps be possible only under certain particular conditions. In any case, the above considerations suggest that a purely evaporative stalactite mechanism may exist in which no secondary snow generation need occur.

Table 1: Vertical Extent of Stalactites.

Date	Measured (ft)	From tephigram (ft)	Mean R.H. (ice)
3/1/54	2000	4000	71%
30/1/54	500	1000	61%
16/2/54	4000	4000	35%

11. PATTERNLESS PRECIPITATION.

Much of the snowfall observed was associated with distinctive cell-and-trail pattern aloft (such as is shown in fig. 1a), though at the lower levels the patterns from adjacent trails merged into a more or less homogeneous type of echo. This type of pattern was observed during about 2/3 of the hours of snowfall in January-February 1954. During the remaining 1/3 of the snowfall there was a notable lack of pattern aloft, the echo being rather homogeneous and featureless (fig. 1b). Tops of this echo were fairly smooth and tended to lower gradually with time toward the end of the storms, although at times faint vestiges of pattern emerged from the upper surface, rather as if the echo was fed from aloft by weak trails which were themselves undetectable.

The pattern characteristics of 14 complete storms are shown in fig. 18. Of these storms, 5 remained patterned and 3 unpatterned throughout; the remaining 6 consisted of a patterned phase followed by an unpatterned one. In no case did the storm begin unpatterned and change to a patterned one. Pattern appeared to be more closely associated with warm than with cold fronts, and with southwesterly flow aloft at 700 mb. In general, a lowering of the echo top occurred with time toward the end of the storm, accompanied by a diminishing precipitation rate. This lowering trend was noted in 9 of the 14 storms (indicated by "L", fig. 18); of these 9 cases, 7 were associated with unpatterned echo.

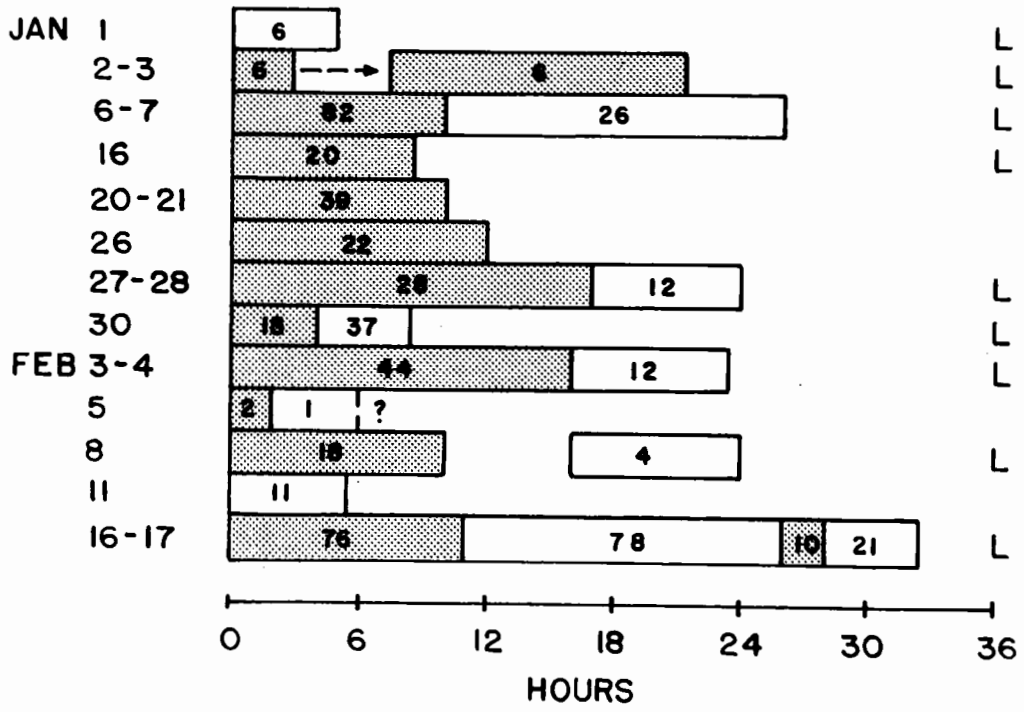

FIG. 18. Radar-pattern characteristics of 14 storms, January-February 1954, showing the durations of patterned (shaded) and of unpatterned (unshaded) precipitation. Numbers indicate the associated total snowfall (10^{-2} in melted); storms with a lowering trend of echo top are indicated by the symbol L.

Measurements indicate a settling rate of the echo top of about 10 cm sec^{-1}, which is somewhat lower than the terminal speeds of dendrites and small needles (20-30 cm sec^{-1}, according to Nakaya, 1954); furthermore, the rate of descent of a trail is usually greater than the terminal speed of the constituent particles. Thus, it is difficult to explain descent of this echo top on the basis of simple trail theory.

If, toward the end of a patterned storm, the cells become progressively weaker, successive trails will be detectable at successively lower levels; this effect would appear first as a progressive cutting-off of consecutive trail tops at lower and lower heights until that height is reached at which adjacent trails merge, when it would result in a gradual lowering of the top of the relatively homogeneous low-level echo. On the other hand, unpatterned precipitation may be the result of non-cellular snow growth. In Part II, a type of convective mechanism is suggested, the result of crystal growth in air in which there exists a substantial vapor excess over ice equilibrium. If only a very slight excess is present, such cellular development would not be expected; rather, one might look for a more homogeneous continuous type of snow growth at vapor contents just slightly above ice equilibrium, probably associated with an extensive but rather slow upward motion of the air mass. In general, the air below the generating level is moving back relative to the cells and trails, and so may experience a

prolonged trajectory through falling snow. By the time this air reaches the last few snow trails its vapor content will have been reduced to ice equilibrium, or very nearly so. Within such ice-filled air, a slight general vertical motion would result in slow crystal growth at a vapor density just above the ice equilibrium value, occurring more or less uniformly throughout the lowest air mass. Thus, the unpatterned echo, observed during the last 1/3 of many of the storms, may be an indication of a non-cellular snow-growing process.

More recent data, obtained from radar records of the CPS-9 at Montreal and reduced to CAPI form (Langleben 1957) are revealing the echo structure in greater detail at all heights and within a 75 mile radius. This presentation reveals, for example, the occasional simultaneous occurrence of cell-and-trail pattern along with patternless echo. Some cases are found in which abrupt transitions from patterned to unpatterned echo occur within the operating range of the equipment. Certainly this new CAPI presentation has indicated that echoes within one storm may be of several types, and may change type abruptly, so that any generalization based upon the limited height/time data would be dangerous. However, these more recent data confirm that local cellular generation is by no means the only process of snow formation, and that another process (or perhaps some suitable modification of the cell mechanism) must be sought to account for the occurrence of unpatterned precipitation,

either alone or in conjunction with the cellular process, even at high levels.

12. SUMMARY AND CONCLUSIONS.

Records from the zenith-pointing radar, displayed on height/time coordinates, reveal the presence, on numerous occasions, of small discrete snow generating units from which the snow falls in a trail which is shaped by the wind field. These records are conveniently interpreted by deriving the plan-trajectory of the falling precipitation, using simple geometrical principles. Winds aloft, available at Maniwaki, must at times be modified to conform to the frontal structure over Montreal, which structure is deduced from appropriate radiosonde data in conjunction with frontal contour analyses, prepared independently at the Central Analysis Office, Montreal.

Fourteen cases of generating cells were examined, each at a time corresponding to that of a radiosonde ascent and each case at least 12 hours removed from any other one. Since, with a zenith-pointing radar, the cell itself is often undetected, the height of the cell was deduced from considerations of trail geometry, involving a fitting of the derived pattern with that actually observed. These generating levels were found to lie at heights ranging from 8 to 20 thousand feet, at temperatures from -3 to -33C; two-thirds of the cells examined were at temperatures between -10 and -25C. Thus there appears to be no particularly favored temperature or height for the cells.

As in the previous study of Gunn et al (1954), it was found that snow generation tends to occur just above a frontal surface; the specific frontal surface involved was, in most cases (including the 10 cases of 1952 data) the Maritime front (separating mP air from mA). The frequencies with which the G/L was located in the various possible air masses are shown in Table 2.

Table 2: Frequency of G/L by Air Masses

Air mass	Number of Cases 1954 data	1952 data	Total
mT	3	2	5
mP	8	8	16
mA	3	0	3
cA	0	0	0

Considering both the present (1954) and the earlier (1952) data together, generation occurred twice as frequently in mP air as in all the other air masses combined. Even though the Maritime front and the mP air mass appear more frequently than the others, the probability of the G/L being contained within the mP air mass is almost double that for any of the other air masses. In about 2/3 of the cases, the G/L was located within the lowest quarter of the parent air mass. The air in which the cells were

located was stable in all but 3 of the 14 cases, in agreement with the earlier findings.

Terminal speeds of the precipitation particles were determined by fitting the geometrically-derived pattern to the observed one, and by measuring the slope of the trail at various levels; there was general agreement between the speeds derived by these two methods. Speeds as high as 12 ft sec^{-1} were measured; various corrections were applied, allowing for the effects of density and viscosity, radar sensitivity and the sorting of particles in the wind shear, and the effect of vertical motion of the generating source. A further source of error, and the most serious one, lies in the unknown alignment of generating line arrays which, in the present study, were assumed to lie normal to the direction of motion. That this assumption is usually invalid is indicated by recent studies of CAPI records which reveal clearly the oblique orientation of line arrays at the G/L. For lack of knowledge regarding the orientation, it is impossible to correct the terminal speeds derived in this study. However, an estimate was made of the scatter thus introduced into the results, and it appears that the actual range of terminal speeds extends from about 1 to 6 ft sec^{-1}; thus most of the speeds are appropriate to aggregate snowflakes, confirming the earlier findings of Langleben (1954) and reinforcing the notion that the generating cells themselves are regions of aggregation.

The same factor of orientation produces an uncertainty in

the determination of the G/L, which cannot be estimated. However the present results, regarding the proximity of the G/L to a frontal surface, are in good agreement with earlier results which were unaffected by this uncertainty.

The phenomenon of stalactites is impressively revealed by the zenith-pointing radar. These occur when snow falls from aloft to evaporate in a dry stratum below. The pattern is believed to be due to convective overturning itself, rather than to fresh snow-formation at a new G/L resulting from such overturning.

Precipitation echoes may be distinctly patterned, or may be patternless. About half the storms investigated showed a lack of pattern during the last few hours of snowfall, during which time the echo top gradually subsided. While this may be due to a continually decreasing intensity of cell-generated snow, it may also be due to an entirely different precipitation mechanism, involving perhaps the relatively slow growth of crystals throughout a large volume of a slowly ascending air mass at vapor densities but slightly in excess of ice equilibrium.

PART TWO

SUBLIMATION IN CLEAR AND CLOUDY AIR

PART II: SUBLIMATION IN CLEAR AND CLOUDY AIR

1. INTRODUCTION AND ACKNOWLEDGMENTS.

The radar observations reported in Part I, as well as in earlier work (e.g. Gunn et al, 1954) suggest that snow frequently originates in compact cells aloft, whose dimensions are of the order of a mile. Earlier RHI records, and more recent CAPI ones (Langleben 1956; 1957) show that the cells persist individually over periods of an hour or more, frequently occur in line arrays, and exhibit a fluidity of form which is suggestive of convective activity, even though the environment is hydrostatically stable. These localized cells (occupying but 1/10 to 1/20 of the sky) apparently provide the mechanism through which the liquid water cloud in which they are embedded is converted into precipitation elements in the form of aggregate snowflakes. One is thus led to consider the development of small convective elements in stable air, in which turbulence may be expected to promote the aggregation of ice crystals. A reasonable source of energy for such cellular elements appears to be the latent heat of sublimation of growing ice crystals; it is this source of energy, and the consequences arising therefrom, which are investigated in the following sections.

The author acknowledges the interest and assistance of Dr. W.L. Godson, whose comments and criticisms, at an early stage of this work, have proven of great value.

2. ISOBARIC SUBLIMATION.

As a first approach and in order to gain preliminary insight into the problem, the process of isobaric sublimation will be considered, first in clear air, then in cloudy air. By clear air is meant air in which no liquid water cloud is present, although there may be ice crystals present; by cloudy air is meant air which contains water cloud. The ice crystals which appear and grow within the parcel may have been introduced from external sources (perhaps having fallen from some higher level) or may have appeared as the result of freezing of cloud droplets within the parcel.

Isobaric variations of amounts of water substance (solid, liquid and vapor) are most conveniently studied by considering these amounts as mixing ratios rather than densities. Thus, r, r_L and r_s are the mixing ratios (mass of substance per unit mass of dry air) of the vapor, the liquid and the solid phases, respectively. Equilibrium values of the vapor phase over plane surfaces of water and ice are r_w and r_i, respectively, and at any specified pressure are functions of temperature only. In later sections, where non-isobaric processes are considered, it will be convenient to consider the amounts of the various phases of water substance in terms of their densities ρ, ρ_L and ρ_i.

(a) Clear Air.

Consider a parcel containing unit mass of dry air at temperature T and pressure p, and r gm water vapor (fig. 1, point A), where $r > r_{i(T)}$ (the latter being the equilibrium vapor mixing ratio over plane ice at temperature T, point B). Ice crystals introduced into such an environment will grow by virtue of the vapor excess $r-r_{i(T)}$, reducing the vapor content from r at temperature T to $r_{i(T + dT)}$ at a final temperature T + dT (point C), the temperature increase dT being due to the release of latent heat of sublimation as the ice crystals grow.

If a mass -dr gm of vapor is sublimed, an amount of heat $-L_s dr$ is released, where L_s is the latent heat of sublimation. Neglecting the heat capacities of the vapor, liquid and solid phases of the water substance*, the following equation can be derived:

$$dr/dT = -c_p/L_s \qquad (2.1)$$

where c_p = specific heat of (dry) air at constant pressure.

Referring to fig. 1,

$$r_{i(T + dT)} = r + (dr/dT)dT = r - (c_p/L_s)dT$$

and also

$$r_{i(T + dT)} = r_{i(T)} + (\partial r_i/\partial T)_p dT = r_{i(T)} + \frac{\epsilon L_s r_{i(T)}}{RT^2} dT$$

---

* The heat capacity of 1 kgm dry air is 240 cal; of saturated vapor at 1000 mb, 0C, is 1.7 cal; of 1 gm liquid water is 1 cal; of 1 gm ice is 0.49 cal. These last three represent generous upper limits in the cases to be discussed, and their sum is seen to be negligible compared to the heat capacity of the dry air component of the mixture.

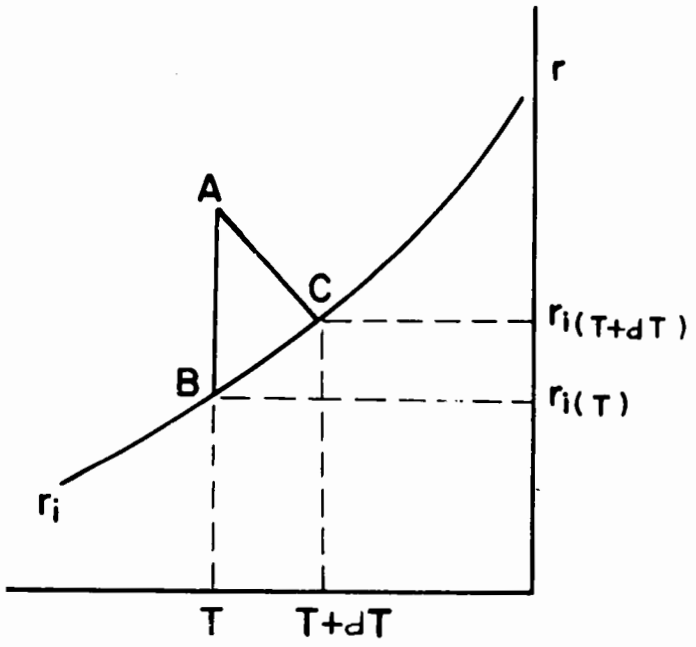

FIG. 1. Isobaric sublimation reduces vapor content to ice-equilibrium (A to C), and is accompanied by a temperature increase from T to T + dT.

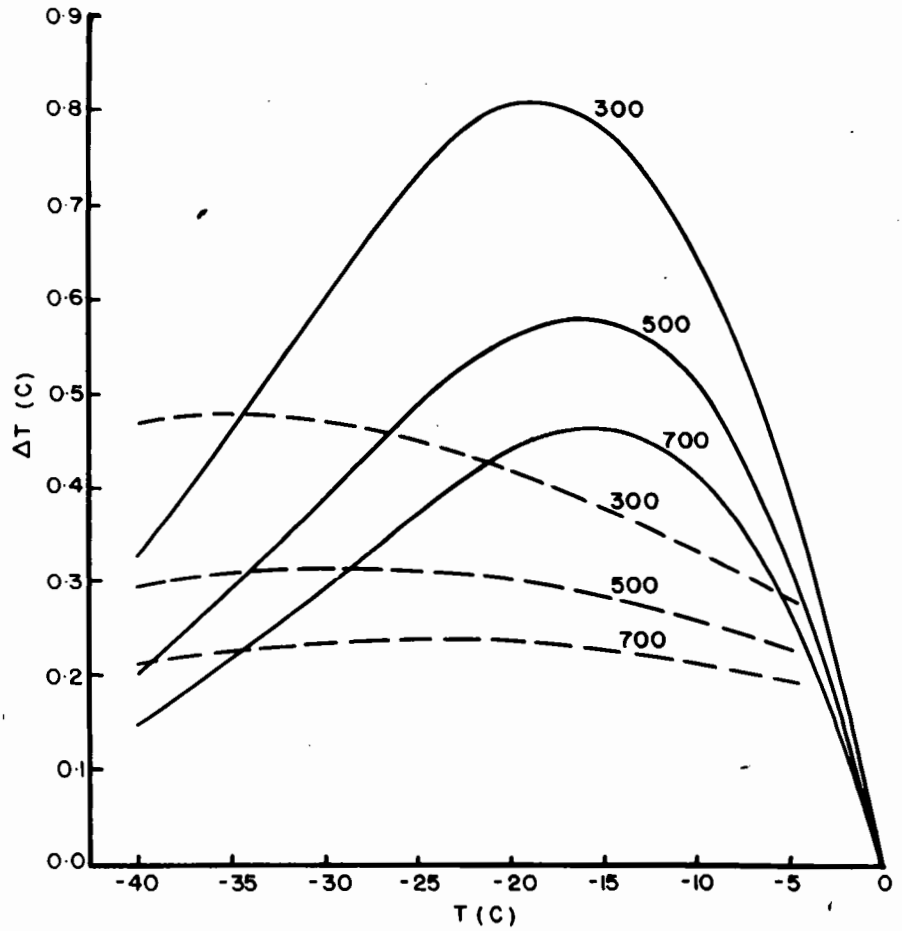

FIG. 2. Isobaric temperature increase as vapor is reduced to ice equilibrium (full curves); the ambient vapor content is taken at water equilibrium. Dashed curves show additional increase due to the presence of cloud of density 1 gm m^{-3}.

where ϵ = ratio of molecular weight of water vapor to that of dry air (=0.622) and R = gas constant for dry air. It follows then that

$$dT = \frac{L_s}{c_p} \cdot \frac{r - r_i}{1 + \frac{\epsilon L_s^2 r_i}{c_p R T^2}} \qquad (2.2)$$

(where, for brevity, $r_{i(T)}$ has been replaced by r_i; a similar abbreviation is used, with respect to r_w and to the corresponding vapor densities, in all subsequent work).

Here, dT is the isobaric temperature increase due to the release of latent heat as the sublimation process reduces the ambient vapor excess over ice equilibrium to zero; with this vapor reduction accomplished, crystal growth ceases. Eq. (2.2) is a psychrometric equation which defines the ice-bulb elevation in air supersaturated with respect to ice, and has been derived and discussed by Marshall and Langleben (1954).

As an upper limit to r, the ambient vapor content, we may take the equilibrium value $r_{w(T)}$ over a water surface. That this is a reasonable limit, both in water cloud and in clear air, is suggested by the calculations of Howell (1949) and by the observations of Dobson and Brewer (1951). Using this value, the maximum isobaric temperature increase has been computed from eq. (2.2), the results being shown in fig. 2. These curves indicate that appreciable isobaric temperature increases can result from sublimation, particularly at low pressures, and that maximum

increases occur at about -15C.

(b) Cloudy Air.

In cloudy air the initial vapor content may be assumed to be at water equilibrium, providing optimum conditions for the growth of ice crystals; this growth will reduce the vapor content, as a result of which a portion of the liquid phase will evaporate. While sublimation provides latent heat, the cloud evaporation extracts heat; the net heat released into a cloudy parcel is therefore less than in a clear one. A stage will be reached at which the water cloud has just completely evaporated, the vapor content being just at water equilibrium; from this stage, sublimation proceeds alone to complete the isobaric reduction of vapor to ice equilibrium, as described in sec. 2(a).

(i) Reduction to ice equilibrium.

Consider unit mass of air containing initially r_L gm cloud water, no ice, and r_w gm vapor, all at temperature T. Finally, the same air contains no cloud water, r_s gm ice, and $r_{i(T + dT)}$ gm vapor at ice equilibrium at temperature T + dT. The heat balance is given by

$$L_s r_s - L_v r_L = c_p dT \qquad (2.3)$$

If the total mass of water substance remains unchanged, then

$$r_L + r_w = r_s + r_{i(T + dT)}$$

i.e.
$$r_s = r_L + r_w - r_{i(T + dT)}$$
$$= r_L + r_i + (r_w - r_i) - r_{i(T + dT)}$$

$$= r_L + (r_w - r_i) - (\partial r_i / \partial T)_p \, dT$$

$$= r_L + (r_w - r_i) - \frac{\epsilon L_s r_i}{RT^2} \cdot dT \qquad (2.4)$$

Combining eqs. (2.3) and (2.4), it follows that

$$dT = \frac{L_s}{c_p} \cdot \frac{r_w - r_i}{1 + \frac{\epsilon L_s^2 r_i}{c_p R T^2}} + \frac{L_s - L_v}{c_p} \cdot \frac{r_L}{1 + \frac{\epsilon L_s^2 r_i}{c_p R T^2}} \qquad (2.5)$$

Comparing with (2.2), it is seen that

$$\frac{dT\ (\text{cloud})}{dT\ (\text{clear})} = 1 + \frac{L_s - L_v}{L_s} \cdot \frac{r_L}{r_w - r_i} \qquad (2.6)$$

Thus, the total isobaric temperature increase, when water cloud is initially present and when the vapor content is finally reduced to ice equilibrium, is equivalent to the isobaric increase in clear air increased by a fraction which is proportional to the liquid water content of the cloud initially present.

The relative contributions, to the total heating, of a vapor excess over ice equilibrium and of liquid water may be compared when, for example, $r_L = r_{w(T)} - r_{i(T)}$, i.e. when the liquid water content is equal to the maximum ambient vapor excess. Then the relative increase due to the liquid water is $(L_s - L_v)/L_s$, which is of the order of 1/8, or about 12%. Thus the reduction of a vapor excess by sublimation contributes roughly eight times as

much to the total temperature increase as does the presence of an equal amount of liquid water. The additional increase due to the presence of 1 gm liquid water is shown in fig. 2 (dashed curves); for cloud contents such as are observed in stratiform cloud (about 0.1 gm m^{-3} according to Pettit, 1954, and Lewis, 1951) this additional contribution is clearly negligible over a fairly wide range of temperature.

(ii) Reduction to water equilibrium.

Of more importance to future considerations is the case where the vapor content is reduced to water equilibrium, the liquid water cloud being just completely evaporated.

If, in unit mass of dry air a mass dr_s of ice is sublimed, while a mass dr_L of liquid water is evaporated, the heat balance is given by

$$L_s dr_s - L_v dr_L = c_p dT \tag{2.7}$$

The total mass of water substance being considered invariant, then

$$dr + dr_s - dr_L = 0 \tag{2.8}$$

If the vapor content remains at water equilibrium (i.e. $r = r_w$), then from eqs. (2.7) and (2.8) and the Clausius-Clapeyron equation, the following expression is derived for the temperature increase:

$$dT = \frac{L_s - L_v}{c_p} \frac{dr_L}{1 + \frac{\epsilon L_s L_v r_w}{c_p R T^2}} \tag{2.9}$$

Thus, the evaporation of a mass dr_L of cloud water by the sublimation-evaporation process results in a temperature increase dT defined by (2.9), the vapor content remaining at water equilibrium throughout. The same result can be derived by first evaporating completely the water cloud and then reducing the resulting high vapor excess to water equilibrium by sublimation.

Comparison of eq. (2.9) with (2.2) shows that the reduction of a mass of <u>vapor</u> by sublimation is much more effective as a thermal source than is the reduction of a like mass of <u>cloud</u>, the ratio of the isobaric temperature increases being

$$\frac{L_s}{L_s - L_v}\left(1 + \frac{\epsilon L_s L_v r_w}{c_p R T^2}\right)\left(1 + \frac{\epsilon L_s^2 r_w}{c_p R T^2}\right)^{-1}$$

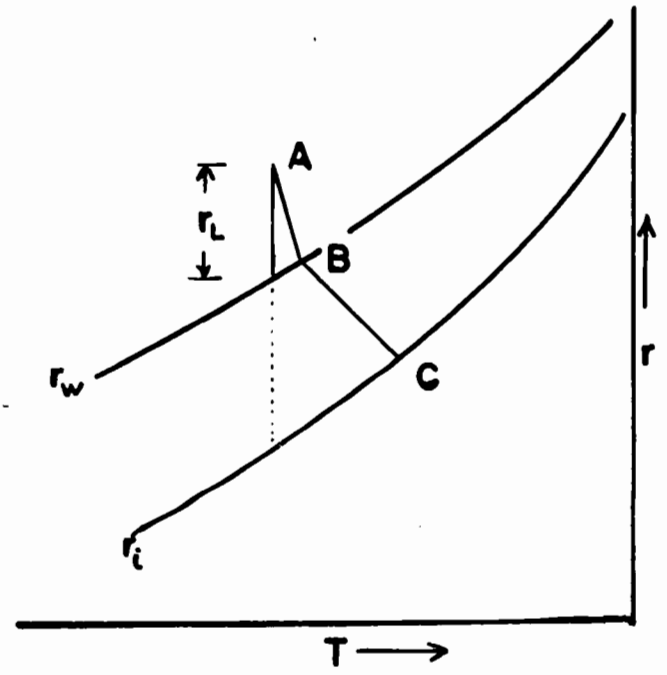

FIG. 3. Sublimational growth in cloud exhausts the water content r_L (A to B), after which the vapor content is further reduced to ice equilibrium (C). The isobaric temperature increase A to B is a small fraction of that from B to C.

values of which lie roughly between 8 and 10. This is indicated schematically in fig. 3, in which A represents the initial state of a parcel containing r gm of water-substance in the form of vapor plus liquid. Sublimational growth exhausts the water content at B (according to eq. (2.9)), then reduces the vapor content to ice equilibrium at C (according to eq. (2.2)); the temperature increase from A to B, while cloud is still present, is much less than from B to C (in clear air). Thus a vapor excess in cloud-free air is worth much more than the presence of an equivalent mass of cloud, insofar as isobaric heating is concerned.

Of more importance to later considerations, in which the effects of ice crystal growth and growth rates are examined, is the temperature increase per unit mass of vapor sublimed, in clear air and in cloudy air. From eqs. (2.7) and (2.8) the following can be derived:

$$dT = \frac{L_s - L_v}{c_p} \frac{dr_s}{1 + \frac{\epsilon L_v^2 r_w}{c_p R T^2}} \tag{2.10}$$

This equation relates the isobaric temperature increase, in cloudy air, to the mass of ice sublimed. From eqs. (2.1) and (2.10), the ratio of the temperature increase in clear to that in cloudy air, for equal masses of material sublimed, is

$$\frac{L_s}{L_s - L_v}\left[1 + \frac{\epsilon L_v^2 r_w}{c_p R T^2}\right] .$$

This ratio varies between 12 and 20 over the normal range of pressures and temperatures encountered; at 700 mb, -15C, it takes the value 12.8. Thus, the presence of water cloud constitutes a powerful inhibition to heating, the importance of which will be developed in later sections.

(c) Freezing of Water Cloud.

It may happen that the cloud water converts into the ice phase by freezing rather than by the evaporation-sublimation process. Freezing of a mass dr_L of cloud water will result in an isobaric temperature increase dT where $dT = L_f dr_L / c_p$, L_f being the latent heat of fusion. Since no vapor transition is involved, the vapor content of the air remains unaltered at the original value. Point B, fig. 4, indicates the state of the air

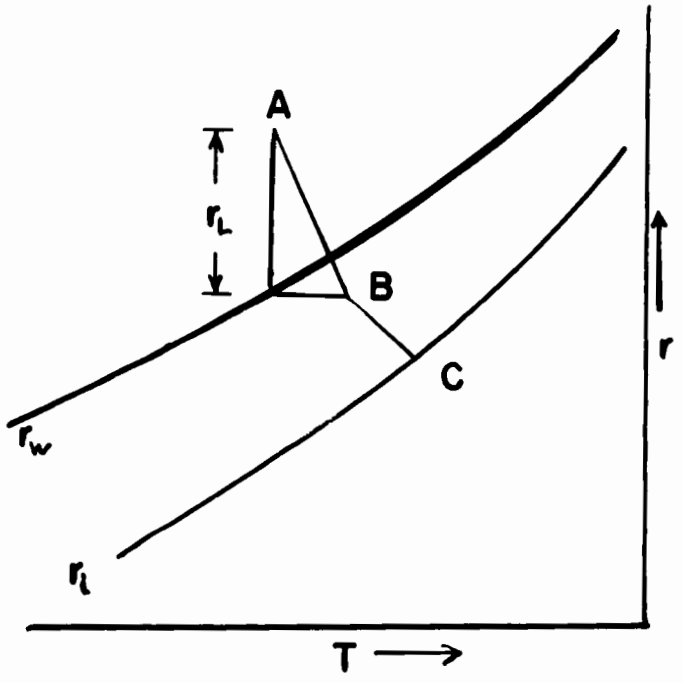

FIG. 4. Freezing of cloud content r_L increases temperature isobarically from A to B; sublimation, reducing the vapor content to ice equilibrium, produces further warming (B to C).

following the freezing. At the increased temperature T + dT the air may be either super- or under-saturated with respect to ice, depending upon whether dT is less or greater than the difference between the ambient frost and dew points. Freezing may be complete or partial.

(i) Complete freezing.

If the entire cloud mass is frozen, the air is in the state indicated by point B, fig. 4, and contains ice but no liquid cloud. Sublimation now reduces the vapor density to ice equilibrium (point C). If the initial cloud content is sufficiently great that the air, after freezing, is undersaturated with respect to ice, then sublimation of ice to vapor will establish ice equilibrium. It can be shown that the same end point (C) is reached whether the initial cloud is transformed by complete freezing or by the process of evaporation-sublimation; this follows due to the numerical equivalence of $(L_s - L_v)$ and L_f.

(ii) Partial freezing.

If only a fraction α of the initial cloud content r_L freezes, the residual liquid water is available to resaturate the warmed air; resaturation is achieved isobarically with a temperature increase given by

$$dT = \frac{L_f \alpha r_L}{c_p \left(1 + \frac{\epsilon L_v^2 r_w}{c_p R T^2}\right)} \simeq \frac{L_s - L_v}{c_p} \cdot \frac{\alpha r_L}{\left(1 + \frac{\epsilon L_v^2 r_w}{c_p R T^2}\right)} \qquad (2.11)$$

Comparison with eq. (2.10) shows that the isobaric freezing of a mass of cloud water $\propto r_L$, at water equilibrium, yields the same temperature increase as is achieved by the sublimation in cloud (also at water equilibrium) of a like mass of ice; whether the ice phase appears by freezing or by sublimation, the isobaric heating is the same.

If, following partial freezing, there is not enough residual cloud to effect complete resaturation, there results a parcel of air containing ice crystals only, slightly undersaturated with respect to water. It can be shown in this case that, following sublimation to ice equilibrium, the same final temperature is reached as would have been had the cloud been transformed into ice by the evaporation-sublimation mechanism.

Thus, whether cloud water is converted by freezing (either complete or partial) or by evaporation-sublimation, the same end points (isobaric temperature increases) are achieved both at water and ice equilibrium; the isobaric temperature increase is independent of the mode of transition of the water- to the ice-phase, and of the fraction initially frozen.

3. NON-ISOBARIC SUBLIMATION.

The foregoing sections have dealt with the complete isobaric reduction of vapor content to ice equilibrium or to water equilibrium, and with the resultant temperature increase. However a warmed parcel of air acquires buoyancy relative to the environment,

and will ascend to a new level of hydrostatic equilibrium. During ascent, further changes in the vapor content occur. In the following sections the resulting vertical development and the velocity of ascent will be discussed. It is assumed, for the present, that the atmosphere is "inactive", i.e. that there exists no general over-all vertical motion; later sections will deal with the more realistic case of the "active" environment. While the isobaric processes were conveniently studied with reference to mixing ratios, it is more convenient to consider the non-isobaric processes with reference to the corresponding densities.

(a) Clear Air.

Consider clear air in which vapor exists at water equilibrium, in which ice crystals will grow. Consider a small element of isobaric growth and heating, followed by adiabatic ascent to a new level of hydrostatic equilibrium; this ascent will be dry adiabatic since sublimation is being accounted for separately and isobarically. In terms of vapor density ρ , eq. (2.1) becomes

$$-(d\rho/dT)_p = \frac{c_p p}{RL_{sT}} + \frac{\rho}{T} \qquad (3.1)$$

whence the isobaric temperature increase dT_p accompanying the loss, by sublimation, of vapor $-d\rho$, becomes:

$$dT_p = - \frac{d\rho}{\frac{c_p p}{RL_s T} + \frac{\rho}{T}} \tag{3.2}$$

There follows dry adiabatic ascent through a height $dT_p/(\gamma_d - \gamma)$, where γ_d and γ are the dry adiabatic and ambient lapse rates, respectively; the resulting adiabatic temperature change dT_A is

$$dT_A = - \frac{\gamma_d dT_p}{\gamma_d - \gamma} = \frac{\gamma_d d\rho}{\left(\gamma_d - \gamma\right)\left(\frac{c_p p}{RL_s T} + \frac{\rho}{T}\right)} \tag{3.3}$$

The total temperature change dT is thus, from (3.2) and (3.3):

$$dT = \frac{\gamma}{\gamma_d - \gamma} \cdot \frac{d\rho}{\frac{c_p p}{RL_s T} + \frac{\rho}{T}} \tag{3.4}$$

The total change in vapor density consists of the initial isobaric reduction $(d\rho)_p$ plus the change $(d\rho)_A$ associated with the dry adiabatic ascent; the latter is given by:

$$(d\rho)_A = \left(\frac{c_p}{R} - 1\right)\frac{\rho}{T} \cdot dT_A \tag{3.5}$$

and so the total change $d\rho$ is

$$\begin{aligned} d\rho &= (d\rho)_p + (d\rho)_A \\ &= \left[1 + \left(\frac{c_p}{R} - 1\right) \frac{\gamma_d}{\left(\gamma_d - \gamma\right)\left(\frac{c_p p}{RL_s T} + \frac{\rho}{T}\right)}\right](d\rho)_p \end{aligned} \tag{3.6}$$

Thus, the total rate of change of vapor content with temperature can be expressed, by combining (3.4) and (3.6), by the equation:

$$\frac{d\rho}{dT} = \frac{c_p p}{RL_s T}\left(\frac{\gamma_d}{\gamma} - 1\right) + \left(\frac{c_p}{R} \cdot \frac{\gamma_d}{\gamma} - 1\right)\frac{\rho}{T} \qquad (3.7)$$

This differential equation expresses vapor content as a function of temperature, in a parcel of air within which sublimation is occurring and as a result of which buoyant ascent is occurring.

Fig. 5 applies eq. (3.7) and its algebraic solution to a parcel in which the initial vapor density lies midway between ice and water equilibrium at temperature -15C and pressure 700 mb (point A). Lines of equilibrium vapor density over ice and water are shown, and lines of constant height-of-rise slant downward from left to right.

If the sublimation were to proceed isobarically, the state of the parcel would proceed along line AC. In an isothermal environment, the condition of the parcel is specified by AB. Paths to the left of AB are for environments in which the temperatures decrease with height at rates of 4, 6, 7 and 8 deg km^{-1}. For lapse rates such as those with which snow generating cells are observed (Part I) the total reductions in vapor density are seen to be several times the initial excess over ice equilibrium.

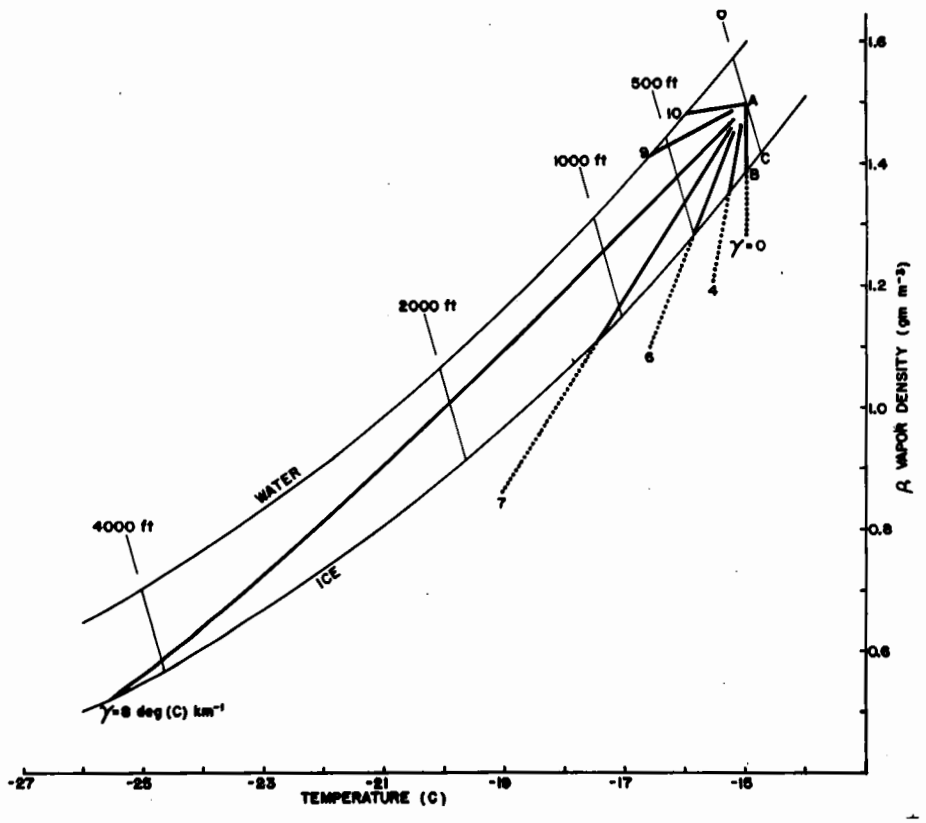

FIG. 5. The heavy lines radiating from A show the variation of vapor density within a parcel in which sublimation is occurring, for various environmental lapse rates. Ascent occurs until the vapor is reduced to ice equilibrium; heights of rise are indicated by the labelled lines. Initial pressure is 700 mb, temperature -15C, and the initial vapor content midway between ice and water equilibrium.

(i) Height of ascent.

Ascent of the parcel occurs only as long as sublimation continues, i.e. until the vapor content is reduced to ice equilibrium. From fig. 5 it is clear that, even in an isothermal environment, some slight vertical development is possible, of the order of a few hundred feet. In the more normal environment in which generating cells occur, vertical development of the order of several thousands of feet (comparable to the observed vertical extent of cells) becomes possible. If the ambient lapse rate is such that $d\rho/dT \leqq d\rho_i/dT$, then there is no intersection of the parcel path with the ice equilibrium curve and no limit to the vertical development; this occurs when $\gamma \geqq \gamma_i^*$.

(ii) Saturation and formation of water cloud.

Inspection of fig. 5 reveals that, for a sufficiently high lapse rate (e.g. 0.9 deg km^{-1}) the vapor content of the parcel approaches water equilibrium, so that continued ascent leads to supersaturation and the formation of water cloud. Thus, a critical lapse rate exists which, if exceeded, leads to the (water) saturation of a parcel which (as in the example of fig.5)

---

* The critical lapse rate for which $d\rho/dT = d\rho_i/dT$ is precisely γ_i only when $\rho = \rho_i$; in the present study, $\rho_w > \rho > \rho_i$, under which circumstances the critical lapse rate equals γ_i within a few percent.

may have been initially undersaturated. This critical lapse rate (γ_k) is that for which d ρ /dT (within the parcel) equals d ρ_w/dT; from eq. (3.7) and the Clausius-Clapeyron equation, it follows that

$$\gamma_k/\gamma_d = \left[1 + (L_s r_w/RT)\right] \Big/ \left[1 + (\epsilon L_s L_v r_w/c_p RT^2)\right] \quad (3.8)$$

Thus, if $\gamma < \gamma_k$, the vapor density within the parcel departs more and more (with ascent) from water equilibrium; but if $\gamma > \gamma_k$ then saturation, and cloud formation, is to be expected. From inspection of γ_k and γ_w, it is seen that $\gamma_k < \gamma_w$, though the difference is small; nevertheless there exists a narrow range of stable lapse rates within which sublimational growth, in a parcel initially undersaturated with respect to water, can lead to saturation and the formation of water cloud.

If the ambient lapse rate exceeds γ_w then, with saturation of the parcel, a condition of absolute instability is present. If sublimation ceases once saturation is achieved, water cloud will continue to thicken due to the continuing instability. If sublimation continues, however, the ensuing processes will be complicated in that the various rates of sublimation and condensation will be involved.

(iii) Conditional instability.

The classical concept of hydrostatic instability rests upon the behaviour of a parcel following a mechanical

impulse. Instability exists, and is realized, if following an initial vertical displacement the parcel accelerates, continuing to move away from its origin; stability is present if the parcel decelerates and returns to its initial position. Environmental conditions favorable for instability depend upon the process by which the parcel-density changes during ascent, i.e. whether the parcel is dry or saturated. Conditional instability exists when the ambient lapse rate lies between the dry and the saturated adiabatic values; then a parcel, forced aloft beyond the lifting condensation level (at which cloud forms) to the level of free convection will be accelerated vertically, the water content increasing continually. But whatever the nature of instability, whether absolute or conditional, the classical concept requires that a mechanical impulse be applied for its realization.

It is evident from the preceding section that a special type of conditional instability exists which does <u>not</u> require mechanical lifting for realization. For in a conditionally unstable environment, $\gamma > \gamma_k$; if the vapor content lies between ice and water equilibrium, the air, while "dry" in the classical sense, can be made to yield water cloud through the introduction of ice crystals, and absolute instability will arise. The possibility of such a stratum of air being "activated" through the introduction of ice crystals (perhaps falling into the layer from higher cirrus) is one which must be considered by the synoptic analyst. Due to

dynamic ascent of an air mass the vertical temperature and humidity structure may be altered in such a way as to produce this particular type of instability; while further ascent would lead ultimately to the realization of instability, the ice crystal mechanism may trigger off cloud formation at a somewhat earlier time. Large scale dynamic ascent complicates the process, however, as will be discussed in sec. 6; suffice it to say here that the effect of large-scale ascent is to reduce the critical lapse rate beyond which water cloud can form.

(b) Cloudy Air.

If the parcel contains water cloud (and vapor at water equilibrium), the sublimational removal of vapor is accompanied by cloud evaporation as equilibrium is maintained. Evaporation reduces the net heating (sec. 2(b)); further, as the temperature changes during ascent, the equilibrium vapor density changes. If ρ is the density of vapor plus liquid, then the variation of ρ within the parcel is specified by the following equation (analogous to eq. (3.7) for clear air):

$$\frac{d\rho}{dT} = \frac{c_p p}{(L_s-L_v)RT}\left(\frac{\gamma_d}{\gamma} - 1\right) + \frac{\rho}{T}\left(\frac{c_p}{R}\cdot\frac{\gamma_d}{\gamma} - 1\right) - \frac{L_v}{L_s-L_v}\left[\frac{d\rho_w}{dT} - \frac{\rho_w}{T}\left(\frac{c_p\gamma_d}{R\gamma} - 1\right)\right] \qquad (3.9)$$

The variation of ρ with T is plotted in fig. 6 for various lapse rates in an environment at 700 mb, -15C; the initial value of the ordinate, at A, includes 0.1 gm m^{-3} of water cloud. The intersections of the paths with the water equilibrium curve indicate the temperatures

(and heights) at which the cloud is completely consumed. At these points, the air, although saturated, is cloud-free, and further sublimation reduces the vapor content in the manner described in sec. 3a; the portions of the paths below the water equilibrium curve of fig. 6 indicate the variations within the cloud-free parcel according to eq. (3.7).

For stable lapse rates, slopes of the paths above the water equilibrium curve are greater than of those below; thus, in such stable air, the cloud content is much less effective than vapor alone in contributing to ascent. The ultimate heights reached at ice equilibrium are evidently scarcely affected by the initial presence of water cloud of any reasonable density. Water cloud becomes more effective, however, as the ambient lapse rate steepens, equal masses of cloud and of vapor become more equally effective, and before the (water) adiabatic lapse rate is reached sublimation is actually increasing the cloud water content.

From figs. 5 and 6 it is clear that each gram of vapor in excess of ice equilibrium initially present yields several grams of snow; however the corresponding amplification in yield from water cloud is negligible.

(i) Depletion of water cloud.

It has been shown (eq. (2.9)) that an isobaric temperature increase dT_p results, in cloudy air, from the isobaric conversion to ice of $(dr_L)_p$ gm cloud water, where

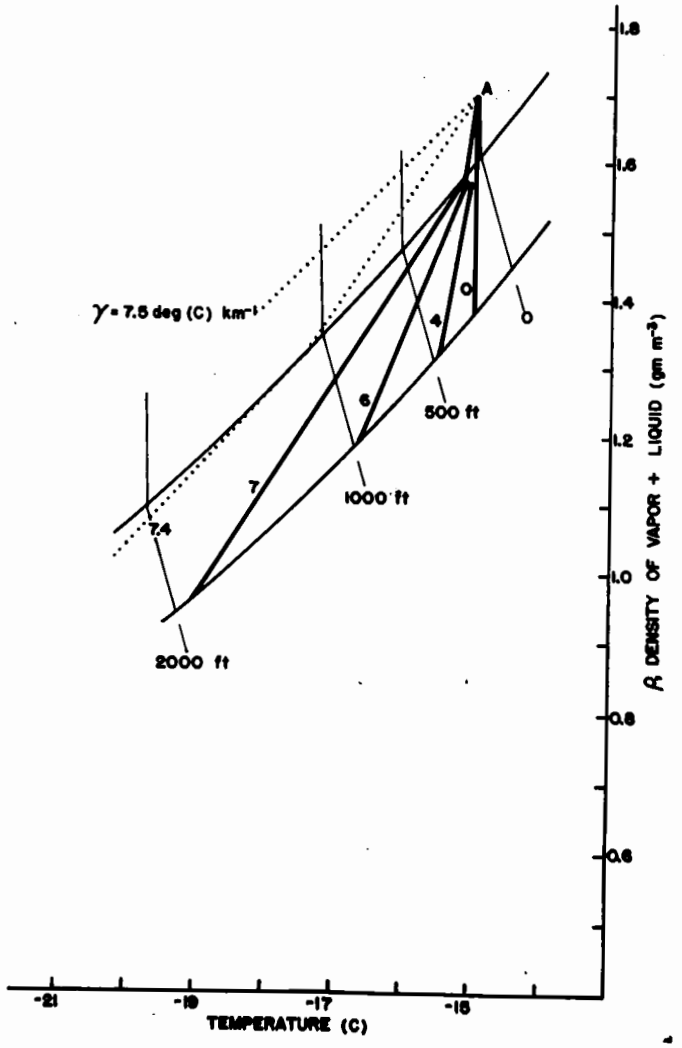

FIG. 6. As in Fig. 5, the lines radiating from A are paths followed by a parcel in which sublimation or freezing is occurring, for various environmental lapse rates. The initial value of the ordinate at A includes 0.1 gm m^{-3} of water cloud. Initial pressure and temperature, 700 mb and -15C. With stable lapse rates, cloud content is depleted, but with lapse rates in excess of about 7.5 deg km^{-1} the cloud content increases.

$$(dr_L)_p = - \frac{c_p}{L_s - L_v}\left(1 + \frac{\epsilon L_s L_v r_w}{c_p RT^2}\right) dT_p \qquad (3.10)$$

Subsequent buoyant rise of the parcel involves adiabatic cooling dT_A and the replacement of cloud water, which can be accounted for by considering the buoyant ascent via the saturated (water) adiabat; i.e. the parcel ascends (saturated) adiabatically through the vertical distance $dz = dT_p/(\gamma_w - \gamma)$. During this ascent, the cloud water content is increased by

$$(dr_L)_A = c_p dT_A/L_v - (RT/L_v)(dp/p). \qquad (3.11)$$

But $dT_A = -\gamma_w dT_p/(\gamma_w - \gamma)$; $dp/p = -(c_p \gamma_d/RT)dz$; and $dz = dT_p/(\gamma_w - \gamma)$; whence eq. (3.11) becomes

$$(dr_L)_A = \frac{c_p}{L_v}\left[\frac{\gamma_d - \gamma_w}{\gamma_w - \gamma}\right] dT_p \qquad (3.12)$$

The net rate of increase of cloud water content with height is therefore

$$dr_L/dz = - \frac{c_p}{L_v}\left[\frac{L_v}{L_s - L_v}(\gamma_w - \gamma)\left(1 + \frac{\epsilon L_s L_v r_w}{c_p RT^2}\right) - (\gamma_d - \gamma_w)\right] \qquad (3.13)$$

The liquid water content may increase or decrease with height depending upon the magnitude of γ ; the critical value of lapse rate for which the water content remains invariant with height is found by setting (3.13) equal to zero, from which it is found that the critical lapse is equal to γ_k, as defined by (3.8). The same result can be obtained by setting (3.9) equal to $\frac{d\rho_w}{dT}$.

Thus, if $\gamma < \gamma_k$, the liquid water is consumed, an initial water content dr_L being depleted within a height interval dz defined by (3.13); the rapidity with which this consumption is accomplished depends of course upon the growth rate and number of the ice crystals. Calculation based upon eq. (3.13), and examination of fig. 6, indicates the relatively small heights within which cloud is consumed. Even with a lapse rate as high as 7.5 deg km^{-1} (about 98% of the saturated adiabatic value), cloud with a density as high as 1 gm m^{-3} is exhausted within about 400 m; stratiform cloud of more usual rather lower densities will be depleted within a few tens of meters.

(ii) Height of ascent.

It is clear from fig. 6 and from the foregoing paragraphs that the cloud content will be depleted within a relatively small height interval. Once the cloud water is exhausted, the parcel is free to ascend cloudlessly until the vapor content is reduced to ice equilibrium, as discussed in sec. 3(a). From figs. 5 and 6 it is apparent that the initial presence of cloud - even of rather substantial liquid water content - contributes relatively little to the total vertical development; presence of stratiform cloud of the densities usually observed can therefore be ignored, insofar as its contribution to vertical development is concerned.

4. PROCESSES ON THE TEPHIGRAM.

Some of the concepts discussed in the foregoing sections can be applied readily by the synoptic meteorologist, by reference to the tephigram. It is useful, for example, to recognize ice-supersaturation, to determine the extent of vertical development, and to determine the possibility of condensation in a conditionally unstable environment. The following sections relate some of the earlier findings to the tephigram, or whatever thermodynamic chart is in use.

(a) Ice Supersaturation.

It is current practise to report and to plot the humidity data on the tephigram in terms of the dew point. At any temperature a specific dew point exists which, if exceeded, indicates ice-supersaturation. This critical dew point can easily be determined from standard tables of equilibrium vapor pressure or density (e.g. Smithsonian Meteorological Tables). A rough but useful rule (see e.g. Appleman 1954) may be stated thus: ice supersaturation exists when the difference (in deg C) between the dry bulb and the dew point temperatures is less than one-eighth the dry bulb temperature itself (also in deg C). For example, if the dry bulb is -16C, and if the dew point is lower by less than 2 degrees, then supersaturation exists with respect to ice.

(b) Variation of T_i; Vertical Development.

It can be shown, on the basis of a ρ -T diagram, that

dry adiabatic ascent of a parcel through a height Δz, cooling from T_0 to T_1 is accompanied by a reduction of ice bulb temperature from T_{i0} to T_{i1}, where $(T_{i0} - T_{i1})/\Delta z = \gamma_i$; i.e. the ice bulb temperature changes according to the saturated (ice) adiabatic lapse rate. This is precisely true only if $\rho = \rho_i$, but (in the cases under consideration, where $\rho_w > \rho > \rho_i$) it holds with sufficient accuracy (within a few percent) for the present purpose.

During the isobaric sublimation process, the ice bulb temperature remains unchanged. Therefore the total change of ice bulb temperature within the rising parcel, in which crystal growth is occurring, is at the saturated (ice) adiabatic lapse rate. Vertical development may be considered in steps (fig. 7); isobaric sublimation increases the temperature from A to A', the ice bulb temperature remaining unchanged at T_{i0}(B). Dry adiabatic ascent follows (A' to A''), during which the ice bulb temperature changes from B to B''. Further isobaric heating, adiabatic ascent, and variation of the ice bulb temperature continues until the ice bulb temperature has become equal to the dry bulb (at C); at this height, crystal growth ceases, and vertical development is halted.

(c) Variation of T_w; Condensation.

With regard to the wet bulb temperature T_w, the situation is not as straightforward, since isobaric sublimation increases the wet bulb temperature from T_{wo} to T'_{wo} (fig. 8a); if the dry bulb increases isobarically by $(\Delta T)_p$ from T_o to T'_o the wet bulb increases

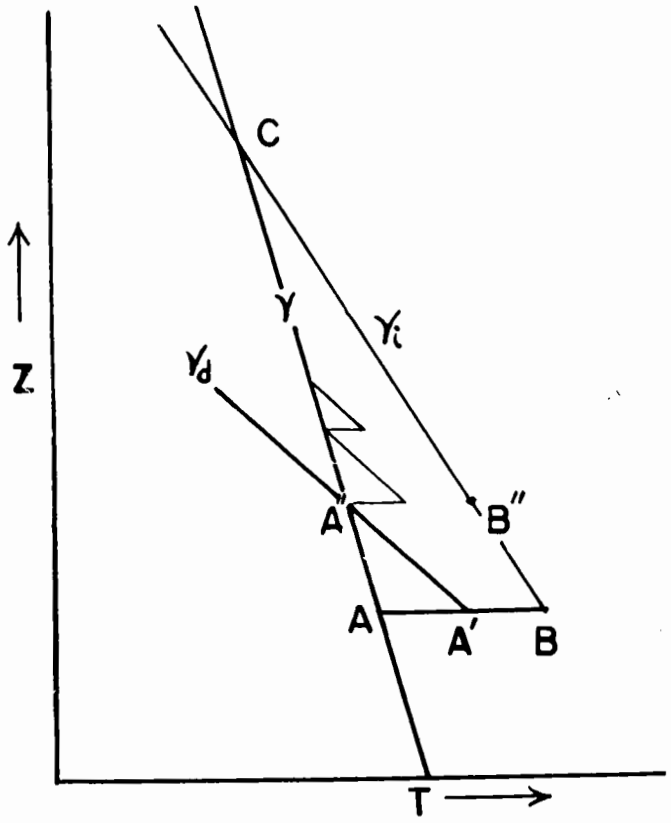

FIG. 7.

Isobaric sublimation in air at temperature A, ice bulb temperature B, increases temperature to A'; buoyant ascent reduces temperature to A'', ice bulb to B''. Further such steps carry the parcel to C, where the temperature equals the ice bulb, and crystal growth and ascent ceases.

by

$$\Delta T_w = \frac{L_s - L_v}{L_s} \frac{1}{1 + \frac{\epsilon L_v^2 r_w}{c_p R T^2}} \cdot (\Delta T)_p$$

as shown in sec. 2(b). The subsequent ascent changes the wet bulb temperature to T_{w1}, following the saturated (water) adiabatic lapse rate. The net lapse rate γ'_w of wet bulb temperature can be shown to be given by the equation:

$$\frac{\gamma'_w}{\gamma_w} = 1 - \frac{L_s - L_v}{L_v} \cdot \frac{1}{1 + \frac{L_v r_w}{RT}} \left(1 - \frac{\gamma}{\gamma_d}\right) \qquad (4.1)$$

Thus, $\gamma'_w < \gamma_w$, and is dependent upon the ambient lapse rate γ.

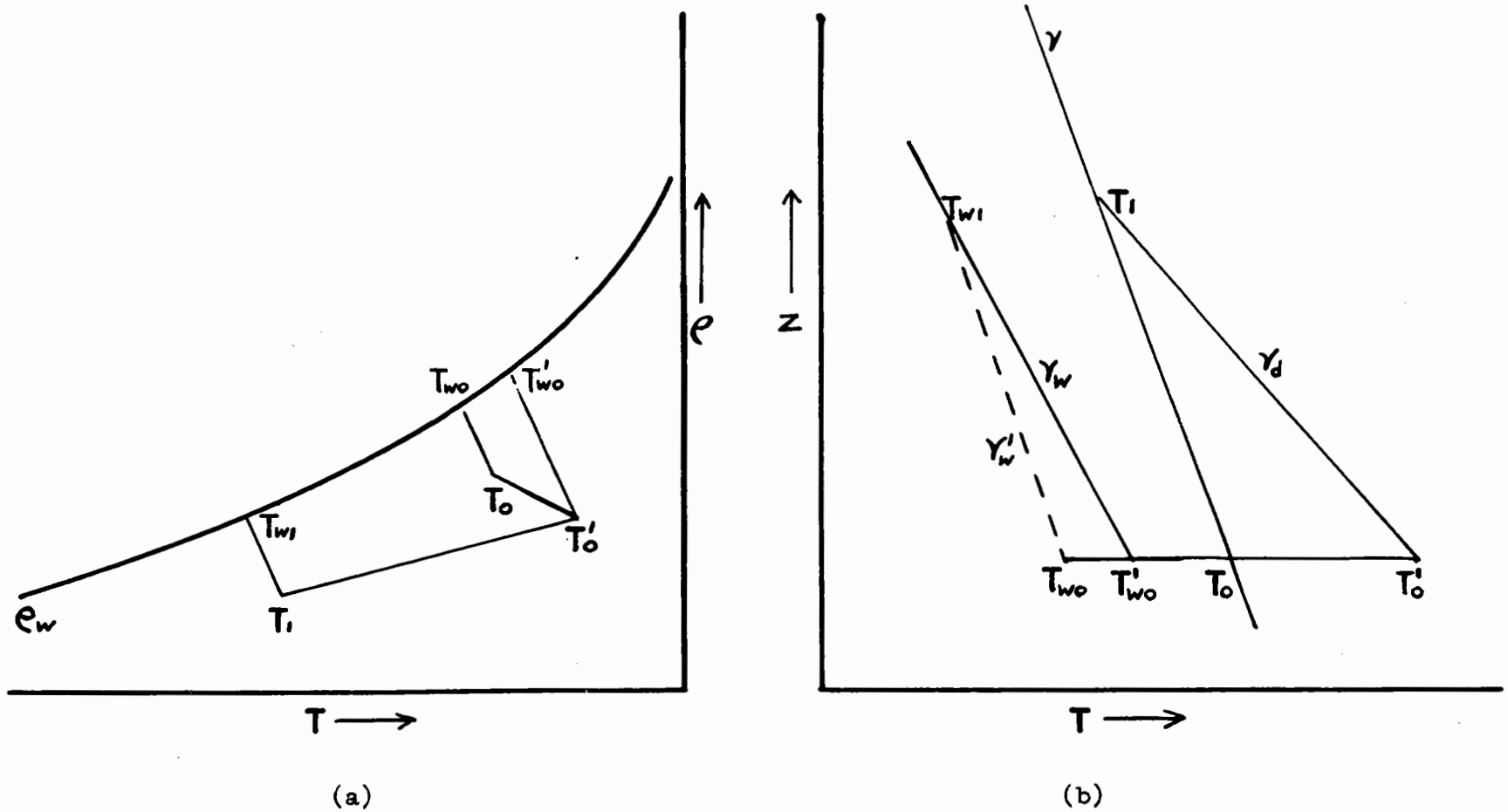

(a) (b)

FIG. 8. Variation of the wet bulb temperature within a parcel of air in which sublimation is occurring, shown (a) against coordinates of vapor density versus temperature, and (b) against coordinates of height versus temperature.

This process is shown schematically upon a tephigram in fig. 8b; the isobaric temperature increase T_o to T'_o is accompanied by an increase of wet bulb from T_{wo} to T'_{wo}, and subsequent ascent further changes the wet bulb to T_{wl}. Then the wet bulb lapse rate γ'_w is $\dfrac{T_{wo} - T_{wl}}{\Delta z}$.

If $\gamma > \gamma'_w$, then at some height the wet bulb becomes equal to the dry bulb temperature, saturation is achieved, and further ascent results in cloud formation; if $\gamma < \gamma'_w$ no such saturation will be achieved. The critical condition $\gamma = \gamma'_w$, applied to eq. (4.1) shows that cloud will or will not form according to whether $\gamma \gtrless \gamma_k$, γ_k being as defined in eq. (3.8). If no water cloud is initially present, the condensation level Z_c may be computed from the equation

$$Z_c = \frac{T_o - T_{wo}}{\gamma - \gamma'_w} \qquad (\gamma > \gamma'_w) \tag{4.2}$$

In order to assist the synoptic analyst in recognizing the possibility of vertical development due to sublimation processes, and particularly in assessing the likelihood of formation of water cloud, it would be advantageous to add to the tephigram the ice adiabats and the γ_k-curves. With the further addition of saturation mixing ratio curves with respect to ice, calculations of the liquid water and ice contents of mixed clouds could be made. A transparent overlay, containing these supplementary curves, would constitute a useful addition to the present tephigram.

5. VERTICAL VELOCITIES.

Having considered the ascent of a parcel of air in sec. 3, we turn now to the rate of ascent. The basic assumption is made that the ascending parcel remains in constant hydrostatic equilibrium with the environment, that is to say, that the buoyant response of the parcel is instantaneously coincident with the injection of thermal energy, none of which is expended in accelerating the parcel from rest. Some of the consequences of this assumption will be discussed later. It is worth noting that similar use has been made of this concept by Hewson (1948), who studied the dissipation of clouds by subsidence, the subsidence being induced by radiational cooling; this sequence of events had been described earlier by Napier Shaw as "heating through cooling".

(a) Clear Air.

Consider the growth, in cloud-free air, of a mass of ice $d\rho_s$, resulting in an isobaric increment of temperature followed in turn by (dry) adiabatic ascent to a new level of hydrostatic equilibrium. According to sec. 3(a) the total temperature change is given by

$$dT = -\frac{\gamma}{\gamma_d - \gamma} \frac{d\rho_s}{\frac{c_p p}{R L_s T} + \frac{\rho}{T}}$$

But if the parcel ascends dz, then $dT = -\gamma dz$, whence the vertical velocity V is given by

$$V = \frac{dz}{dt} = \frac{d\rho_s/dt}{\left(\frac{c_p p}{RL_s T} + \frac{\rho}{T}\right)(\gamma_d - \gamma)} \simeq \frac{d\rho_s/dt}{\frac{c_p p}{RL_s T}(\gamma_d - \gamma)} \qquad (5.1)$$

But $\frac{d\rho_s}{dt} = \sum_1 N_i \frac{dm_i}{dt}$, where N_i is the number of growing crystals, each of mass m_i, per unit volume. Thus

$$V = \frac{\sum_1 N_i \frac{dm_i}{dt}}{\frac{c_p p}{RL_s T}(\gamma_d - \gamma)} \qquad (5.2)$$

Houghton (1950) has derived the growth rates of various types of ice crystals, and for plates or dendrites $\frac{dm}{dt} \propto m^{\frac{1}{2}}$; so, for such crystals, growing at a specified pressure and temperature, at a specified supersaturation with regard to ice, the resulting "sublimational updraft" velocity V is proportional to $\sum m^{\frac{1}{2}}$ and inversely proportional to $(\gamma_d - \gamma)$. In the case of growing spheres the velocity is proportional to $\sum_1 m^{1/3}$.

Using the constants appropriate to an environment at 700 mb and -15C, at water equilibrium, V has been computed, for dendrites, as a function of particle mass, assuming a monodisperse distribution, and a lapse rate of 6.6 deg km^{-1} (corresponding, at the specified pressure and temperature, to the median stability index with which snow generating cells were found to be associated, see Part I sec. 7). The results of the calculations are shown in fig. 9.

It is clear from this figure that substantial vertical velocities may appear in clear air as the result of sublimational growth in (water) saturated air. Even in an extremely stable isothermal atmosphere (in which the velocities are only about 1/3 the values of fig. 9) the velocities may be appreciable. The significance of such updrafts may be recognized by comparison with the terminal speeds of dendrites and of aggregates (after Nakaya, 1954, and Langleben, 1954), as indicated in the figure.

(b) Cloudy Air.

In cloudy air, a portion of the latent heat released by sublimational growth is expended in evaporating cloud water in order to retain water equilibrium. It has been shown that the resultant isobaric temperature increase in cloudy air is substantially less than in clear air for the sublimation of like masses of water substance. The isobaric temperature increase in cloudy air is (from eq. 2.10)

$$(dT)_p = \frac{L_s - L_v}{c_p} \frac{dr_s}{1 + \frac{\epsilon L_v^2 r_w}{c_p R T^2}}$$

and the parcel, still at the original pressure but at a slightly higher temperature, is saturated with respect to water. During the subsequent ascent and expansion, water equilibrium is maintained as condensation takes place, supplying additional heat to the parcel; this additional heat input can conveniently be taken into account by considering ascent to occur saturated adiabatically.

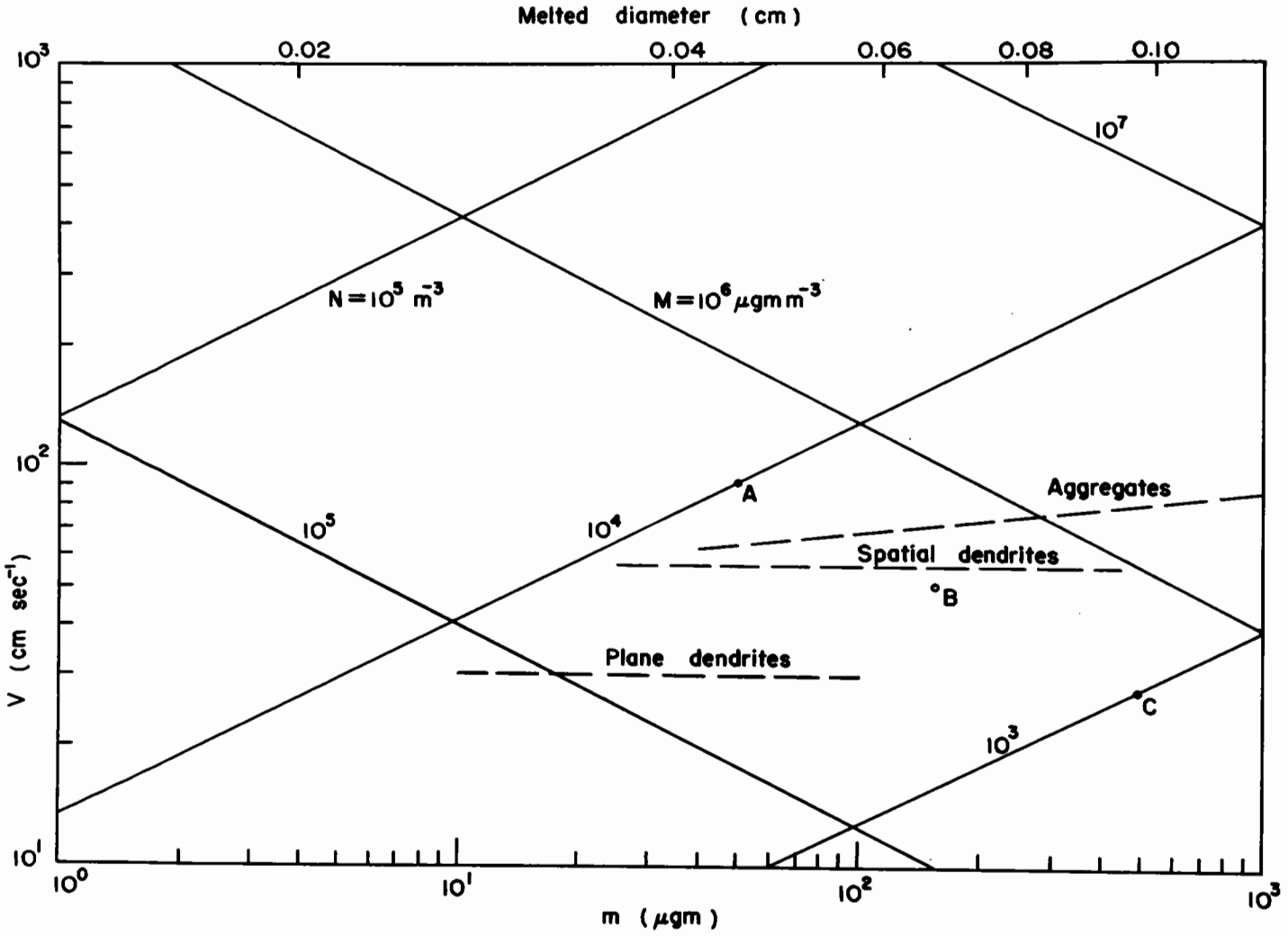

FIG. 9. Sublimational updraft velocity due to growth of N dendrites m^{-3}, each of mass m, in cloud-free but water saturated air at 700 mb, -15C, lapse rate 6.6 deg km^{-1}. Ice content is M, for a monodisperse distribution. Dashed lines indicate terminal speeds of dendrites and aggregates.

The total temperature change, once hydrostatic equilibrium is restored, is then

$$dT = \frac{L_s - L_v}{c_p} \frac{dr_s}{1 + \frac{\epsilon L_v^2 r_w}{c_p R T^2}} - \gamma_w dz \qquad (5.3)$$

Since $dz = \frac{(dT)_p}{\gamma_w - \gamma}$ and $dT = -\gamma dz$, it follows that

$$V = \frac{L_s - L_v}{c_p \left(1 + \frac{\epsilon L_v^2 r_w}{c_p R T^2}\right)(\gamma_w - \gamma)} \cdot \frac{dr_s}{dt} \qquad (5.4)$$

For the same total growth rate per unit volume $\left(\sum_i N_i \frac{dm_i}{dt}\right)$ the velocities in clear and in cloudy air are in the ratio

$$\frac{V(\text{cloudy})}{V(\text{clear})} = \left[\frac{L_s - L_v}{L_s}\left(1 + \frac{\epsilon L_v^2 r_w}{c_p R T^2}\right)^{-1}\right]\left[\frac{\gamma_d - \gamma}{\gamma_w - \gamma}\right] \qquad (5.5)$$

The factor within the first square bracket represents the inhibition due to the evaporation of water cloud; the second factor (which is greater than unity) represents the slight improvement in cloudy air due to the additional heat input as condensation occurs during ascent. Under the conditions for which fig. 9 was computed (700 mb, -15C, $\gamma = 6.6$ deg km^{-1}) the effect of the presence of cloud is to reduce the updraft velocities to about 1/13 their clear air values.

(c) Aggregation.

The effects of aggregation may be examined, at least in a qualitative sense, by referring to an example in conjunction with

fig. 9. Consider, for example, 10^4 dendrites m^{-3}, each of mass 50 μgm. In the environment of fig. 9, crystal growth will result in a sublimational updraft (in clear air) of about 1 m sec^{-1} (point A). Suppose now that the crystals aggregate by tens, resulting in 10^3 aggregates each of mass 500 μgm; the resulting updraft, indicated by point C, has been substantially reduced (by a factor of $10^{-\frac{1}{2}}$ in this case). Prior to aggregation, the crystals would be carried aloft in the updraft; following aggregation, the aggregates would precipitate. At an intermediate stage of aggregation (by threes or fours), indicated by point B, single crystals would be carried aloft and aggregates would precipitate. Thus single crystals which are supported in the updraft may become aggregates which are no longer supported, and precipitate out of the air mass. It is assumed that a dendritic aggregate grows at the same rate as a single dendritic crystal of the same mass, which is in fact not likely to be the case. Most of the diffusional growth onto the aggregate will occur on the outside, where ventilation is free; within the entangled body of the mass, ventilation will be inhibited and the growth rate somewhat less.

If the snow crystal distribution were monodisperse, and if the crystals were to aggregate by n's (i.e. n crystals clump to form one aggregate), then the updraft velocity would be reduced to $n^{-\frac{1}{2}}$ its original value; similarly, if the reverse were to occur and each crystal splinter (or each aggregate break up) into n equal-sized dendritic fragments, the velocity would increase by a factor $n^{\frac{1}{2}}$. Thus aggregation and splintering (or de-aggregation) may have an important effect upon the sublimational updraft

velocity.

(d) Downdrafts, and Ice Saturation.

The evaporation of snow, falling into a dry stratum of air, will result in chilling and downdrafts, as discussed in Part I (sec. 10). In moist air, water equilibrium places an upper limit on the vapor excess which "drives" crystal growth; at 700 mb, -15C, this maximum excess is about 0.2 gm m^{-3}. The vapor deficit which "drives" the evaporation, however, can be much greater, being about 1.4 gm m^{-3} in completely dry air at the above temperature and pressure. Thus, downdrafts due to evaporation may be many times as great as the updrafts indicated in fig. 9.

As in the case of sublimational growth, vertical motion of the chilling air parcel ceases either when all the snow-content is evaporated or when the air reaches ice saturation, the latter occurring when the ice bulb temperature within the parcel has increased to the ambient dry bulb temperature (in stable air). If the parcel acquires sufficient downward momentum, it may overshoot the equilibrium level and achieve supersaturation with respect to ice; any snow remaining will then grow, the latent heat operating to return the parcel to the equilibrium level. Thus, a parcel of snow-filled air may become, at the lowest extremity of its downward motion, a centre of renewed snow growth.

(e) Limiting Updraft Velocities.

The question arises as to the reality of the rather large updraft velocities which are implied (under suitable conditions) by the equations derived in this section. These equations have been derived upon the basis of continual equilibrium of the parcel with the environment, implying no acceleration. Certainly some energy must be expended in order to accelerate the parcel from rest. With regard to the ascent (once begun), Scorer and Ludlam (1953) have studied the drag on a buoyant bubble, and the limiting velocity; they present a limited number of data which suggest a linear relation between the temperature excess and the limiting velocity of a bubble. It seems likely that a more or less steady temperature excess, and velocity, is established, representing equilibrium between the buoyant force and the opposing forces of drag and loss of buoyancy due to mixing.

The maximum isobaric temperature excess, obtainable in clear air when the vapor content is reduced completely from water to ice equilibrium, is of the order of $\frac{1}{2}$ deg C (see fig. 2), which excess could (according to Scorer and Ludlam) result in a bubble velocity of 1-2 m sec^{-1}. Ludlam (1956) suggests that a bubble of several hundred meters' diameter, with an initial temperature excess of this magnitude, is not likely to acquire a vertical speed much in excess of 1 m sec^{-1}; however, he is considering ascent in clear stable air in which the temperature excess diminishes

with ascent, even without mixing. If growing ice crystals are retained within, or continually supplied to, the parcel there is a greater likelihood of a temperature excess being maintained; also, in cloudy air, while mixing will serve to reduce the excess, it will at the same time tend to maintain a high vapor content within the parcel, thus prolonging the period of most rapid crystal growth and supply of thermal energy. In stable air, therefore, it seems reasonable to expect that updrafts as high as several meters per second may be achieved. In the case of unstable, or conditionally unstable, air the major role of crystal growth (as a source of heat-supply) is probably that of a trigger, leading to the realization of the instability; once established, the instability will lead to updrafts of the magnitudes usually observed in cumulus and cumulonimbus (up to about 20 m sec^{-1}).

If the updraft velocity is in fact less than predicted by present theory, then the rate of resupply of cloud water is reduced, the cloud being consumed within a somewhat smaller height interval than indicated in sec. 3. In unstable air, a limited updraft velocity would make possible the depletion of liquid water content in cumulus. Similarly, in clear air, the net rate of reduction of vapor content within the ascending parcel will be increased.

6. ACTIVE ENVIRONMENT.

In the foregoing sections it has been assumed that the environment, in which crystal growth and the resulting vertical

development, velocity, and variation in cloud content occur, is "inactive", i.e. that there exists no general large-scale vertical motion of the environment. In the case of frontal or orographic precipitation, of course, this is far from the case. When there exists such general vertical motion, the environment may be called "active", and various changes occur within the environment as the result of this activity; the presence of growing ice crystals introduces further changes, of the sort described in the preceding sections, these being superimposed upon the large scale dynamic activity. In the following sections the effects of this basic environmental activity will be considered.

(a) The Apparent Lapse Rate.

Consider a vertical column of air AA' (fig. 10) which ascends vertically at a rate w, it being assumed that all particles within the column rise at the same rate so that there is no vertical stretching or shrinking of the column (i.e. no lateral divergence). In time Δt the column is displaced vertically by $w\Delta t$ to the position BB'. Consider now a parcel within the column, at A, in which sublimation is proceeding at such a rate as to result in a vertical velocity, relative to the surrounding air in the column, of V. In time Δt this parcel will have risen from A to C, a distance of $(V + w)\Delta t$. Now the updraft V is calculated upon the assumption that the parcel remains in equilibrium with the environment (sec. 5), so that at C the parcel temperature is the same as the ambient temperature T_C.

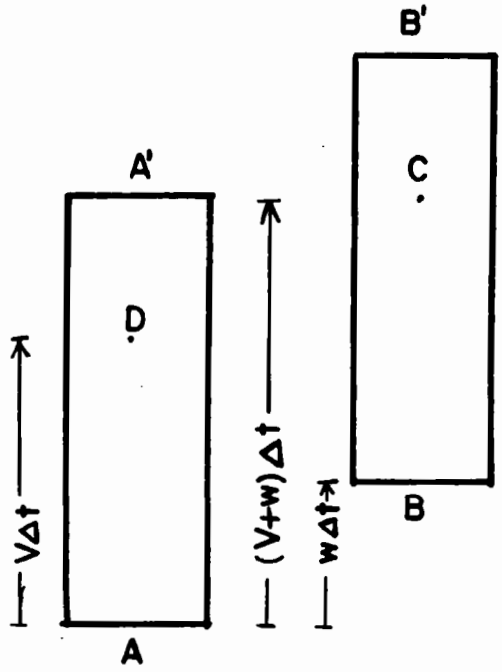

FIG. 10.

In an inactive air mass AA', an ice-filled parcel would ascend in unit time from A to D; in an active air mass, ascent is from A to C, resulting in a steeper lapse of temperature within the parcel.

If the column is saturated, then

$$T_C = T_D - \gamma_w w \Delta t$$

If the lapse rate within the column AA' is γ, then

$$T_C = T_A - V \gamma \Delta t - w \gamma_w \Delta t$$

Since the temperature difference $T_C - T_A$ occurs within a vertical distance $(V + w)\Delta t$, the apparent lapse rate γ_p, experienced by the parcel, is

$$\gamma_p = (T_A - T_C)/(V + w)\Delta t = \left\{V\gamma/(V + w)\right\} + \left\{w\gamma_w/(V + w)\right\}$$

i.e. $$\gamma_p/\gamma = (1 + w\,\gamma_w/V\,\gamma)\Big/(1 + w/V) \qquad (6.1)$$

A similar expression (but containing γ_d instead of γ_w) applies in dry air.

Eq. (6.1) shows that in stable air the effect of the general environmental vertical component w is to increase the apparent lapse rate so that the parcel may be considered, in effect, to be ascending through a somewhat less stable environment.

If, in a saturated column in which no general vertical motion occurs (an inactive environment), the ambient lapse rate is γ_p, then the sublimational updraft velocity is (eq. 5.4):

$$V_p = K/(\gamma_w - \gamma_p) \qquad (6.2)$$

If however the air mass is active and has a lapse rate γ (so that γ_p is specified by eq. 6.1), then (6.2) becomes:

$$V_p = K(V + w)/V(\gamma_w - \gamma)$$

But $K/(\gamma_w - \gamma) = V$, the updraft in the inactive environment whose lapse rate is γ. Thus,

$$V_p = V + w \qquad (6.3)$$

i.e. the sublimational updraft in an environment whose lapse rate is γ_p is simply the sum of two velocities, the first being the sublimational updraft as computed for the inactive environment (of lapse rate γ) and the second being the general vertical velocity w.

The effect of lateral convergence is to stretch the column with time, introducing a variation of w with height. The environment at C will then have originated some distance below D and in stable air will arrive at C with a lower temperature than w o u l d otherwise have been the case; thus, convergence tends to increase γ_p.

(b) Dry Air.

In a dry environment, general vertical motion will tend to bring the vapor content closer to water equilibrium. Thus the desiccating effect of sublimation in a stable inactive air mass

may be balanced or even counteracted by the general ascent in an active one.

From eq. (3.7), the vapor content within a rising parcel in which sublimation is occurring is given by

$$d\rho/dt = -\gamma V \left[\frac{c_p p}{RL_s T} \left(\frac{\gamma_d}{\gamma} - 1 \right) + \left(\frac{c_p}{R} \frac{\gamma_d}{\gamma} - 1 \right) \frac{\rho}{T} \right] \quad (6.4)$$

Added to this is the change in vapor density due to dry adiabatic vertical motion w, given (from eq. 3.5) by

$$\frac{d\rho}{dt} = -\gamma_d w \left[\frac{c_p}{R} - 1 \right] \frac{\rho}{T} \quad (6.5)$$

Adding these two simultaneous rates and noting that

$$\left(\frac{d\rho}{dt} \right)_{\text{Total}} = -\left(\frac{d\rho}{dT} \right)_{\text{Total}} (V + w) \gamma_p$$

we get (after considerable rearrangement, and using eq. 6.1),

$$\left(\frac{d\rho}{dT} \right)_{\text{Total}} = \frac{c_p p}{RL_s T} \left(\frac{\gamma_d}{\gamma_p} - 1 \right) + \left(\frac{c_p \gamma_d}{R \gamma_p} - 1 \right) \frac{\rho}{T} \quad (6.6)$$

Eq. (6.6) is identical to (3.7) except for the replacement of γ by γ_p. Thus, the variation of vapor density within the parcel can be computed by (3.7), in the case of an active environment, by using the apparent lapse rate γ_p instead of the ambient lapse rate γ; specifically, fig. 5 can be applied by using the curves appropriate to γ_p.

This being the case, then water equilibrium is approached within the parcel when $\gamma_p > \gamma_K$, i.e. when $\gamma > \gamma_K - \frac{w}{V} (\gamma_d - \gamma_K)$.

Thus, the critical lapse rate is reduced when the environment is active rather than inactive. For any given ambient lapse rate γ and vertical velocity w, water equilibrium is approached when

$$V < w \frac{\gamma_d - \gamma_K}{\gamma_K - \gamma} \tag{6.7}$$

Since V is a function of the number, size and type of growing ice crystals, (6.7) can be used to define the critical crystal mass and number ($\sum m^{\frac{1}{2}}$ for dendrites) below which the vapor content of the parcel approaches saturation.

If $\gamma_p < \gamma_i$, vapor density decreases toward ice equilibrium and V decreases. However, increasing crystal mass will tend to increase V. The net variation in V will depend upon the relative effects of these two factors. Suppose the net effect is a reduction in V. Then γ_p increases (see eq. 6.1) and $\frac{d\rho}{dT}$ decreases (eq. 6.6 and fig. 5), and if continued, results in an increase in V. Conversely, if the initial tendency is toward an increase in V, this tendency will tend to reverse itself. Thus, in either case, V will tend to a more or less steady value.

(c) Cloudy Air.

By a similar examination of the cloudy-air case, it can be shown that the variation of the liquid mixing ratio r_L (given by eq. 3.13 in the case of the inactive environment) is given in the active case by

$$dr_L/dz = (VS + wF)/(V + w) \qquad (6.7)$$

where

$$S = -\frac{c_p}{L_v}\left[\frac{L_v}{L_s - L_v}(\gamma_w - \gamma)\left(1 + \frac{\epsilon L_s L_v r_w}{c_p R T^2}\right) - (\gamma_d - \gamma_w)\right]$$

$$= \left(\frac{dr_L}{dz}\right)_s \text{ due to sublimation in the inactive environment}$$

and

$$F = \frac{c_p}{L_v}(\gamma_d - \gamma_w)$$

$$= \left(\frac{dr_L}{dz}\right)_F \text{ due to saturated adiabatic ascent.}$$

Eq. (6.7) can be drived from (3.13) by the substitution of γ_p for γ. The critical lapse rate, beyond which cloud content is increased rather than depleted is found, from (6.7), to be that for which $S = -Fw/V$ which can be shown to be equivalent to the condition $\gamma_p = \gamma_K$. Thus, in cloudy air as well as in cloud-free air, the effect of the general environmental vertical motion can be conveniently taken into account by using the appropriate equations, already derived for the inactive environment, but substituting for the ambient lapse rate γ the apparent one γ_p; graphs such as figs. 5 and 6 can therefore be applied in either the active or inactive case so long as the proper lapse rate is used.

Given the ambient lapse rate γ, and the upglide velocity w, eq. (6.7) permits the calculation of the critical value of V which, if exceeded, results in cloud depletion; since V depends upon γ and upon $\sum m^{\frac{1}{2}}$ (for dendrites and plates), the corresponding critical crystal content can be computed. Critical values of $\sum m^{\frac{1}{2}}$ as a function of lapse rate, for various values of w, are shown in

fig. 11; these curves are based upon an ambient pressure and temperature of 700 mb and -15C. Fig. 11 indicates that, over a wide range of stable lapse rates and of environmental upglide velocities, the critical ice crystal content $\sum m^{\frac{1}{2}}$ lies within a relatively restricted range, between 10^4 and 10^5 $\mu gm^{\frac{1}{2}}$ m^{-3}.

Fig. 12 shows the height at which cloud of initial density 0.1 gm kgm^{-1} is depleted, as a function of air mass stability, curves being plotted for several environmental upglide velocities (w) and for several crystal contents ($\sum m^{\frac{1}{2}}$). For crystal contents greater than 10^5 $\mu gm^{\frac{1}{2}}$ m^{-3}, and over a wide range of lapse rates, such cloud is depleted within a few tens of meters. Following depletion, further ascent occurs in clear air, but never reaches complete equilibrium since the vapor excess over ice equilibrium tends to be continually improved by the general environmental ascent. In clear air, the vapor content of the parcel is specified by the path, in fig. 5, appropriate to the apparent lapse rate γ_p; as ice equilibrium is approached, the sublimational updraft V decreases and γ_p increases. The vapor density tends to approach ice equilibrium more and more gradually, and so the later part of the clear air ascent tends to be at a speed very nearly equal to w and at a vapor content but slightly above ice equilibrium. However, the major part of the reduction of the vapor content will have occurred within a height which is relatively great compared to the height within which the water cloud is depleted; thus, in a stable active air mass, as in an inactive one, the presence of water

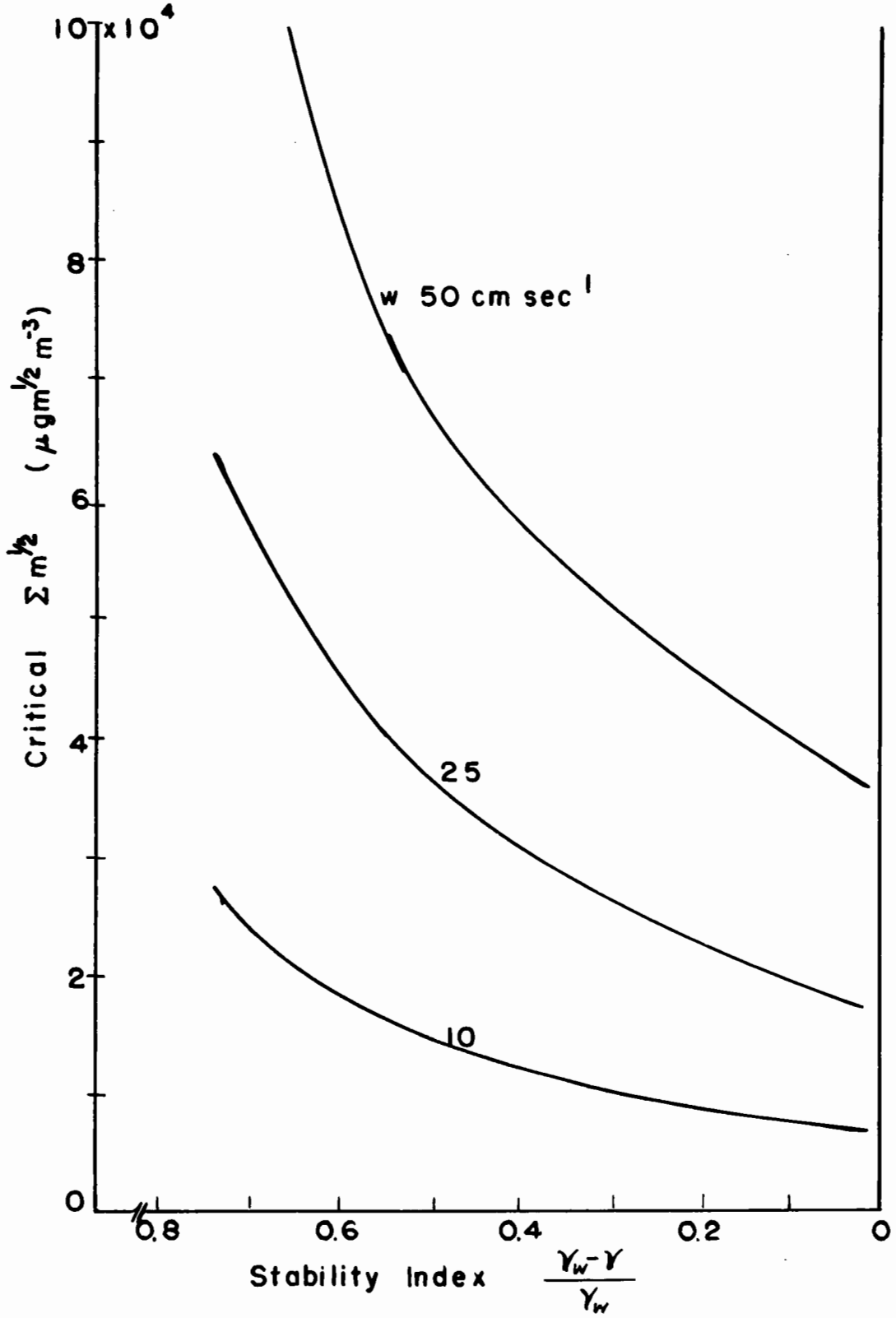

FIG. 11. Critical values of $\sum m^{\frac{1}{2}}$, at various stabilities and environmental vertical velocities. Pressure and temperature, 700 mb, -15C. Cloud content is depleted when crystal content exceeds the critical value.

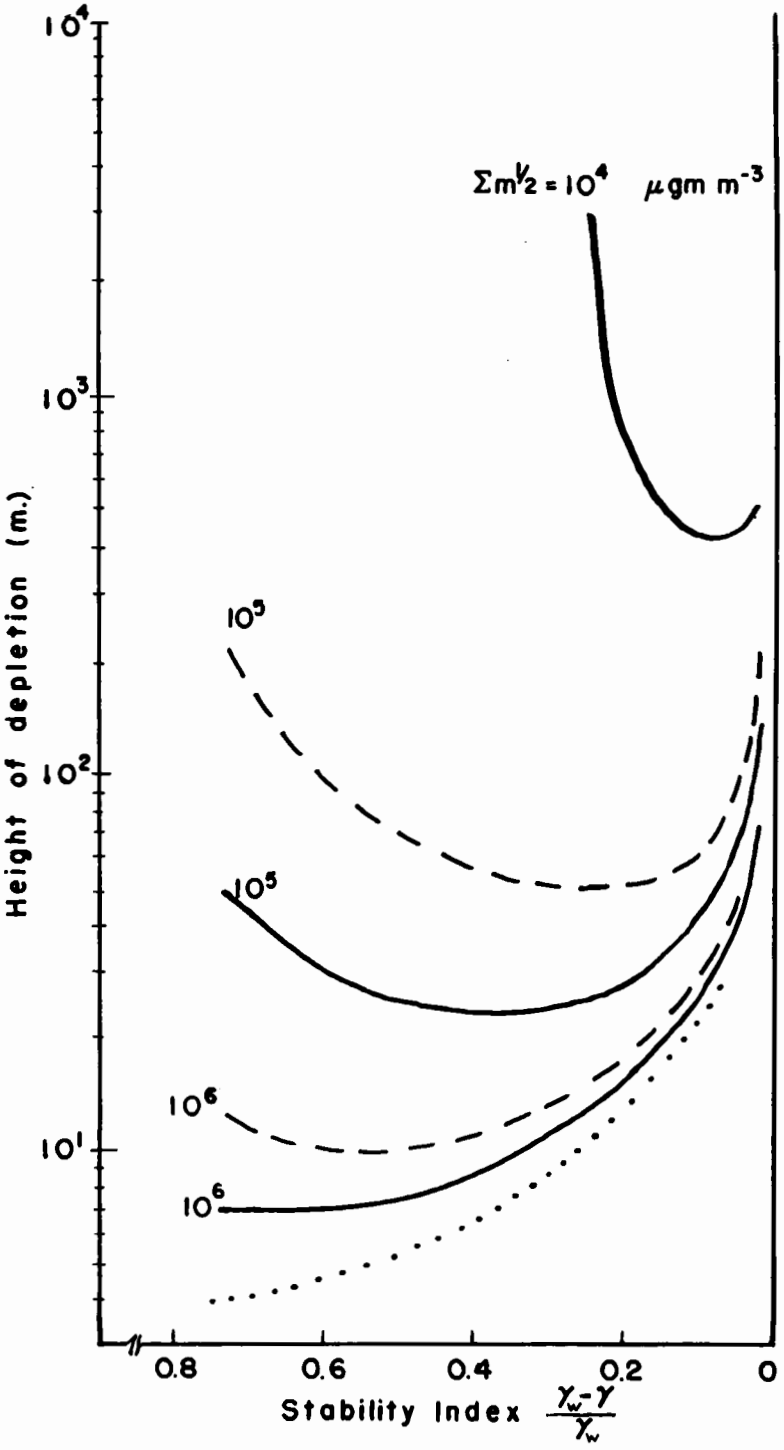

FIG. 12. Heights at which cloud of initial liquid content 0.1 gm m^{-3} and crystal content Σ m$^{\frac{1}{2}}$ is depleted. For environmental vertical velocities of zero, 10 and 25 cm sec^{-1}, the heights are as indicated by the dotted, full, and dashed curves, respectively.

cloud makes a relatively minor contribution to the overall ascent.

7. CLOUD BOUNDARY SHEAR.

The difference in sublimational updraft velocities in moist clear air and in cloudy air suggests the possibility of a shear developing across a cloud boundary. If ice crystals appear within a region including such a boundary, the resulting updrafts may be greater by a substantial factor in the clear air just adjacent to the cloud than in the cloud itself. This difference, or shear, is indicated in fig. 13, in which sublimational updrafts in clear and in cloudy air, and their difference, or shear, are plotted as functions of lapse rate. The shear is a maximum for a specific lapse rate which depends upon the pressure and temperature, varying between about 5.5 and 7.5 deg km^{-1} over the range of conditions in which generating cells are usually observed. The optimum lapse rate for maximum shear was computed for each of the 14 cases of cells discussed in Part I, and were compared with the observed lapse rates at the generating levels. In 10 of the 14 cases, the actual lapse rate differed from the optimum by 10% or less; considering all 14 cases, the mean relative deviation was $2\frac{1}{2}\%$, with the ambient lapse rate tending to be a little less than optimum. Thus, the air mass stability at the generating level appears to be nearly the optimum value for maximum cross-boundary shear. Such shear, and the turbulence which would be expected as a result, would presumably favor the aggregation of crystals into snowflakes.

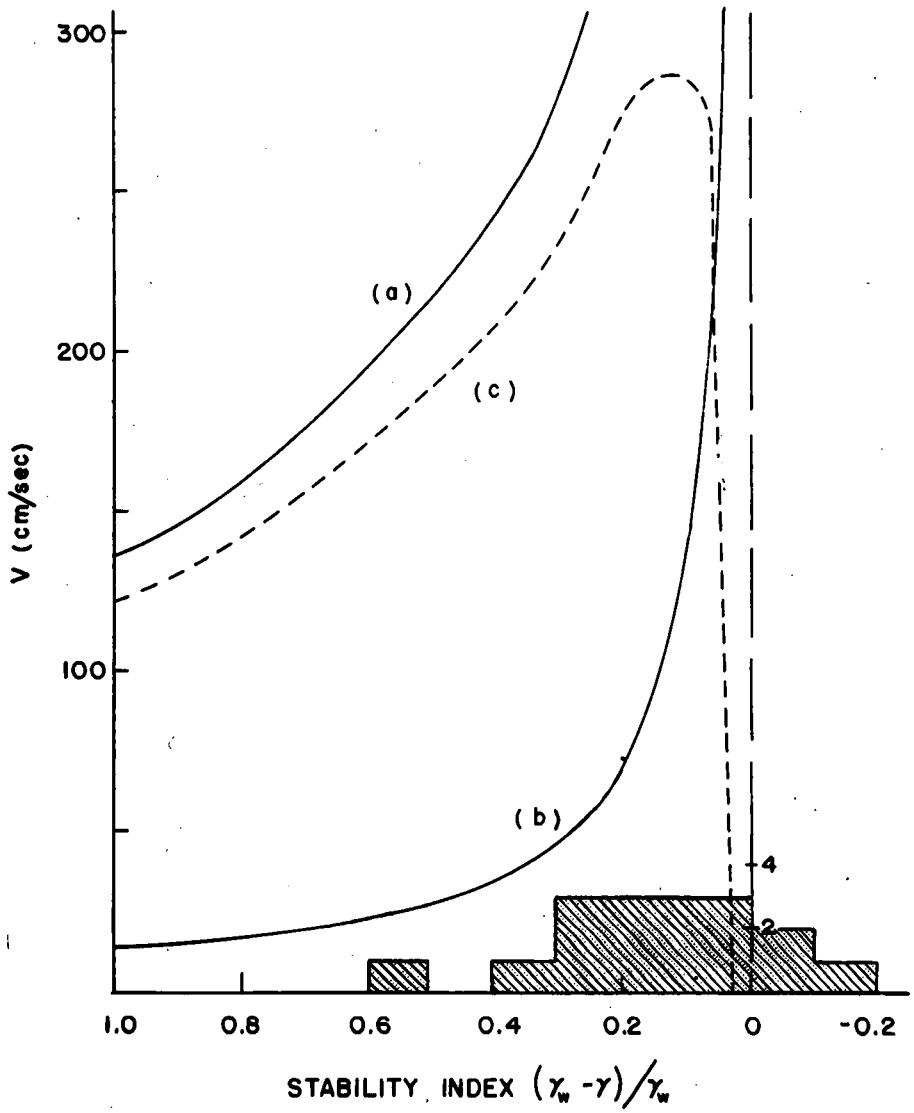

FIG. 13. Updraft velocity as a function of stability index (a) in clear air, (b) in cloudy air. The difference (c) between these velocities represents a shear across a cloud boundary. A concentration of 10^5 crystals m^{-3}, of mass 10 μgm, is assumed. Histogram shows air mass stabilities for cases discussed in Part I.

In view of a likely upper limit to the parcel velocity, of the order of a few meters per second (in stable air) as discussed in sec. 5(e), the shear (as indicated, for example, in fig. 13) may be unrealistic at low stabilities. The effect of a limiting updraft velocity will be to reduce the shear at low stabilities, and to shift the peak towards a more stable lapse rate.

8. GENERATING CELLS.

Radar observations indicate the presence of aggregate snowflakes in the snow trails at all levels, suggesting the cell as a centre of aggregation. Magono (1953) points out that single crystals are likely to be poor "collectors" since their terminal speeds are invariant with size, and suggests that the necessary collisions can occur only between crystals and already-formed aggregates. Mason and Ludlam (1951) suggest that crystals may have appreciable relative motion in the horizontal, due to their fluttering during fall, claiming that aggregate flakes are often observed in which the constituent dendrites are interlocked in a more or less co-planar fashion. The accretion of droplets onto plane crystals will double or triple their terminal speeds and hence improve the probability of collision of rimed with unrimed crystals. A liquid surface film will favor aggregation, and it has until recently been generally considered that this occurs only at temperatures near melting; however, recent laboratory studies (Jensen, 1956; Hosler, Jensen and Goldshlak, 1957) have shown that sticking and clumping of crystals can occur at temperatures as

low as -40C in a water saturated environment. Thus, cloudy air offers an environment favoring aggregation, which will be even more likely if turbulence is present. Furthermore, if enough accretion does occur in cloud to materially increase terminal speeds, then turbulence, by bringing rimed crystals (in cloud) into juxtaposition with unrimed ones (from outside) will further serve the cause of aggregation. It is suggested, therefore, that turbulence across a cloud boundary, due to differential sublimational updrafts, makes that boundary a favored region for aggregation, and that the snow generating cell may be associated with this active boundary.

If ice crystals appear within a sheet of water cloud (perhaps falling into it from some higher level), new internal cloud boundaries may appear as the result of unequal desiccation due to local variations in cloud density and ice content. Also, crystal growth within the vapor-rich but cloud-free stratum immediately below the cloud base will result in the development of greater updrafts originating in this layer than in the cloud above; these more intense and cloud-free updrafts may be imagined as penetrating the cloud mass in "chimneys" of relatively intense convection, helping to produce internal boundaries across which turbulence and aggregation can occur. As aggregation proceeds, the updraft diminishes to the point where the aggregates, no longer supported aloft, are precipitated out to form the snow trail. On this basis, the cell might be considered as a snow-filled

hole in the stratiform water cloud (see fig. 14).

This aggregation process may well be a self-regulating one. Crystal growth leads to buoyancy which leads to shear, turbulence and aggregation; aggregation in turn reduces the updraft and the shear, tending thus to stabilize the process.

9. PRECIPITATION RATES.

Classical theory of precipitation rates (see e.g. Bannon, 1948) is based upon the premise that all excess vapor above water equilibrium is precipitated out of an ascending column of air, the cloud content remaining more or less constant, or at least varying little in comparison with the changes in vapor content. It is also assumed that all the air at the saturated levels is contributing to the precipitation. Now the greatest proportion of the precipitation of January-February, 1954 derived from precipitation rates of about $\frac{1}{2}$ mm hr^{-1}; furthermore, inspection of fig. 2 of Part I shows that rates in excess of $\frac{1}{2}$ mm hr^{-1} were usually associated with cell-and-trail pattern, and lesser rates with patternless radar echo. The higher hourly precipitation rates evidently derived from the cellular generation of snow in localized regions within a relatively thin layer of the troposphere. According to classical theory, a saturated layer 2-3 km thick (at 700 mb, -15C), ascending at 10 cm sec^{-1}, will yield only about 0.1 mm hr^{-1}. Thus, substantially higher precipitation rates must have been occurring from within the cells than could have resulted, on

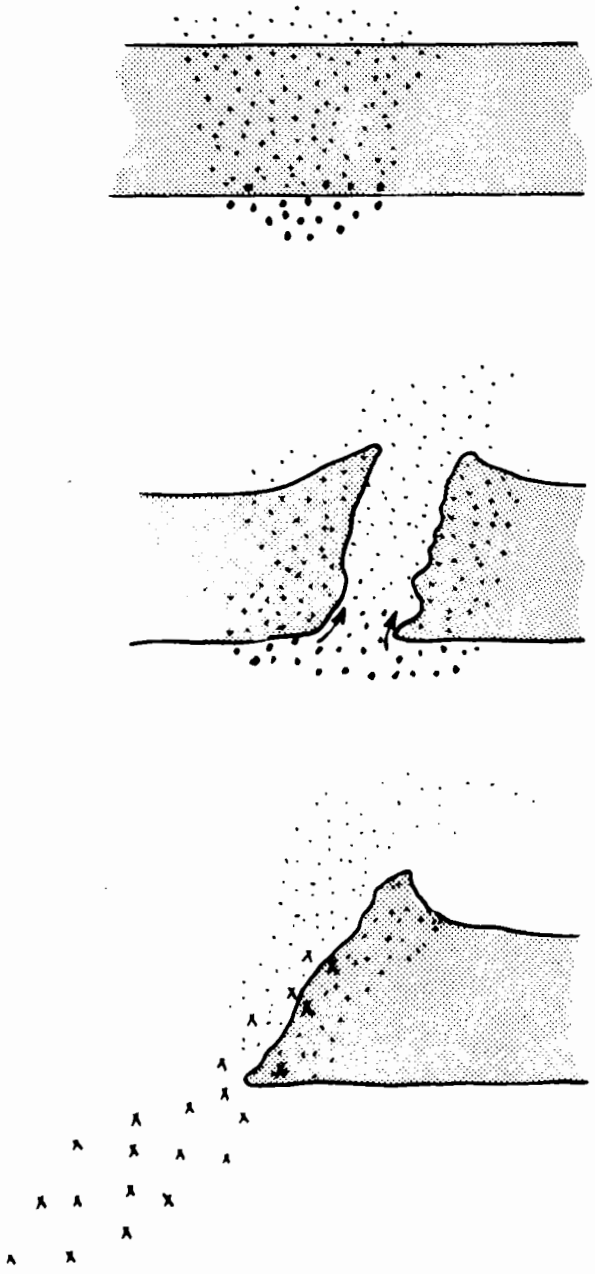

FIG. 14. Schematic diagram showing the development of new internal cloud boundaries. Growing ice crystals within the water cloud (top) result in the appearance of near-vertical "chimneys" of snow-filled air (centre). The new cloud boundary, a region of turbulence and aggregation (bottom) may constitute the snow generating cell.

the classical basis, from any reasonable rate of general ascent of the saturated cloud layer in which they were embedded. Furthermore, it is possible to have cellular snow generation in the absence of general environmental vertical motion (when classical theory predicts no precipitation), so long as ice crystals appear and grow within whatever water cloud is present.

According to classical theory, ascent of saturated air sufficient to increase the liquid content by 0.1 gm yields that same amount as precipitation. But fig. 6 shows that the sublimational reduction of 0.1 gm of cloud water results in a rather higher yield since, even with the cloud depleted, snow growth continues until ice equilibrium at a reduced temperature is achieved. Furthermore, if the cloud content is being depleted by sublimation in spite of the environmental vertical motion, the rate of snow growth within the ascending cloudy parcel is greater than the rate of increase of liquid content in the surrounding environmental cloud (and hence greater than the precipitation rate from that cloud, according to classical theory). Thus, the classical treatment of precipitation rates will tend to underestimate the rate within a cell. Considering, however, that cellular generation occurs within a limited portion of the cloud mass, the precipitation rate at the ground will be reduced, and may happen to be comparable to the classically-derived rate. Where cells are concerned, there seems to be no reason why agreement is to be expected between classically computed and observed

precipitation rates. While the classical concept has enjoyed considerable success in the determination of whether or not precipitation is to be expected, and where, this may be due to the fact that vertical motion produces the cloud system in which cells form, rather than the precipitation itself.

In stable air, sublimational snow growth feeds upon and consumes the cloud content, provided that enough snow is present ($\sum m^{\frac{1}{2}}$ in excess of about 10^4 μgm m^{-3}, as indicated in fig. 11). Recognizing that this depletion is occurring within a relatively small fraction of the parent cloud, the rate of resupply of liquid water to the surrounding cloud would not have to be great to enable the cloud mass to persist, against the cellular desiccation, over a long period of time.

10. SUMMARY AND CONCLUSIONS.

In moist air, the latent heat made available by growing ice crystals may be sufficient to result in significant vertical development, and in vertical velocities comparable to the terminal speeds of the ice crystals themselves. The rate of thermal input, and the corresponding updraft velocity, is seriously inhibited in the presence of water cloud, the evaporation of which draws on the thermal energy; thus, substantially greater sublimational updrafts are possible in clear air than in cloudy air. Whether the cloud content converts to ice by evaporation-sublimation or by freezing, the total heat involved is the same; however, if sublimation and

freezing occur at different rates, these rates are additive. Vertical motion ceases when the vapor content of the parcel is reduced to ice equilibrium; vertical development thus achieved, in an environment in which the lapse rates are of the magnitude observed when snow generating cells occur, are of the order of magnitude of the observed vertical extent of such cells.

Sublimation draws on the liquid content of water cloud, but the subsequent buoyant ascent tends to restore it. In an inactive air mass, these two factors find a balance when the ambient lapse rate has a critical value slightly less than the saturated (water) adiabatic value; in stable air, water cloud is consumed, but for lapse rates in excess of the critical value, cloud content increases. In stable air, the initial presence of water cloud makes possible a slight increase in the total height of vertical development, but this increase is negligible for stratiform cloud of the usual liquid water content. In an active air mass, large scale ascent (frontal or orographic) reduces the depletion of cloud content and may indeed cause that content to increase, even in stable air; thus, an active air mass serves to reduce the critical lapse rate to a more stable value.

In air which is conditionally unstable and which contains vapor in excess of ice equilibrium, water cloud may form and absolute instability develop as the result of crystal growth; the possibility of ice crystals serving as a trigger to the

realization of instability, even in the absence of mechanical lifting, is one which should not be overlooked by the synoptic meteorologist.

Ludlam (1956) has considered the formation of "shred cloud" above a fallstreak which extends into a moist stratum. His data indicate the formation of such water cloud in stable air in which, according to the foregoing considerations, such cloud formation is not to be expected, except in an active air mass (in which the critical lapse rate takes a reduced value). Since vertical motion within the air mass is required for the formation of the fallstreak itself, Ludlam's data are not at variance with the present theory.

Since sublimational updrafts in moist clear air exceed those in cloudy air by a substantial factor, appreciable differences in vertical velocity may appear across a cloud boundary. New internal cloud boundaries may appear within water cloud as the result of unequal desiccation of that cloud by crystal growth. Across these new boundaries turbulence, arising as the result of differential updraft velocities, will favor the aggregation of crystals. Aggregation reduces the updraft, enabling the aggregates to precipitate out of the boundary region. It is suggested that such internal cloud boundaries constitute the snow generating cells, in which aggregation occurs and from which the aggregates fall to form the snow trail below.

Since, with cellular snow generation, the precipitation

derives from scattered sources occupying but a small fraction of the parent cloud mass, the cells apparently serve as intermediaries through which the parent cloud mass is converted into the precipitation which arrives at the ground. Classical theory of precipitation rates does not consider such an intermediate process, and so cannot be considered satisfactory in those cases where the cellular process is involved.

The precipitable ice content of a moist parcel is considerably greater when the process of sublimational vapor reduction occurs non-isobarically than when it occurs isobarically. In particular, the total vapor reduction may be many times the water content of any reasonable cloud initially present. In the active environment, general vertical motion serves to increase the liquid content of the parent cloud, against which the relatively scattered cells act as desiccating agents. Whether or not the entire cloud sheet is ultimately consumed depends upon the relative rates of desiccation (within the cells) and of resupply (by the air mass activity). If the cellular desiccation is not too great, water cloud will continue to provide a nourishing environment for cell activity for a relatively long period of time.

PART THREE

GROWTH BY ACCRETION AND SUBLIMATION

PART III: GROWTH BY ACCRETION AND SUBLIMATION

1. INTRODUCTION AND ACKNOWLEDGMENTS.

Growth of liquid precipitation elements can be attributed to condensation, coalescence, or a combination of both; many investigations have been made of these processes, of which East's (1957) is among the most recent, dealing with the development of precipitation in cumulus (CU) through the all-water processes of condensation-coalescence. In cold cloud, growth of solid precipitation elements may be by sublimation of ice crystals, by the aggregation of many crystals into snowflakes, by accretion, or by combinations of these processes. Accretion occurs when a solid particle, falling through supercooled cloud, collides with and collects droplets which freeze upon impact to form rimed crystals or flakes, graupel, or hail.

Studies of accretion have in general been confined to relatively large particles, for which accretion is the predominant growth mechanism; such studies include, for example, those of Ludlam (1950), of Magono (1953) and of Wexler (1953). Houghton (1950) has compared sublimational growth of ice crystals with growth by coalescence of water droplets, the latter process yielding a substantially improved growth rate over the former for particles whose equivalent diameter exceeds a few hundred microns; the conclusion is that the initial growth of precipitation elements is by sublimation, but that subsequent growth to precipitation size is by coalescence. However, in this study, Houghton was comparing two separate and independent

processes, rather than the simultaneous occurrence of two growth-processes.

Mason and Ludlam (1951) treat the growth rate of a particle as the sum of the sublimational and accretional rates, considering them independent; they conclude that accretion predominates once the particle has exceeded some specific size. However, it is not permissible to treat the two growth rates as independent, since the sublimational growth rate must be affected by the increase in particle temperature due to the latent heat of fusion as freezing material is accreted. Thus, as accretion sets in, the sublimational component will be reduced; it is important, in the earliest stages of accretional growth, that this effect be evaluated, and this is done in the following sections.

The accretion process is of importance to the production of hail, and a knowledge of hail initiation must be built upon a knowledge of the initial growth of the primitive accretion particle and of the transformation from a sublimation element to an accretion element. Accretion appears to play an important role in the generation of thunderstorm electricity. The Thunderstorm Project (Byers and Braham, 1949) reported very few flight encounters of hail in thunderstorms, but this may have been due in part to the localization of hail within the storm; identification of the primitive forms such as graupel would be difficult from an aircraft. However Kuettner (1950) claims that graupel is the most frequently observed hydrometeor in thunderstorms occurring over the Zugspitze (at ten thousand feet),

being always associated with high electrical fields; large hail was found to be a rare and by no means a necessary occurrence in the 125 storms which he studied. Thus, while hail may not necessarily accompany every thunderstorm, it appears that graupel does.

A useful beginning may be made by studying the formation and growth of graupel as it occurs in spring and fall in relatively cold air; interpretation of the results may be extended to summer conditions, at comparably low temperatures aloft but with the rather higher liquid water contents and updraft velocities appropriate to cumulonimbus (CB). At the same time it is important to recognize how and why graupel does not form, since winter CU is observed which yields snowflakes rather than accreted particles; indeed, both graupel and snow have been noted to occur simultaneously, falling from adjacent portions of the same cloud mass. This phenomenon may have its summer counterpart in the occurrence, in the near vicinity of a thunderstorm, of areas of more or less continuous rain, in which radar reveals the bright band so typical of melting snow aloft. In this regard, Kuettner (1950) found that snow crystals prevail during the later periods of a thunderstorm, following the shower (graupel) and lightning centre.

The work reported in the following sections owes a great deal to earlier studies of the coalescence mechanism, by Dr. T.W.R. East and Prof. J.S. Marshall. In particular, Dr. East's droplet size distributions, derived by him for cumulus cloud, form the basis for computations of accretional growth in that type of cloud.

2. SUBLIMATION AND ACCRETION.

If a particle gains mass m by accretion at a rate $(dm/dt)_A$, then heat is added to the particle at a rate

$$Q_1 = L_f(dm/dt)_A$$

Similarly, sublimational growth adds heat to a spherical particle of radius S at a rate

$$Q_2 = L_s(dm/dt)_s$$
$$= L_s \cdot 4\pi SCD\Delta\rho$$

where C = ventilation factor, D = diffusivity of water vapor in air, and $\Delta\rho$ = excess of vapor density of the environment over that at the crystal surface.

Heat is removed, by conduction from the surface of the growing particle, at the rate

$$Q_3 = 4\pi SKC(T_S - T_A)$$
$$= 4\pi SKC\Delta T$$

where K = thermal conductivity of the environment, T_S = temperature at the face of the particle and T_A = ambient temperature.

In the steady state, $Q_1 + Q_2 = Q_3$, and it follows that

$$(d\rho/dT)_A = (K/DL_s)\left[1 - L_f(dm/dt)_A(4\pi KSC\Delta T)^{-1}\right] \qquad (2.1)$$

Eq. (2.1) is the equivalent, for the sublimation-accretion process, of eq. (3.1) of Part II. Now $K/DL_s = (\Delta\rho/\Delta T)_s$ for sublimation alone, assuming sublimation to be according to the diffusion process alone (Marshall and Langleben, 1954); thus,

$$(\Delta\rho/\Delta T)_A = (\Delta\rho/\Delta T)_s\left[1 - L_f(dm/dt)_A(4\pi KSC\Delta T)^{-1}\right] \qquad (2.2)$$

and since $\Delta T = T_S - T_A > 0$ (i.e. the particle is warmer than the air), then

$$(\Delta \rho / \Delta T)_A < (\Delta \rho / \Delta T)_S$$

Note that when $(\Delta \rho / \Delta T)_A = 0$, sublimation must cease since the vapor excess is reduced to zero; this occurs when a sufficiently large accretion rate occurs, given by

$$(dm/dt)_A = L_f^{-1}(4\pi KSC \Delta T),$$

and if the environment contains vapor at water equilibrium (as will usually be the case if liquid droplets are available for accretion) then ΔT in the above equation is the difference between the frost- and the dew-points.

(a) The Temperature Excess.

From eq. (2.2), and from considerations similar to those of Part II sec. 2 , it follows that

$$(\Delta T)_A = \frac{\delta \rho}{(K/DL_s + d\rho_i/dT)} + \frac{L_f (dm/dt)_A}{4\pi DL_s SC(K/DL_s + d\rho_i/dT)} \qquad (2.3)$$

where $\delta \rho = \rho - \rho_i$ (fig. 1). Now the first term is the temperature excess of the particle due to diffusive sublimation alone, and the second is the <u>additional</u> excess due to the accretion process; this accretional term is proportional to the accretion rate $(dm/dt)_A$, and is the equivalent of the temperature excess of the particle due to sublimation in the presence of a vapor excess (above ice equilibrium) of $L_f(dm/dt)_A(4\pi DL_s SC)^{-1}$.

(b) The Vapor Density Excess.

It can also be shown that

$$(\Delta\rho)_A = (\Delta\rho)_s \left[1 - L_f(d\rho_i/dT)(dm/dt)_A(4\pi KSC\,\delta\rho)^{-1}\right] \tag{2.4}$$

where $(\Delta\rho)_s$ is the vapor density excess when sublimation occurs alone. Thus, the vapor density excess, which "drives" the sublimation process, is reduced by the accretion process, and sublimational growth is thus inhibited (fig. 1).

With a vapor excess $(\Delta\rho)_A$, sublimational growth proceeds at a rate given by

$$(dm/dt)_{sA} = 4\pi SCD(\Delta\rho)_A$$

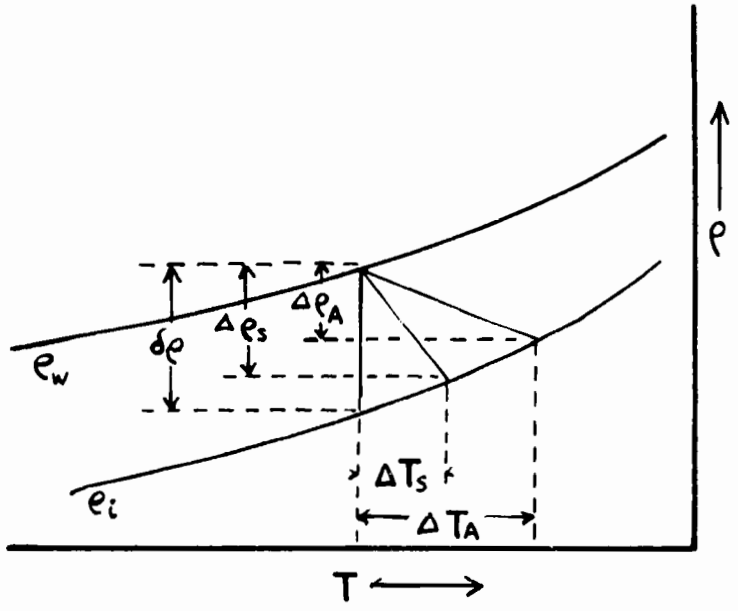

FIG. 1. Sublimation alone results in temperature and vapor density excesses ΔT_s and $\Delta\rho_s$. With accretion, the temperature excess increases to ΔT_A and the vapor excess decreases to $\Delta\rho_A$, thus inhibiting sublimation.

$$= 4\pi SCD(\Delta\rho)_s - \frac{L_f \frac{d\rho_i}{dT}}{L_s\left(\frac{K}{DL_s} + \frac{d\rho_i}{dT}\right)} \cdot \left(\frac{dm}{dt}\right)_A$$

$$= \left(\frac{dm}{dt}\right)_s - \frac{L_f \frac{d\rho_i}{dt}}{L_s\left(\frac{K}{DL_s} + \frac{d\rho_i}{dT}\right)} \cdot \left(\frac{dm}{dt}\right)_A \qquad (2.5)$$

where the subscript sA indicates the sublimational component of growth in the presence of accretion. This equation shows that the component of growth rate due to sublimation, in the presence of accretion, is equal to the purely sublimational growth rate which would obtain in the absence of accretion, less an amount which is proportional to the accretional growth rate.

Now the total growth rate

$$(dm/dt)_T = (dm/dt)_{sA} + (dm/dt)_A$$

$$= (dm/dt)_s + \left[1 - \frac{L_f \frac{d\rho_i}{dT}}{L_s\left(\frac{K}{DL_s} + \frac{d\rho_i}{dT}\right)}\right] \left(\frac{dm}{dt}\right)_A \qquad (2.6)$$

showing that the total growth rate is equivalent to the purely sublimational growth rate which would obtain in the absence of accretion, plus an increase due to accretion, less a reduction, also due to accretion. Now the ratio R_M of the accretional decrease to the accretional increase in growth rate is

$$R_M = \frac{L_f \frac{d\rho_i}{dT}}{L_s\left(\frac{K}{DL_s} + \frac{d\rho_i}{dT}\right)} \qquad (2.7)$$

Table I	R_M(%)		
T°C	p (millibars)		
	1000	700	500
0	5.9	4.9	3.9
-10	3.5	2.7	2.1
-20	1.7	1.2	0.9

This ratio, expressed as a percentage, is tabulated in Table I; from these values, it is clear that the reduction is but a small fraction ($< 6\%$) of the increase. Although accretion reduces the sublimational component of growth (by increasing the surface temperature of the particle), this reduction is negligible compared to the increase in growth rate due to the accretion itself. Therefore, in computing total growth rates, one is justified in calculating and simply adding the two components, sublimational and accretional, as if they were independent. The same treatment is justified when the radial growth rates are used, as will be shown in the next section.

3. DENSITY OF THE GROWING PARTICLE.

The density of the particle is of importance in determining its terminal speed and hence collection efficiency. Particle density may vary during growth as material of different density is added, either by sublimation or by accretion.

(a) Density of the Particle and of the Added Material.

Densities of hailstones are usually estimated to be of about 0.7-0.8 (see e.g. Weickmann, 1953). Densities of graupel have been measured by Nakaya (1954) who reports a value of 0.125, invariant with particle diameter (which ranged from about $1\frac{1}{2}$ to 6 mm). Magono (1954), theorizing on the terminal speed of graupel, finds agreement with observed values when the density is of that order, but he presents a diagram (fig. 2) showing a marked variation of density with size. Apart from this variation, fig. 2 is noteworthy for the low densities of the smallest particles.

That the density of the accreted material is dependent upon the ambient temperature and liquid water content is suggested by riming data of Clark (1948) and by the results of wind tunnel experiments by Melcher (1951) (as quoted by Weickmann, 1953). Also Reynolds (1879) considered the "packing" of the accreted droplets to be dependent upon the velocity of impact. Generally speaking, the warmer the temperature, the higher the liquid water content and the higher the velocity of impact, the denser is the accreted material. Thus, for the smaller particles on which accretion is just beginning, a relatively low density of accreted material is reasonably to be expected; with increasing size and fall speed, this density should increase, as Magono's data do indeed indicate. Furthermore, if particle growth continues to any reasonable size, the density of the particle will approach closely that of the added material (as will be shown in sec 3(c)). Thus, the observed density of graupel may be considered to be indicative of that of the collected material.

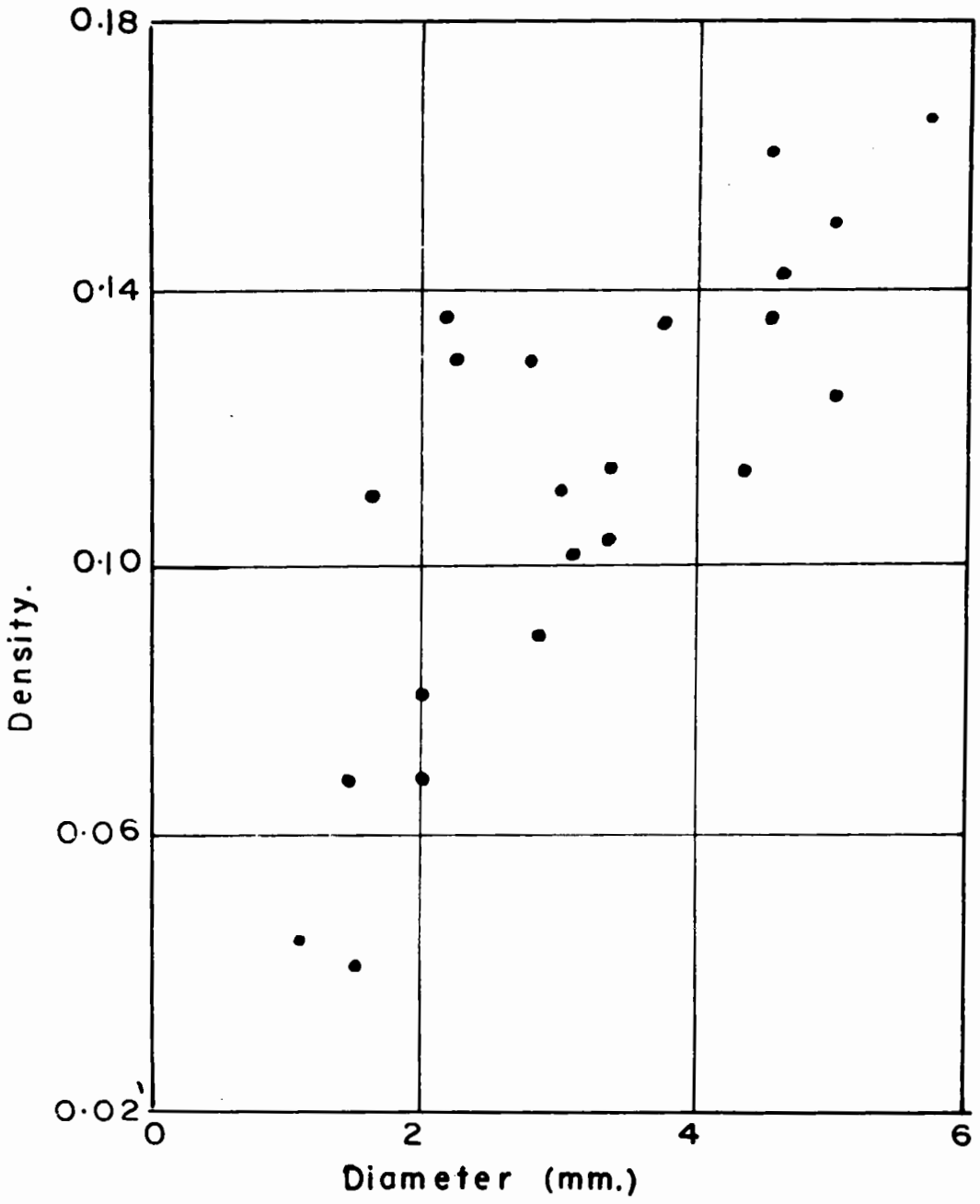

FIG. 2. Observed densities of graupel (after Magono, 1954).

Although the density of bulk ice is 0.9, that of the sublimed material may be somewhat lower, due to the porous needle-like or dendritic form of growth. According to Magono (1954) needles have a density of about 0.15. Thus, the density of the material added to the particle, whether by accretion or by sublimation, may be of rather low density. For the purposes of the present calculations, 0.2 was taken as the density of the accreted material; values of both 0.2 and 0.9 were used for the density of the sublimed material.

(b) Effective Density.

If material of density σ_s is sublimed onto a spherical particle of radius S at a rate $(dm/dt)_s$, then

$$(dS/dt)_s = (4\pi\sigma_s S^2)^{-1}(dm/dt)_s$$

A similar expression holds for accretion, the density of accreted material being σ_A. The total growth rates may be defined by the following equations:

$$(dm/dt)_T = (dm/dt)_s + (dm/dt)_A$$

and

$$(dS/dt)_T = (dS/dt)_s + (dS/dt)_A$$

and furthermore,

$$(dS/dt)_T = (4\pi\sigma_T S^2)^{-1}(dm/dt)_T$$

where σ_T is the net or "effective" density of the material acquired by both sublimation and accretion occurring simultaneously. From the above equations, it follows that

$$\sigma_T = (1 + \alpha\beta)(1 + \beta)^{-1}\sigma_s \qquad (3.1)$$

where $\alpha = (\sigma_A/\sigma_s)$ and $\beta = (dS/dt)_A(dS/dt)_s^{-1}$.

In terms of <u>radial</u> growth rates, it can be shown (as in sec. 1) that the total rate is the sum of the purely sublimational rate (in the absence of accretion) <u>plus</u> the accretional growth rate <u>less</u> a reduction due to accretion; the ratio R_S of the reduction to the increase (analogous to the ratio R_M of the preceding section, where mass growth rates were considered) is

$$R_S = (\sigma_A/\sigma_T)R_M = \alpha(1+\beta)(1+\alpha\beta)^{-1}R_M \quad (3.2)$$

It follows that $R_S \leq R_M$ for any value of β, provided that $\alpha \leq 1$, which condition applies in the growth calculations which follow. Thus, referring to Table I, it is clear that there is as much, if not more, justification for neglecting the small decrease in growth rate due to the accretional inhibition of sublimation in the case of radial as there is for mass growth rates.

(c) Density Changes of a Growing Particle.

If, to a spherical particle of radius S, mass dm is added uniformly at density σ_T, then $dm = 4\pi\sigma_T S^2 dS$. The increased mass is

$$m + dm = \frac{4\pi}{3}\sigma S^3 + dm$$

$$= \frac{4\pi}{3}\sigma S^3 + 4\pi\sigma_T S^2 dS.$$

But it is also

$$m + dm = \frac{4\pi}{3}(S + dS)^3(\sigma + d\sigma).$$

Equating these equivalent expressions, we find that

$$\frac{d\sigma}{\sigma_T - \sigma} = \frac{3dS}{S} ;$$

and integrating,

$$\sigma - \sigma_T = (\sigma_0 - \sigma_T)(S_0/S)^3 \qquad (3.3)$$

Thus, if a spherical particle of radius S_0 and density σ_0 grows to radius S by the addition of material of density σ_T, the particle density becomes σ, as defined by eq. (3.3). The change in the particle density can be rather rapid as growth proceeds; eq. (3.3) shows that the difference in density between the particle and the added material is reduced to 1/8 its original value when the radius is doubled.

For the purpose of growth calculations, σ_T can be determined from the densities of the accreted and sublimed material, together with the relative radial growth rates (eq. 3.1), and the variation of particle density computed from (3.3).

4. TERMINAL SPEEDS.

The terminal speed of the particle is of great importance to the growth rate by accretion, and is of some significance (through the ventilation coefficient) to growth by sublimation; it is therefore necessary to know the terminal speeds of particles over a wide range of densities. While considerable work has been done on the terminal speeds of water droplets (of unit density) there has been little attention paid to those of less dense particles.

Langmuir (1948) has published computations of terminal velocities of water droplets at 785 mb, -2C. From his paper (eqs. 19 and 21) it was determined that, for a given Reynolds number (which is the independent variable in his table 2), the appropriate particle radius is proportional to $\sigma^{-1/3}$, and the corresponding terminal velocity to $\sigma^{-1/3}$. Thus, each radius and its corresponding velocity in Langmuir's table was converted into a new radius and a new velocity for a number of particle densities; plots were made of terminal velocity versus particle radius for various densities from 1.0 to 0.1, and were used in the subsequent calculations.

5. THE DROPLET SIZE DISTRIBUTION.

A spherical particle of radius S, mass m, grows by the accretion of droplets of radius r at a rate given by:

$$dm/dt = \int_0^r \pi (S + r)^2 UEW(r)dr \qquad (5.1)$$

where $U = v_S - v_r$, the relative fall velocity of the particle with respect to the droplet; E = collision efficiency of the particle with respect to droplets of radius r; and W(r)dr = liquid water content contained by droplets of radius r to r + dr. Growth rates due to coalescence in CU have been treated at length by East (1957), who derived the appropriate droplet size distributions for CU of various liquid water contents; in the present work, East's distributions were used in the growth calculations in CU. Diem's (1948) distribution was used for altostratus (AS), and was considered independent of liquid water content. Separate calculations were

made for various particle densities (and hence various derived values of the parameters U and E of the above equation).

6. GROWTH CALCULATIONS.

Given the droplet size distribution and a specified particle density, the mass growth rates due to accretion were computed for a number of particle radii using a finite-difference form of eq. (5.1). These were converted into radial growth rates according to a specified density of accreted material. Calculations were made for particle densities of 0.9, 0.5 and 0.2, using the appropriate terminal speeds. The sublimational growth rates were likewise computed, and both sets of curves were plotted together. Addition of the rates provided three sets of total radial growth rates, one for each particle density. At every point along the total growth curves the ratio β (sec. 3) is known and, with σ_A and σ_S specified, α is a known constant; thus, a value of effective density σ_T can be calculated at every point along the growth rate curves. In this way, isopleths of σ_T were superimposed upon the growth rate curves.

Growth was begun with a particle of initial radius 20 μ and density 0.9, for which the total growth rate was determined from the graph. Growth was calculated stepwise; for each step, the appropriate value of σ_T was used. At the end of each step, eq. (3.3) was used to determine the new particle density. As the particle density decreased, growth rates were interpolated from the curves; for any given particle radius, log $(dS/dt)_T$ was found

to vary nearly linearly with S. At the same time, radial growth was converted into mass growth and the distance fallen was computed in steps, using terminal speeds appropriate to the mean particle density during the interval.

Fig. 3 shows the relevant growth curves in CU of density 1 gm m^{-1}; density of the sublimed material is 0.9 and of accreted material 0.2. Three curves sloping downward from left to right indicate the sublimational growth rates for particles of densities 0.2, 0.5 and 0.9; the difference in these curves is attributable to the ventilation factor, which is a function of terminal speed. The corresponding accretional growth rates are shown by the three curves sloping steeply upward from left to right. Addition of these two sets of curves yields the three total growth rate curves, which show pronounced minima. Thin dashed lines indicate the effective density σ_T. Finally, the actual growth rate of the particle itself is indicated (heavy dashed curve). A set of such curves was prepared for each computation.

Growth in AS was computed for liquid water contents of 0.1, 1.0 and 2.0 gm m^{-3}; density of the accreted material was taken as 0.2, and of the sublimed material 0.2 and 0.9. It was assumed that there was no updraft in the cloud.

The CU was modelled on the basis of conditions which have been observed to yield showers of graupel at Montreal. Cloud base and tops were taken at 910 mb, -1C, and 700 mb, -15C, respectively. Liquid water contents were computed on the basis of unmixed saturated

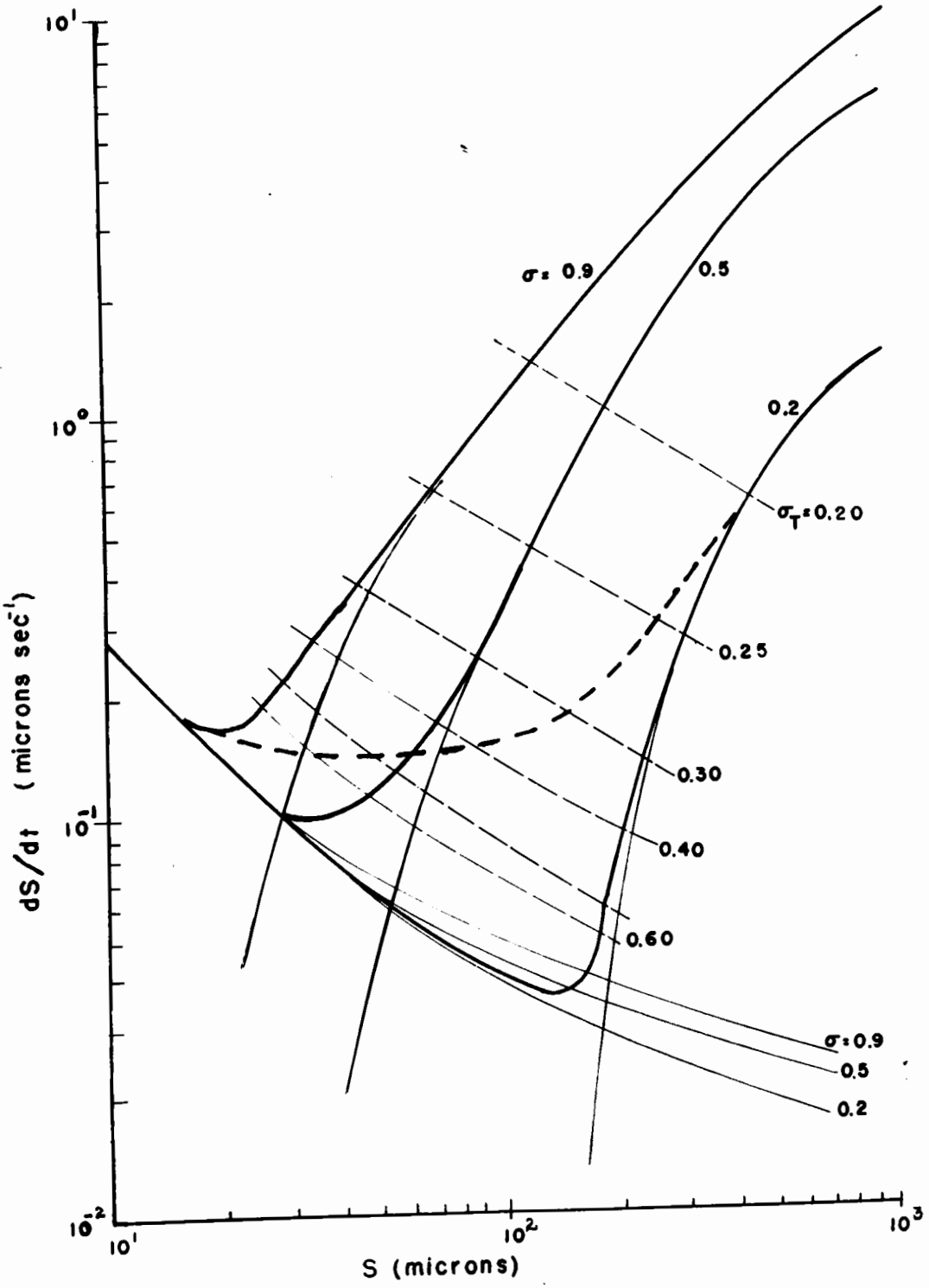

FIG. 3. Growth rate of a particle as a function of radius, in 1 gm m^{-3} CU, 700 mb, -15C. Densities of sublimed and accreted material are 0.9 and 0.2 respectively: curves are shown for particles of densities 0.9, 0.5, and 0.2. Curves sloping down from left to right are for sublimation alone; curves sloping upward from left to right are for accretion alone. Heavy curves show total growth rates, and heavy dashed curve shows growth rate of a particle of initial radius and density of 20μ and 0.9. Thin dashed lines indicate effective density σ_T .

(water) adiabatic ascent, which gave a cloud top density of about 2.7 gm m^{-3}. Accretional growth rates were based upon droplet size distributions derived by East (1957). Particle growth was begun in the cloud top, and no updraft was considered. In this particular case, the particle density and the densities of added water substance were all considered constant at 0.2, a choice which was made on the basis of the results obtained in the densest AS cloud, as will be discussed in a following section.

7. THE EFFECTIVE COLLECTION EFFICIENCY.

The mass growth rate of a particle by accretion is given by eq. (5.1), in which the integrand includes the collision efficiency E, which is a function of S, r, and U (and hence of density σ). In order to compare the accreting characteristics of particles of various densities in various types of cloud droplet distributions, it is useful to compute an "effective collection efficiency" E_s, defined by the equation

$$dm/dt = \pi S^2 v_s W E_s$$

i.e.
$$E_s = \frac{dm/dt}{\pi S^2 v_s W} = \frac{dm}{(\pi S^2 v_s dt)W}$$

= fraction of liquid water content, contained within the swept volume, which is accreted, or

= mass growth per unit swept volume per unit liquid water content.

Fig. 4 shows a plot of E_s as a function of S for particle densities of 0.2, 0.5 and 0.9, in AS and in CU of 1.0 and 4.0 gm m^{-3}. Discussion of these curves is reserved for sec. 8.

8. RESULTS OF GROWTH CALCULATIONS.

(a) The Effective Collection Efficiency.

The effective collection efficiency E_S incorporates the effects of droplet size distribution and of terminal speeds. Following the initial increase from zero, it shows a tendency to level off before increasing again to a maximum value; this levelling-off appears consistently in nearly all the curves of fig. 4, and shifts to higher particle radii at lower particle densities.

The term EW(r)dr in the integrand of eq. (5.1) increases steadily as S increases. The mean collection efficiency, defined by $(1/W)\int_o^r EW(r)dr$, behaves likewise. The ratio of the effective efficiency to this mean efficiency involves the ratios (a), $\left[1 + (r/S)\right]^2$ and (b), $\left[1 - (v_r/v_S)\right]$; the former decreases, the latter increases, as S increases. At low particle radii (a) decreases rapidly compared to the increase in (b), but since E is also increasing rapidly, the effective efficiency E_S increases. At large particle radii both (a) and (b) are slowly approaching unity, so that E_S is increasing at about the same rate as E. At intermediate particle radii, however, the rapid decrease with S of (a) is comparable to the joint increases in E and in (b),

particularly beyond the range of Stokes' Law, where the particle terminal speed becomes proportional to a decreasing power of S. The net effect is a decline in the rate of increase of E_S over a limited range of S, as shown in fig. 4.

In any specified cloud, the denser particle is the more effective collector; collection efficiency improves with particle radius, approaching a maximum value. However an extension of the curves of fig. 4 to radii beyond 1000μ would undoubtedly show a decrease in E_S (which is in fact already evident in the uppermost curves of the figure); such a decrease at large radii is evident in Langmuir's (1948) table 4 and in Hitschfeld and Gunn's (1951) fig. 1.

The effects of variable particle density can be seen by an inspection of fig. 4. For example, if a particle of initial density 0.9 grows to double its size through the addition of material of density 0.1, its density is reduced to 0.2; this will reduce the effective collection efficiency substantially, particularly at low radii and in thin cloud, where it may in fact eliminate accretion entirely. Thus, the reduction of particle density serves as a powerful inhibition to accretion. Conversely, an increase in particle density will increase the collection substantially.

The effective collection efficiency is less sensitive to changes in particle density for large dense particles than for small light ones. Thus, a large dense particle (of radius about 1mm and density in excess of 0.5) is more apt to maintain a high collection rate than a smaller lighter one.

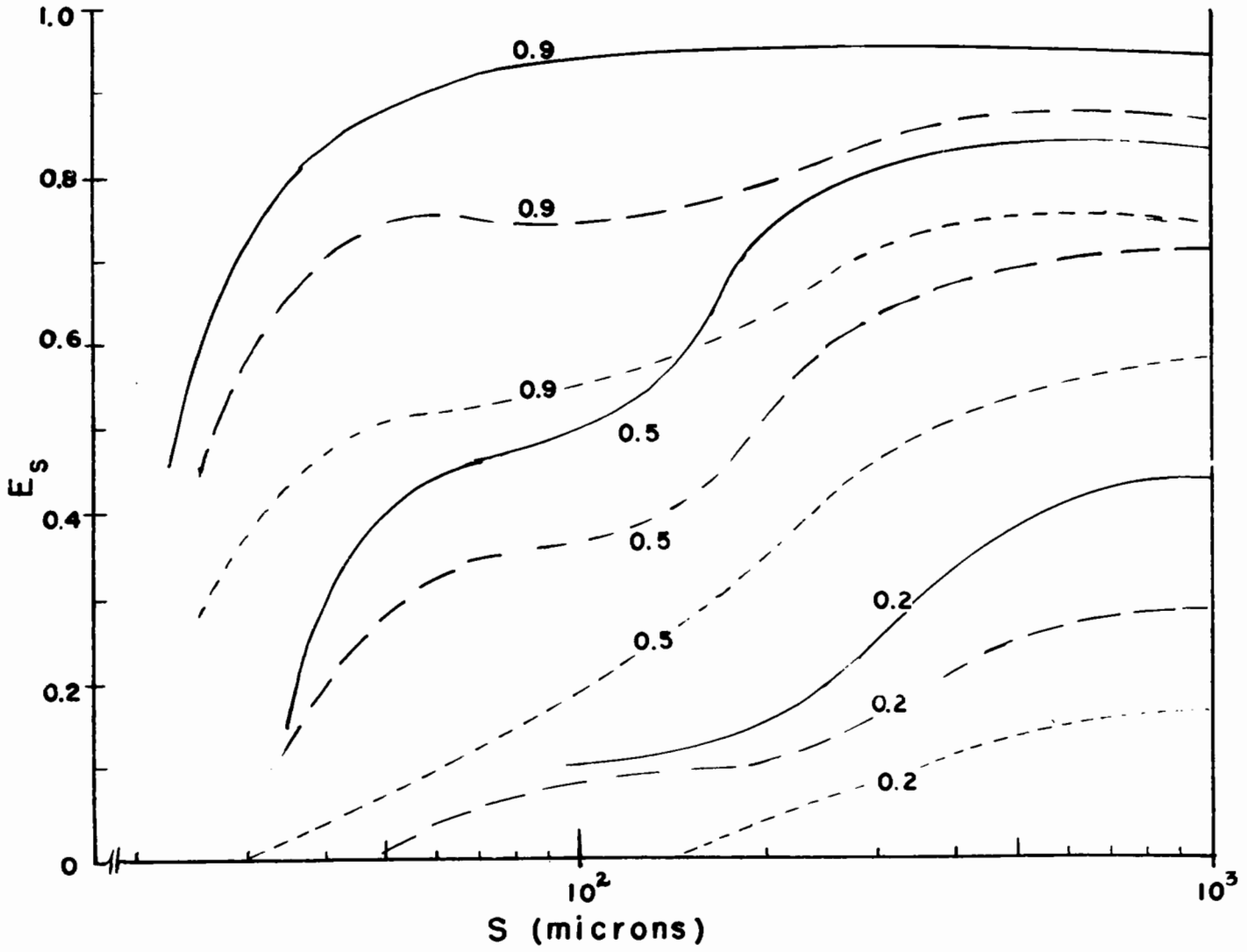

FIG. 4. Effective collection efficiency as a function of radius, for spherical particles of densities 0.9, 0.5 and 0.2. CU, 4 gm m^{-3} ____; CU, 1 gm m^{-3} _ _ _; AS ___.

(b) Growth by Sublimation and Accretion.

Fig. 5 shows the results of the growth calculations, plotted as mass versus time. Radii of the spherical particles and the vertical distances fallen (assuming no vertical air motion) are marked along the curves.

Curves A and B are for sublimational growth alone, at 700 mb, -15C, using two densities of the sublimed material (0.9 and 0.2, respectively). The reduced density not only improves the radial growth as mass is added, but improves the mass growth rate itself, which is proportional to the radius. After about 10 minutes' growth, the mass of the lighter particle remains roughly 3 times that of the denser one, with a corresponding improvement in radius.

Curves C and D show growth in 0.1 gm m^{-3} AS; in both cases accretion is at density 0.2, but sublimation is at 0.9 in the former and 0.2 in the latter case. Curves C and D, compared with A and B respectively, indicate the improvement in growth due to the cloud. With the high density sublimation, the improvement is substantial, but with the low density sublimation it is not particularly noteworthy; terminal speeds at low density are too low to permit any substantial accretion.

However, as cloud density increases to 1 gm m^{-3} (curves E and F) a marked improvement occurs after 10-15 minutes' growth, but it is apparent now that in cloud of this water content the effect of variation of density of sublimed material is almost

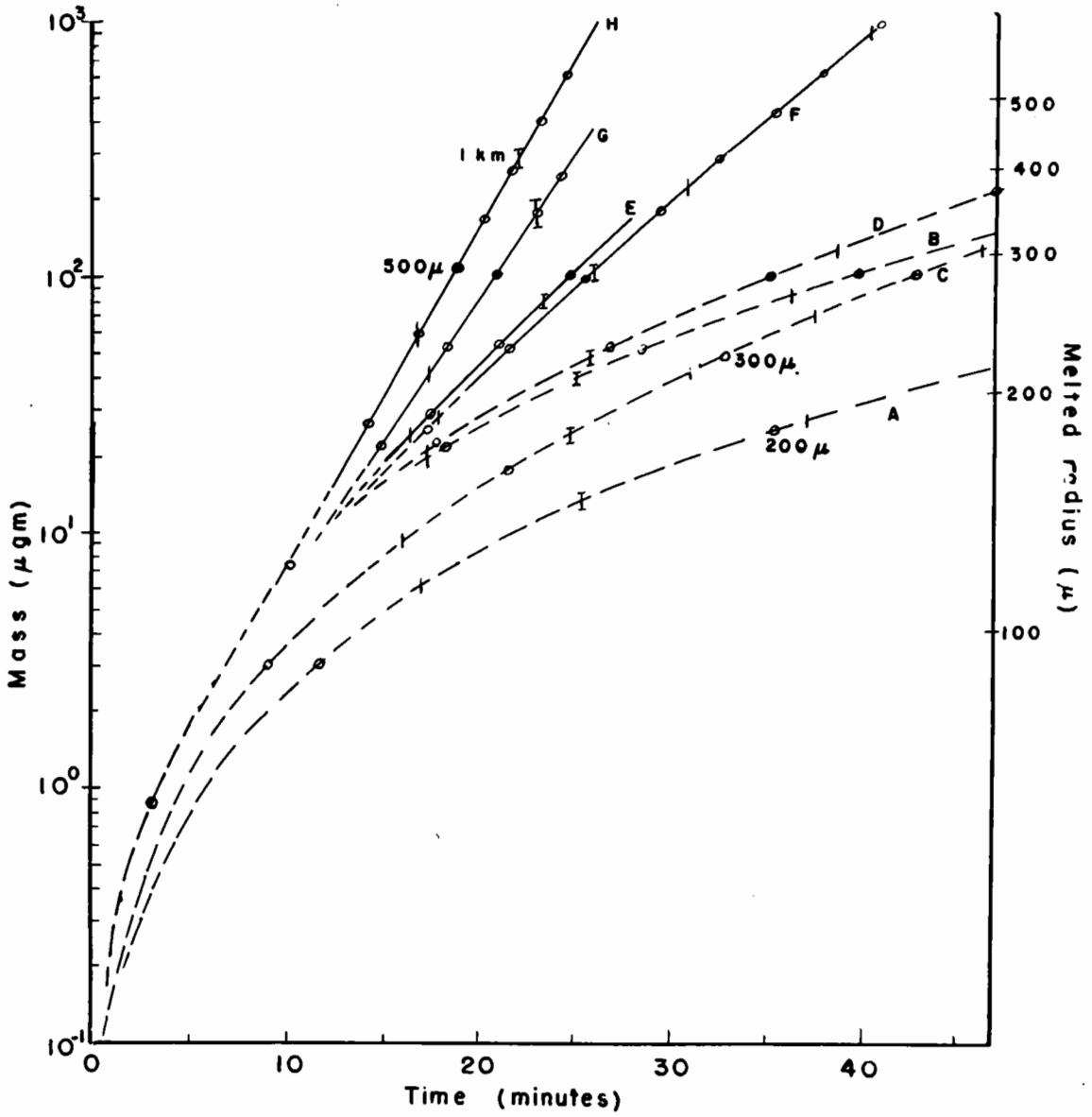

FIG. 5. Growth of spherical particles from radius 20μ.
Sublimation alone; A, $\sigma_s = 0.9$; B, $\sigma_s = 0.2$.
Sublimation and accretion:
C, in 0.1 gm m^{-3} AS, $\sigma_s = 0.9$, $\sigma_A = 0.2$.
D, same as C, but $\sigma_s = 0.2$.
E, in 1.0 gm m^{-3} AS, $\sigma_s = 0.9$, $\sigma_A = 0.2$.
F, same as E but $\sigma_s = 0.2$
G, 2 gm m^{-3} AS, $\sigma_s = \sigma_A = 0.2$.
H, in model CU, $\sigma_s = \sigma_A = 0.2$.
Particle radii indicated (circles) at 100μ intervals, 500μ radius indicated by solid circle. Distances fallen ($\frac{1}{2}$, 1, 2 etc. km) indicated by vertical marks, the 1 km mark being thus (I).

insignificant; accretion, playing a more prominent role, rapidly nullifies the high density sublimation, and particles in both cases have very nearly the same density after the first minute or so. The effect of a further increase in cloud content (AS of 2 gm m^{-3}) is shown by curve G, which was computed on the basis of a density throughout of 0.2 for the particle and the added material; in view of the similarity of curves E and F, and of the rather rapid reduction in particle density as light material is both accreted and sublimed, curve G is probably representative of any initial particle density and any density of sublimed material.

Particle growth in the model CU is shown by curve H. The liquid water content is variable, but growth to 1000μ radius occurred in the top 1.5 km of the cloud in which the liquid content was about 2 gm m^{-3}. Thus, curves G and H serve to compare the effect of the droplet distribution in CU with that in AS, cloud densities being roughly equal. While CU proves to be a better environment, the difference is not marked, since similar masses and radii are reached in times which differ from one another by less than 5 minutes.

(c) Predominant Mode of Growth.

The total mass growth rate is effectively the sum of the mass growth rates due to sublimation and to accretion. The fraction (of the total rate) due to sublimation alone is shown as a function of particle radius in fig. 6; the curves correspond to those similarly lettered in fig. 5. In relatively dense cloud (curves

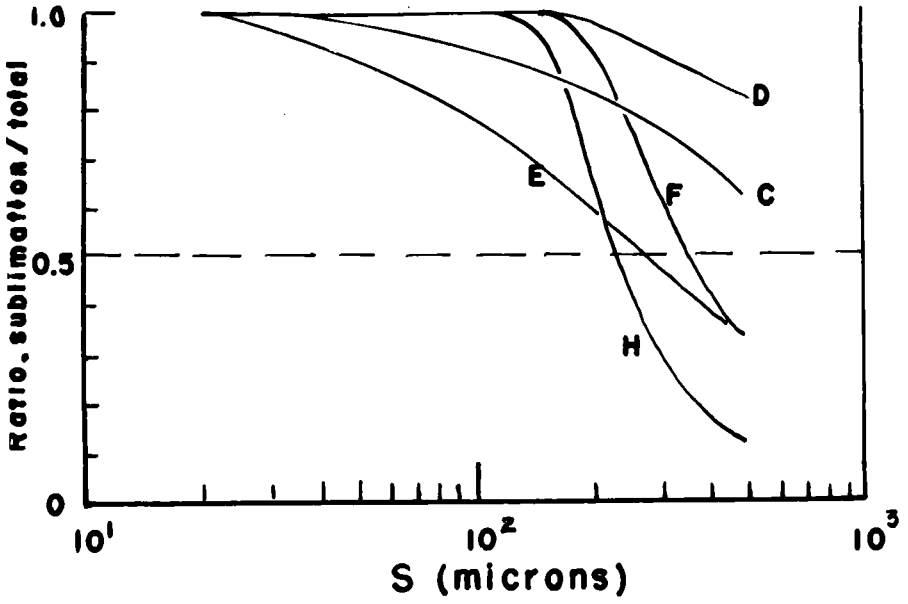

FIG. 6. Ratio of sublimational mass growth rate to total growth rate, as a function of particle radius. Letters indicate same conditions as in Fig. 5.

E, F and H) accretion becomes predominant at a much earlier stage than in thin cloud, the shift toward accretional predominance being particularly sudden in the cases of low density sublimation (F and H). With the density of the particle diminishing, the effective collection efficiency remains near zero until radii of 100-200μ are reached, when it improves more or less steadily with radius. In dense cloud sublimation predominates during the first 10-20 minutes of growth (to 200-400μ). The effect, in dense cloud, of high density sublimation (curve E) is to introduce accretional growth at a fairly early stage, since the particle density (and hence its terminal speed) remains high for a longer period of time. In thin AS (0.1 gm m^{-3}), however, sublimational mass growth predominates to radii well beyond 500μ.

9. SUMMARY AND CONCLUSIONS.

Sublimation and accretion, occurring together, are not independent, since the heat of fusion involved in the latter process acts to reduce the former. The reduction to sublimational growth, however, is a sufficiently small fraction of the accretional growth that little error is involved in assuming the processes to operate independently and additively. This assumption has been implied, without proven justification, in various published papers; that this assumption is a reasonable one is now recognized.

The effective collection efficiency is highly dependent upon particle density, which in turn depends upon the densities of the material added by the two processes, sublimation and accretion; it is also dependent upon droplet size distribution in the cloud, being greater in CU than in AS, and being greater in denser CU. If both sublimed and accreted material are of low density, the particle density (originally 0.9 for a frozen particle) is rapidly reduced, and the collection efficiency with it; even when dense material is sublimed, both particle density and collection efficiency decline as the particle grows, increasing again only when the particle has achieved its minimum density. If, for any reason, the particle density increases (as it might if material were accreted at high density due to some combination of increased terminal speed, high liquid water content, and relatively warm temperature) then the collection efficiency would increase; this

might occur when graupel, grown originally at low density, finds itself in very dense CU, where rapid high density accretion might be expected to result in hailstone development. With a large enough particle, a substantial variation in particle density (between 0.9 and 0.5) will have very little effect upon its collection efficiency; this is true for somewhat smaller particles in CU than in AS.

With sublimation alone, and with sublimation coupled with accretion in thin cloud (0.1 gm m^{-3} AS), growth is sensitive to the density assumed for the sublimed material; a low density is more favorable to mass growth (the rate of which is proportional to radius, which increases more rapidly at low density). In such a case the particle density (initially 0.9) is reduced rapidly to a low value, terminal speed and collection efficiency are both kept low, and growth is completely sublimational until a radius of about 150μ is achieved. Even then sublimation contributes more than accretion to the growth rate until radii in excess of 300μ are reached in dense cloud, and in excess of about 1000μ in thin cloud.

The present results (for 1.0 gm m^{-3} AS) may be compared with Houghton's (1950), in which he compared sublimational dendritic growth with coalescent growth. Considering the former at -15C and the latter in NS of 1.0 gm m^{-3}, Houghton found equality of growth-rates at a particle mass of about 10-20 μgm, corresponding to a droplet radius of about 130μ; this finding agrees reasonably well with the corresponding radius (melted) of about 200μ, and mass of about 25 μgm, found in the present study.

If a particle leaves the parent cloud before accretion has become the predominant growth process, then it will arrive essentially as a sublimation product; on the other hand, if it has remained within the cloud long enough to have grown significantly by accretion, it will emerge as a particle of graupel. The radii beyond which growth must occur to become predominantly accretional can be obtained from fig. 6. From these curves, together with those of fig. 5, we see that, in thin AS, a graupel-like particle can emerge only from a very deep layer of cloud (over 4 km if sublimation is of high density, and almost double that if of low density); even with vertical air motion of 10 cm sec^{-1}, the required depths of AS are only reduced by about 7%. Furthermore, these cloud depths are minimal. Thus, in AS with the usual rather low liquid water content, an unlikely depth of cloud is necessary for the precipitation of graupel.

On the other hand, dense cloud (1.0 gm m^{-3} or greater) can apparently produce graupel, whose radii exceed 200-300μ, from a cloud depth as little as $\frac{1}{2}$ km, and it would appear that graupel should be of rather common occurrence in cold CU, particularly in view of the fact that no cloud updraft has been considered in the present computations. However many cold CU produce showers of snow rather than of graupel, indicating the predominance of sublimation over accretion. This may be attributed in part to the rather lower densities of graupel than have been used in the calculations. Fig. 4

indicates that the effective collection efficiencies of particles of densities much less than 0.2 will remain at zero until a very substantial radius is achieved. But Magono (1954) reports observations of low density particles with radii as low as 500μ, (fig. 2), suggesting that accretion became predominant at much lower radii. It is not known what meteorological conditions attended the precipitation of these particles, but it seems unlikely that the cloud density could have been high enough to produce them if they grew as spheres. On the other hand the initial particle may have been a crystal with collection characteristics superior to those of a low density sphere. Nakaya (1954) notes that plates and dendrites are frequently the primary particles on which accretion occurs, observing a progressive evolution from the pure crystal through a rimed type to an accretion element. While a dendrite has a rather lower terminal speed than a sphere of like radius, and so sweeps out a lesser volume per unit time, the slim dendritic branches are probably relatively efficient collectors. The net result may be that the dendrite accretes more efficiently than a spherical particle of low density but requires a much greater depth of cloud than the spherical particles of density 0.2 which have been considered here. In other words, if the primary growth is plane dendritic rather than spherical, then graupel can probably only appear, even from CU, provided that a rather greater cloud depth than indicated in fig. 5 is available. On the other hand, the appearance of graupel can be taken as evidence of cloud densities

which are more likely with CU than with stratiform cloud, serving as evidence of the presence of a convective cloud type. In a snow generating cell, embedded in AS of relatively low liquid water content, sublimation will be the predominant mode of growth.

Considering warmer CU in the light of these findings, reference is made to the work of MacCready, Smith, Todd and Beesmer (1956), who have computed times of growth to 50μ radius of spherical ice particles (by sublimation, after Houghton, 1950) and of droplets (by condensation-coalescence, after East, 1957). They show that in "cold" cloud (base temperature below about +12C) ice crystal growth to 50μ is more rapid than droplet growth. Assuming, as the authors did, a density of unity for the ice particle, then the ice particle will become a more efficient collector than the droplet, and will grow more rapidly by accretion. In warm cloud the trend is reversed and coalescence leads the ice process, although in the higher levels of the cloud the ice process and accretion may remain dominant. With lower particle densities, however, the findings of MacCready et al must be modified, since accretional growth will be reduced. If accretion is to assume predominance, with a low density particle involved, then the primary crystal growth by sublimation must outstrip the initial growth of droplets, so that the particle can reach an efficient size for accretional growth before the droplet does. Of two spherical particles growing by sublimation, the one acquiring the less dense material will grow the more rapidly, as shown by

curves A and B, fig. 5; the accretional growth rate of the lighter particle (proportional to $S^2 v_s E_s$) may reach a value in excess of that of a smaller water droplet. A rough calculation indicates that a 75μ particle of density 0.5, in cloud of 4 gm m^{-3}, grows slightly more rapidly by accretion than a 50μ droplet. This suggests that, with low density sublimation, the ice process may operate more rapidly, and may predominate at slightly warmer cloud temperatures, than indicated by MacCready et al.

If, however, the particle retains a high density until accretion begins, and then collects light material, its mass growth rate can only exceed that of a 50μ droplet when it has achieved a rather large radius; if the ice process is to dominate, the primary sublimational growth rate must be somewhat in excess of that of the droplet. This implies a lowering of the cloud temperature suggested by MacCready et al as the boundary between the all-water and the ice processes. A closer examination of the effects of low density accretion upon the above-noted calculations is warranted, since it may shed some light upon the problem of why, from so many well-developed cumuli and cumulonimbi, graupel and hail fail to make an appearance at the ground.

PART FOUR

SUMMARY

PART IV: SUMMARY

The earlier findings of Gunn et al (1954) regarding a snow-generating level in stable air, related to a frontal surface, have been confirmed by the study reported in Part I. For the 14 cases which were examined (as for the 10 of the earlier study), the particular front to which the generating level was most often related was the Maritime front, the cells tending to appear within the lowest one-fifth of the mP air mass. Cells occurred over a wide range of heights and of temperatures.

Estimations of the terminal speed of the particles constituting the snow trails were made by the suitable application of trail geometry, as described by Marshall (1953) and as applied by Langleben (1954) for the same purpose, as well as by fitting derived patterns to the observed ones; present calculations confirm Langleben's findings, viz., that the particle speeds are appropriate to aggregate snowflakes rather than to single crystals. With regard to these determinations, a notable deficiency of the zenith-pointing radar is disclosed, i.e. that the speeds derived from the observed radar pattern are sensitive to the orientation of line arrays of generating elements. On this basis, the rather high terminal speeds derived by the present technique are explained as the result of a broadening of the true range of velocities due to random orientations.

The zenith-pointing radar reveals strikingly the occurrences of stalactites, which occur when snow falls from aloft into a dry stratum. These are attributed to the descent of chilled snow-filled air, in which no secondary snow generation need occur.

About half the storms studied displayed a lack of radar pattern during the last few hours of snowfall, during which time the echo top gradually subsided. This may be attributable to a continually decreasing intensity of cell-generated snow, or to an entirely different snow generating process, involving perhaps the relatively slow growth of crystals throughout an ascending air mass at vapor contents but slightly in excess of ice equilibrium.

In part II, certain consequences of the growth of ice crystals in moist air are examined. The latent heat of sublimation, released into an air parcel during crystal growth, results in vertical ascent which is comparable in magnitude to the observed depths of snow-generating cells. The initial presence of water cloud contributes but negligibly to the height of ascent. Vertical velocities comparable to the terminal speeds of the ice crystals, or even of aggregate snowflakes, may result as crystal growth injects heat of sublimation into the air. The presence of water cloud inhibits the updraft velocity, as also does aggregation.

Sublimation within water cloud may deplete the cloud water in spite of the resupply by ascent. Variations in water

content and in ice crystal content within a cloud may result in unequal desiccation and the appearance of new internal cloud boundaries; across such boundaries, differing updraft velocities will produce shear and turbulence, favorable for aggregation. Such a boundary, it is suggested, may constitute the snow-generating cell. Such cells serve to process the parent water cloud into precipitable snow. On this basis, the classical theory of precipitation rates is an unsatisfactory one, at least insofar as cellular snow generation is concerned.

Radar reveals that the cell process is not the only one to produce snow. It may be that the rather featureless homogeneous type of snow echo, as seen by radar, is due to non-cellular growth in slowly ascending air in which the vapor content remains but little above ice equilibrium. If this is the case, and if the cell theory presented above is reasonable, then one might expect the snowfall from the non-cellular process to be non-aggregated, as opposed to a predominantly aggregated snowfall from cells; a study of simultaneous records of snow type and of radar echo type would be useful in this regard.

Part III deals with the growth, by accretion and sublimation simultaneously, of spherical particles of various densities. It is found that the assumption, implied by various investigators, that sublimation and accretion may be considered independently, is a valid one; although accretion tends to reduce the sublimational growth rate, the reduction is negligible by

comparison with the accretion itself. The effective collection efficiency is highly dependent upon particle density, which depends in turn upon the density of the material sublimed or accreted. Reduction of particle density, due to accretion of low density material, results in a substantial reduction of collection efficiency, and may in fact reduce it to zero.

Growth of spherical particles (with initial radius and density 20μ and 0.9) was computed in several types of cloud, making allowance for the variations in particle density. For sublimation alone, and for sublimation-accretion in cloud of low liquid content (0.1 gm m^{-3}), growth is sensitive to the density of the sublimed material. In denser cloud (1.0 gm m^{-3}) in which accretion plays a greater role, the particle density is rapidly reduced toward that of the accreted material, even when sublimation is at high density. Thus, in dense cloud, accretion exercises the major control over the particle density, and hence over the collection efficiency.

In 0.1 gm m^{-3} altostratus, particle growth is predominantly sublimational until radii in excess of about 500μ are achieved; this growth requires rather deep layers of cloud, even with reasonable vertical motion, and so it seems unlikely that graupel can develop in altostratus of reasonable depth and water content, or in a snow generating cell. In denser cloud, such as sumulus, low density graupel of radius exceeding a few hundred microns would require but a modest cloud depth of the order of $\frac{1}{2}$ km. It

is suggested that the failure of many cold cumuli to produce such accretion elements may be due, at least in part, to particle densities even lower than the value of 0.2 which was taken as the minimum in the present study. On the other hand graupel of density as low as 0.03 has been observed; this may be due to accretion by dendritic crystals rather than spheres. It seems likely that the cloud contents necessary for accretion elements are more likely with cumulus than with stratiform cloud, so that the precipitation of graupel can be taken as evidence of instability.

If, within a cloud mass, the all-water process of condensation-coalescence runs ahead of the sublimation-accretion process, the latter will be inhibited as the cloud content precipitates out as rain. If however the ice process takes the lead, the cloud content will be precipitated mainly in the form of accretion elements. Calculations relevant to this aspect of the precipitation problem have been made by MacCready et al (1957), but for accretion particles of density unity; similar computations for particles of lower densities should be undertaken, and may be expected to shed some light on the conditions favoring the precipitation of graupel or hail, rather than of rain, from various levels within the cloud mass.

REFERENCES.

REFERENCES

Anderson, R., B.W. Boville and D.E. McClellan, 1955: An operational frontal contour analysis model. Quart. J. Roy. Meteor. Soc. 81, 588-599.

Appleman, H., 1954: Design of a cloud-phase chart. Bull. A. Meteor. Soc. 35, 223-225.

Atlas, D., 1956: The origin of stalactites in precipitation echoes. Proc. 5th Wea. Radar Conf. (Asbury Park, Sept. 1955), Belmar, Evans Signal Labs., 321-328.

Bannon, J.K., 1948: The estimation of large-scale vertical currents from the rate of rainfall. Quart. J.R. Meteor. Soc. 74, 57-66.

Browne, I.C., 1952: Precipitation streaks as a cause of radar upper bands. Quart. J. Roy. Meteor. Soc., 78, 590-595.

Byers, H.R. and R.R. Braham, 1949: The thunderstorm, Washington D.C. (U.S. Dept. of Commerce).

Clark, V., 1948: Icing nomenclature. Harvard-Mt. Washington Icing Res. Rep. 1946-1947, Air Force Tech. Rep 5676, pp 415-481.

Diem, M., 1948: Messung der Grösse von Wolken-elementen II, Meteor. Rundschau, No. 9/10, 261-273.

Dobson, G.M.B., and A.W. Brewer, 1951: Water vapour in the upper air. Compendium of Meteorology, Boston (A. Meteor. Soc.), 311-319.

East, T.W.R. and J.S. Marshall, 1954: Turbulence in cloud as a factor in precipitation. Quart. J.R. Meteor. Soc. 80, 26-47.

East, T.W.R., 1957: An inherent precipitation mechanism in cumulus clouds. Quart. J.R. Meteor. Soc. 83, 61-76.

Godson, W.L., 1951: Synoptic properties of frontal surfaces. Quart. J. R. Meteor. Soc. 77, 633-653.

Gunn, K.L.S., M.P. Langleben, A.S. Dennis and B.A. Power, 1954: Radar evidence of a generating level for snow. J. Meteor. 11, 20-26.

Gunn, K.L.S. and J.S. Marshall, 1955: The effect of wind shear on falling precipitation. J. Meteor. 12, 339-349.

Gunn, R. and G.D. Kinzer, 1949: The terminal velocity of fall for water droplets in stagnant air. J. Meteor. 6, 243-248.

Hewson, E.W., 1948: Dissipation of scattered and broken cloud. Quart. J.R. Meteor. Soc. 74, 243-265.

Hitschfeld, W. and K.L.S. Gunn, 1951: A laboratory investigation of the coalescence between large and small water drops. J. Meteor. 8, 7-16.

Hosler, C.L., D.C. Jensen and L. Goldshlak, 1957: The aggregation of ice crystals to form snow. Paper presented at 150th nat. meeting A. Meteor. Soc., New York, Jan. 1957. (Abstract, Bull. A. Meteor. Soc. 37, 540).

Houghton, H.G., 1950: A preliminary quantitative analysis of precipitation mechanisms. J. Meteor. 7, 363-369.

Howell, W.E., 1949: The growth of cloud drops in uniformly cooled air. J. Meteor. 6, 134-149.

Jensen, D.C., 1956: On the cohesion of ice. Penn. State Univ. (contract NSF-G1340).

Kuettner, J., 1950: The electrical and meteorological conditions inside thunderclouds. J. Meteor. 7, 322-332.

Langleben, M.P., 1954: The terminal velocity of snowflakes. Quart. J.R. Meteor. Soc. 80, 174-181.

_____ , 1956: The plan pattern of snow echoes at the generating level. J. Meteor. 13, 554-560.

_____ , 1957: Snow pattern revealed by constant-altitude maps. Proc. 6th Wea. Radar Conf. (Boston, March 1957), 89-98.

Langmuir, I., 1948: The production of rain by a chain reaction in cumulus clouds at temperatures above freezing. J. Meteor. 5, 175-192.

Lewis, W., 1951: Meteorological aspects of aircraft icing, Compendium of Meteorology, Boston, (A. Meteor. Soc.), 1197-1203.

L'hermitte, R., 1952: Les "bandes superieures" dans la structure verticale des echos de pluie. Compt. rend. acad. sci. 235, 1414-1416.

Ludlam, F.H., 1950: The composition of coagulation-elements in cumulonimbus. Quart. J.R. Meteor. Soc. 76, 52-58.

Ludlam, F.H., 1956: The forms of ice clouds II. Quart. J. R. Meteor. Soc. 82, 257-265.

Magono, C., 1953: On the growth of snow flake and graupel. Sci. Rep., Yokohama Nat. Univ., Sec. I, No. 2, 18-40.

Magono, C., 1954: On the falling velocity of solid precipitation elements. Sci. Rep., Yokohama Nat. Univ., Sec. I, No. 3, 33-40.

Marshall, J.S., 1953: Precipitation trajectories and patterns, J. Meteor. 10, 25-29.

_____, and M.P. Langleben, 1954: A theory of snow crystal habit and growth. J. Meteor. 11, 104-120.

Mason, B.J., and F.H. Ludlam, 1951: Microphysics of clouds. Rep. on Prog. in Physics 14, 147-195.

Melcher, D., 1951: Experimentelle Untersuchen von Vereisung-serscheinungen. Zeits. fur angew. Math. u. Phys. II, p 421.

Möller, F., 1951: Thermodynamics of clouds. Compendium of Meteorology, Boston (A. Meteor. Soc.), 199-206.

Nakaya, U., 1954: Snow crystals, natural and artificial. Cambridge, Harvard, U. Press, 510 pp.

Penner, C.M., 1955: A three-front model for synoptic analysis. Quart. J.R. Meteor. Soc. 81, 89-91.

Pettit, K.G., 1954: The characteristics of supercooled clouds during Canadian icing experiments, 1950-53. Proc. Toronto Met. Conf., London (R. Meteor. Soc.), 269-275.

Reynolds, O., 1879: On the manner in which raindrops and hailstones are formed. Mem. Lit. and Phil. Soc. Manchester, 3rd ser., VI, 161-170.

Scorer, R.S. and F.H. Ludlam, 1953: Bubble theory of penetrative convection. Quart. J.R. Meteor. Soc. 79, 94-103.

Soane, C.M. and V.G. Miles, 1955: On the space and time distribution of showers in a tropical region. Quart. J. R. Meteor. Soc. 81, 440-449.

Weickmann, H., 1953: Observational data on the formation of precipitation in cumulonimbus clouds. (Chapt. V in: Thunderstorm Electricity, Chicago, Univ. of Chicago Press, 66-138).

Wexler, R., 1953: Radar echoes from a growing thunderstorm, J. Meteor. 10, 285-290.

APPENDICES.

APPENDIX A

MODIFICATION OF THE SHEAR HODOGRAPH

In sec. 5 of Part I, equations (5.4), (5.4a) and (5.5) are presented as the basis of modification of the shear hodograph; their use is most easily illustrated with reference to a simple example.

In fig. 1 is shown the portion of a hodograph from 4 to 9000 ft (heavy lines), indicating cold air up to 6000 ft, above which lies a hyperbaroclinic (H-) layer to 7000 ft, with warm air above. It is required to determine the form of the wind field above a nearby station at which the frontal boundaries are 1000 ft higher.

Dealing with the upper surface first, at 7000 ft, the x- and y-axes are aligned in accordance with eq. (5.5) of Part I (fig. 2), orientation being such that the perpendiculars onto the y-axis from the 6 and 8000 ft points are of equal length and on opposite sides; the x-axis is perpendicular to the y-axis, directed into the cold air, i.e. to the left of the general shear vector through the layer. The y-components of the shears from 6 to 7000 ft and from 7 to 8000 ft give the values of Δv_H and Δv_W, respectively. Care must be taken in assigning the proper sign to these shears which, in the present example, are both negative; their values, in the present case, are respectively -20 and -2 arbitrary units. Thus, $\Delta v_W - \Delta v_H = 18$ units.

The front is to be raised to 8000 ft, so the coordinate system (x,y) is translated (to x',y'), without rotation, to an origin at that level on the hodograph. Now the new warm air shear ($\triangle v'_W$) just above the relocated frontal surface is given by the vector 8-9, and that in the H- layer by 7'-8, where 7' is a new point (representing a new wind at the base of the new H- layer) which must be located so as to satisfy eq. (5.4a). First, we note that 7' must be so located that the perpendicular from it onto the y'-axis is equal to the perpendicular from 9, and on the opposite side of the y'-axis; thus, 7' must be located on the line aa which is parallel to the y'-axis and as far (perpendicularly) from that axis as is point 9. The position of 7' on aa is such as to satisfy eq. (5.4), i.e. $\triangle v'_W - \triangle v'_H = \triangle v_W - \triangle v_H = 18$. Since $\triangle v'_W$ is known (being the y'-component of the vector 8-9 which in this example is -4 arbitrary units), it follows that $\triangle v'_H = -22$. Thus, point 7' is located on aa at a distance 22 units from the projection of 8 on aa, in a direction from 8 such that the vector 7'-8 is negative.

With the new wind (7') at the base of the H- layer established, it is now necessary to adjust the next lowest wind, in the cold air mass, in accordance with conditions (5.4a) and (5.5). First the original x- and y-axes must be aligned, at the 6000 ft level on the original hodograph; this is done in exactly the same way as for the upper frontal surface, as indicated in

fig. 3. In this particular example, the lower and upper frontal boundaries are oriented in the same direction, but this need not be the case in general. Values of $\triangle v_c$ and $\triangle v_H$ are determined as before, being in the present case +4 and -20 units, respectively; thus $\triangle v_c - \triangle v_H = +24$.

Now, given the 5 and (new) 7000 ft points (the latter indicated by 7'), the 6000 ft point must be located, and it will be located on the y'-axis parallel to the original y-axis and midway (perpendicularly) between points 5 and 7' (to satisfy eq. 5.5). Its location on this line must be such that $\triangle v'_c - \triangle v'_H = +24$, as indicated by point 6', fig. 3.

With both upper and lower frontal surfaces adjusted in such a way as to preserve slope and orientation, the shear hodograph becomes 4-5-6'-7'-8-9, as shown in fig. 1.

If necessary, the frontal surfaces can be raised or lowered several thousand feet by making changes in one thousand foot steps. If the wind data is too coarse, with winds being reported at rather large intervals such as every 5000 ft, it may be desirable to go to the original station data. Difficulties were encountered when a pronounced lowering of the front brought the lower surface down too near the friction layer in which strong non-frontal shears usually exist. The case of a deep frontal zone, several thousands of feet thick, introduces complications, but the general principles of treatment remain the same.

FIG. 1

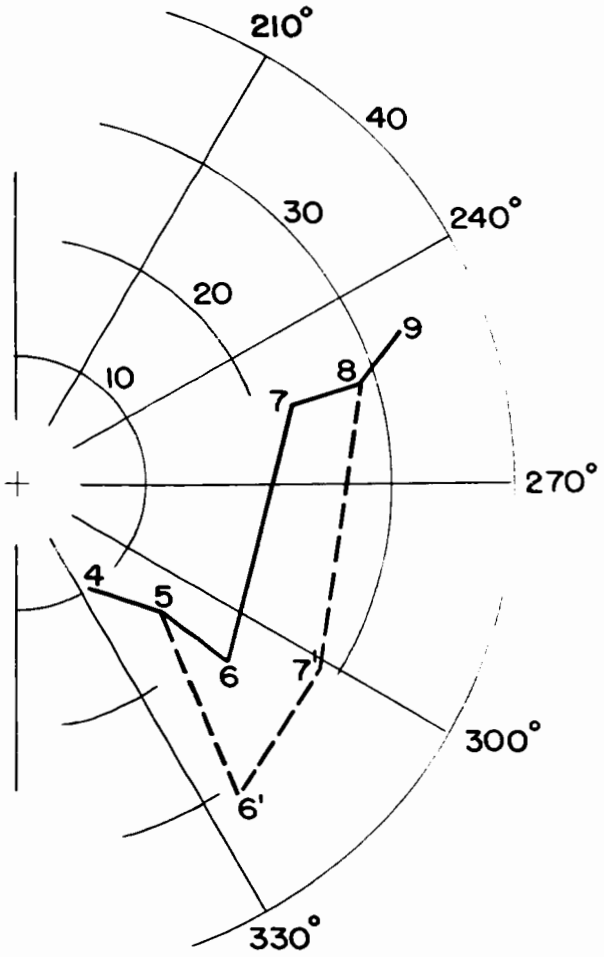

FIG. 2

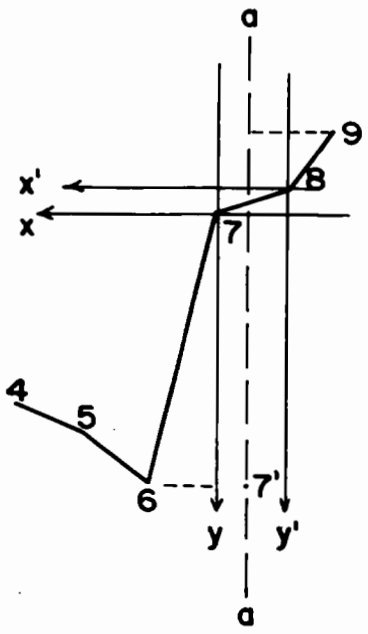

FIG. 3

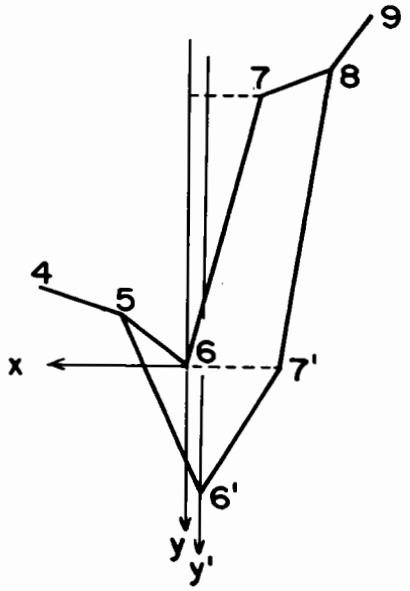

FIG. 1. Schematic hodograph showing original wind distribution (4-5-6-7-8-9). Following elevation of the frontal boundaries (originally at 6 and 7 thousand ft) by 1000 ft, the wind distribution becomes (4-5-6'-7'-8-9).

FIGS. 2,3, illustrate the progressive steps in the determination of the changes in the wind distribution (see text).

APPENDIX B.

CASE #12, 4 FEBRUARY 1954, 0300 GMT.

1. Synoptic Situation.

Late on 3 February a low on the Arctic front dissipated to the north of Montreal as a wave deepened on the Maritime front over the eastern seaboard to become the dominating feature. Aloft, a flat broad trough extended south to the Great Lakes. At 0630 GMT, 4 February, the fronts and precipitation areas were disposed as shown in fig. 1. Snow, which began at Montreal at 2145 on the 3rd, continued through most of the 4th, accumulating a total of 0.56 in (melted); peak rate of snowfall (0.05 in hr^{-1}) occurred between 1200-1300, after which it declined fairly steadily to the end of the storm (see fig. 2, Part I). Snow grains were reported at Montreal Airport between 2030-2330 GMT.

A pool of mP air, conspicuous over Maniwaki on the previous day, was still in evidence; both Maniwaki and Montreal lay under a col in the Maritime front, the height of which remained between 9 and 11000 ft over a 24-hour period (figs. 2, 3). With little slope to the frontal surface in this region, the Maniwaki wind distribution (fig. 4) was not modified. The mP air mass was stable; lapse rates in the mA air varied slightly about the (water) saturated adiabatic, with wet bulb depressions of 1-2 deg C. No humidity data were available above the Maritime frontal surface.

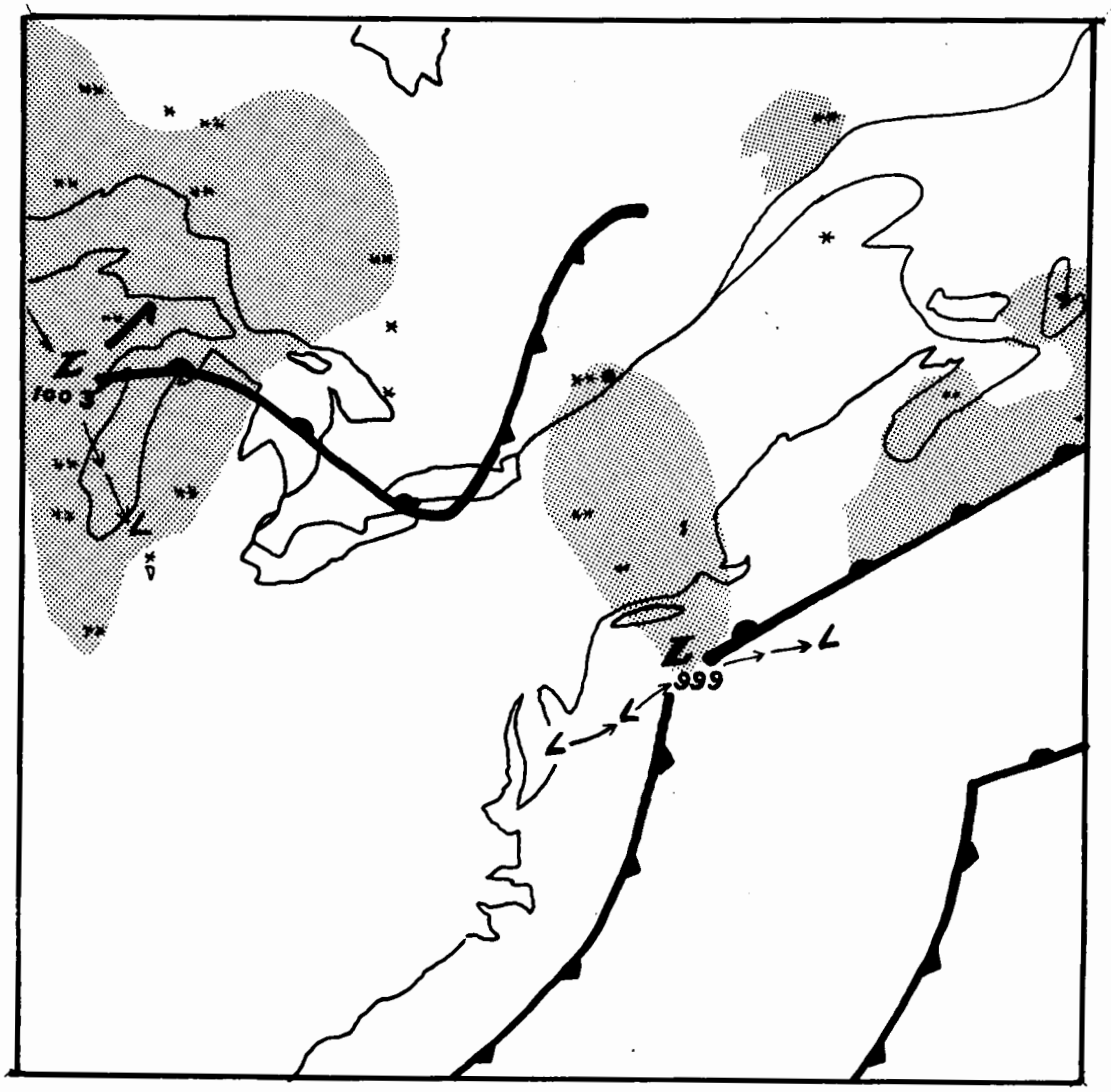

FIG. 1. Fronts and precipitation, 0630 GMT, 4 February 1954. Positions and central pressures of lows indicated, also past and subsequent positions at 6-hour intervals. Areas of continuous precipitation are stippled.

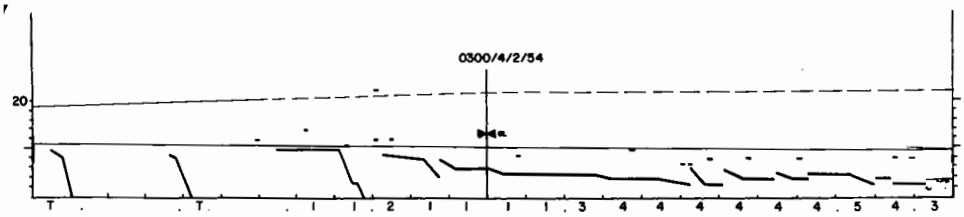

FIG. 2. Time-cross-section over Montreal for 24-hour period, centred on 0300 GMT, 4 February. Ordinate is height (thousands of feet), abscissa is time (hours). Fronts and echo-tops are shown, and the generating level indicated. Figures below the abscissa show hourly precipitation (10^{-2} in, melted).

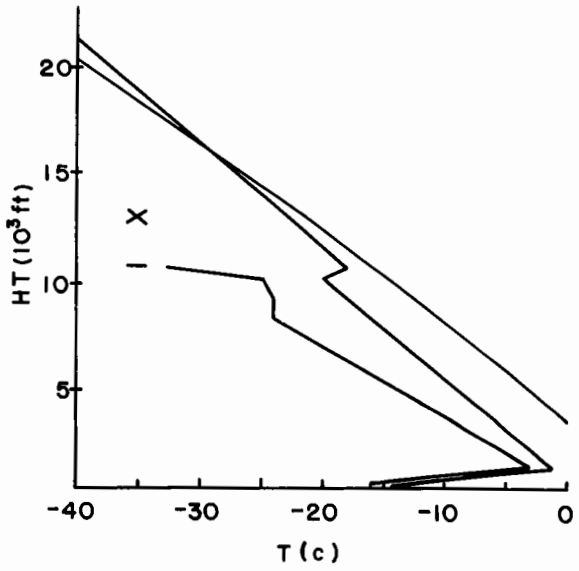

FIG. 3. Temperature and dew-point structure aloft, Maniwaki, 0300 GMT. A saturated (water) adiabat is included for reference. Front, at 11000 ft, is indicated by (-), and the generating level, at 13000 ft, by (X).

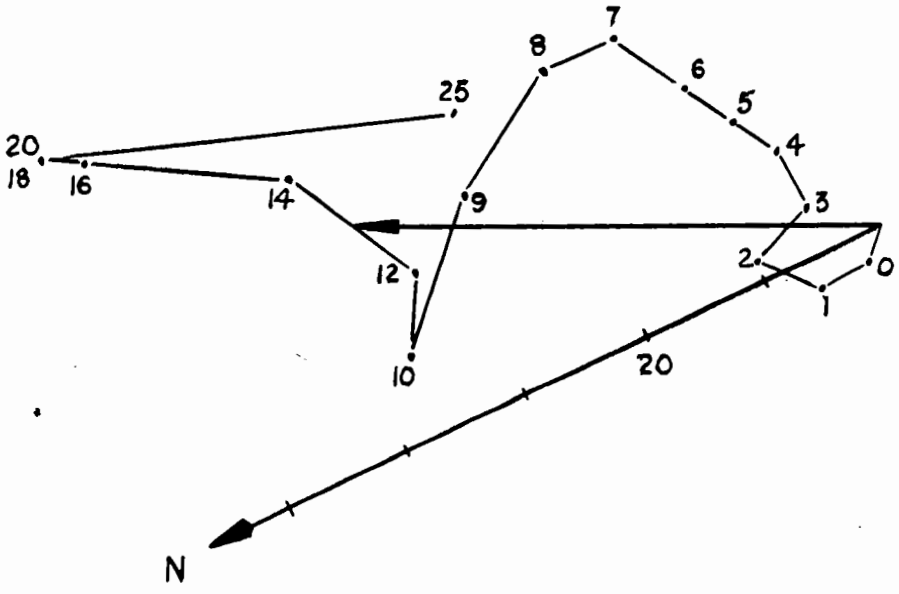

FIG. 4. Wind hodograph (Maniwaki, 0300 GMT) used for computation of trajectories. It is oriented with the generating level wind vector directed to the left. The scale is graduated in ft sec^{-1}.

2. Radar Echoes.

From 1500 to 2120 GMT of the 3rd, two half-hour bursts of echo appeared, each being a closely packed group of trails with tops (apparently cells) at about 10000 ft. The same form of echo reappeared about 2130, to last almost without interruption until 1500 GMT of the 4th. Fig. 5 shows a 3/4-hour portion of the height/time radar record of this echo pattern. Echo-top heights are plotted on the frontal time-cross-section (fig. 2); prior to 0300 these tops lay a few thousand feet above the Maritime front, but later they subsided to several thousand feet below. (with the exception, at 2400 GMT, of an echo top at 21000 ft). These tops appear to be generating cells.

3. Pattern Fitting and Terminal Speeds.

The wind distribution aloft over Maniwaki was not modified; patterns derived from these winds (fig. 6) were fitted to the leading edge of the prominent echo at 2215 GMT, a good fit being obtained down to 7000 ft with a generating level of 13000 ft. Terminal speed, derived by fit, was 3.0 ft sec^{-1}; speeds derived from trail slopes at 10.8 and 6000 ft were found to be 3.0, 4.0 and 4.3 ft sec^{-1}, respectively.

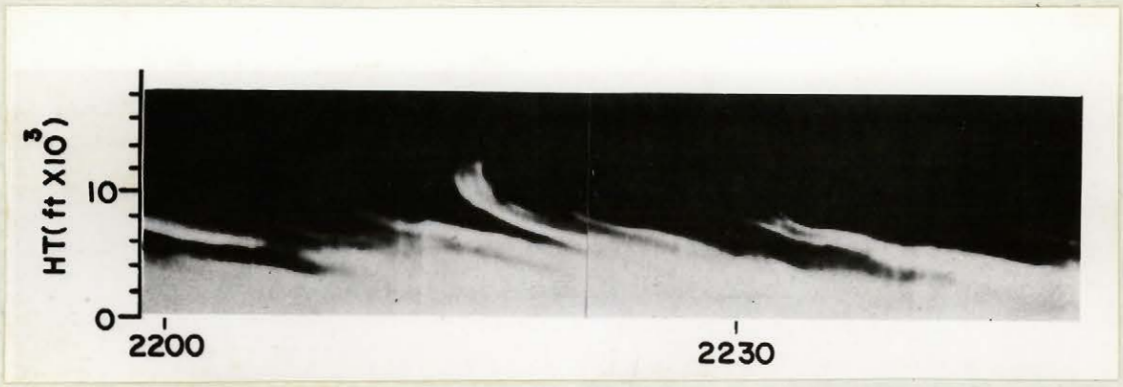

FIG. 5. Portion of the radar height/time record, 2200-2245 GMT, 3 February, showing apparent cell at 13000 ft. This prominent pattern, at 2220 GMT, was matched with the derived pattern of Fig. 6.

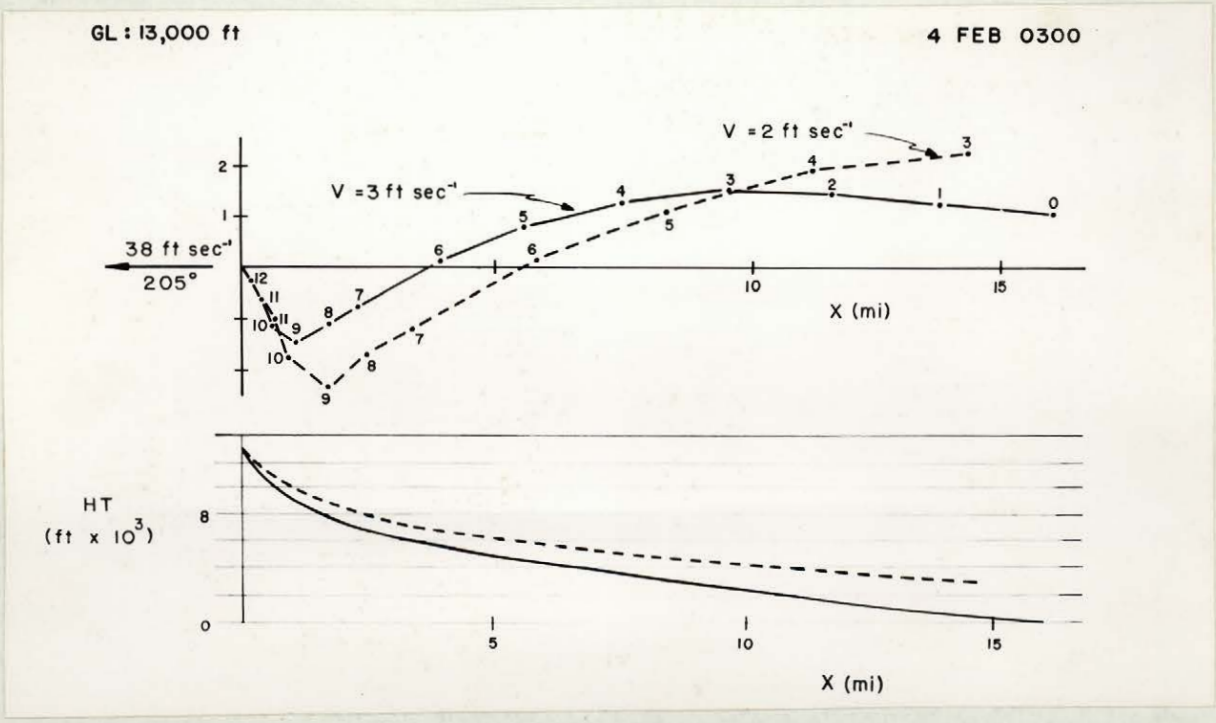

FIG. 6. Top, plan trajectories, derived from the wind field, for particles with terminal speeds of 2 and 3 ft sec^{-1}.
Bottom, projection of the plan trajectories into the vertical plane containing the generating level wind vector. The abscissa can be converted into a time axis; adjustment of this time scale, to achieve fit with the observed echo of Fig. 5, yields a terminal velocity of 3.0 ft sec^{-1} for the snow particles.

APPENDIX C

GENERATING LEVELS AND TERMINAL SPEEDS

		BY SLOPE		BY FIT	
Case no.	G/L (thsds. ft)	Height (thsds. ft)	Terminal Speed (ft sec^{-1})	Terminal Speed (ft sec^{-1})	Remarks
1	11	8	2.5	3.	
		6	2.7		
2	11	6	4.7	4.8	Echo at 0350 GMT.
		2	5.3		
		6	8.7	8.1	Echo at 0405 GMT.
		2	7.9		
3	11	8	7.5	4.	Echo at 1300 GMT, trailing edge.
		6	3.1		
		6	7.8	8.	Echo at 1600 GMT, leading edge.
		-	-	8.	Echo at 1300 GMT, leading edge.
4	20	12	11.2	9.1	
		8	7.0		
		6	8.8		
5	14	8	6.7	7.	Leading edge.
		6	5.2		
		8	5.0	5.4	Trailing edge.
6	17	12	0.8	1.3	
		10	2.7		
		8	7.6		
7	8	6	3.4	6.2	
		4	5.3		
		2	8.1		
8	18	14	11.9	12.4	Leading edge.
		12	12.4		
		14	7.3	6.7	Trailing edge.
		12	5.1		
9	16	14	4.7	4.4	14-12000 ft.
		12	6.1	6.1	12-9000 ft.
		10	8.2		
10	11	10	1.1	1.7	10-6000 ft.
		8	1.4		
		7	1.0		
11	12	6	10.7	6.8	
		4	9.1		
		2	6.8		
12	13	10	3.0	3.0	
		8	4.0		
		6	4.3		

		BY SLOPE		BY FIT	
Case no.	G/L (thsds. ft)	Height (thsds. ft)	Terminal Speed ($ft\ sec^{-1}$)	Terminal Speed ($ft\ sec^{-1}$)	Remarks
13	12	10	6.0	4.	
		8	5.4		
		6	2.6		
		4	2.0		
		2	2.0		
14	14	13	6.7	5.	
		12	6.4		
		10	4.5		
		8	5.5		